IMPACT OF WIND GENERATION ON GRID FREQUENCY STABILITY

By

Nga Nguyen

A DISSERTATION

Submitted to
Michigan State University
in partial fulfillment of the requirements
for the degree of

Electrical Engineering - Doctor of Philosophy

2017

ABSTRACT

IMPACT OF WIND GENERATION ON GRID FREQUENCY STABILITY

By

Nga Nguyen

The integration of renewable energy sources into power systems has gathered significant momentum globally because of its unlimited supply and environmental benefits. Within the portfolio of renewable energy, wind power has been experiencing a steadily increasing growth. Despite its well known benefits, wind power poses several challenges in grid integration. The inherent intermittent and non-dispatchable features of wind power not only inject additional fluctuations to the already variable nature of frequency deviation, they also decrease frequency stability and reliability by reducing the inertia and the regulation capability. To ensure the system security, the integration of wind power must be limited and the wind generation has to operate in the condition that enables wind generator to support the frequency control. As a result, the reliability of wind power must be re-estimated based on the wind power that can be accepted by the system, instead of the total wind production. This research examines the impacts of wind generation on system inertia and the regulation capability as well as the effect on tie-line flows and area control error. The effect of wind power on frequency regulation capability at different penetration levels is also investigated. The mathematical and simulation model to determine maximum wind power penetration level, given a frequency deviation limit, is developed. Based on the proposed mathematical model of wind penetration limit, the negative impact of wind on system reliability is examined. An improved method to coordinate the energy storage with the existing system to improve the wind-integrated system reliability while maintaining the system frequency security is also proposed. An approach to assist the integration of wind power with grid-scale virtual energy storage will be developed and examined. This thesis discusses the pertinent background and state of the art, and describes the proposed approaches and the results obtained.

To my parents, my sister, my husband and my little daughter.

ACKNOWLEDGMENTS

First of all, I would like to express my sincere thanks to my advisor Dr. Joydeep Mitra, who gave me great support during my graduate study. He is the one who taught me the first steps in my research with all of his patience. As one of the students under his supervision, I always have a feeling that he is always there to guide, to support, to protect, and to push us to “grow up” not only in our academic career but also in our daily life. I am really grateful for the patience that he showed for me, while teaching me everything step-by-step and also encouraging and supporting me. Even the way he scolded me was exactly the way my father did. That makes me feel like I am in my family. He is the best adviser that I have ever known with a very wide knowledge, consideration, patience, and kindness. Without his support and his guidance, I would not have made progress in my graduate studies and finish my Ph.D. program. His support is greatly appreciated.

I also would like to thank my committee members, Dr. Jongeun Choi, Dr. Subir Biswas, Dr. Fang Z. Peng, and Dr. Ranjan Mukherjee for their inspiring and helpful classes, valuable suggestions, and being members of my committee.

I would also like to thank my colleagues in the ERISE lab, for their kind support and priceless friendship, Dr. Niannian Cai, Dr. Mohammed Benidris, Dr. Salem Elsaiah, Dr. Samer Sulaeman, Mr. Valdama Johnson, Ms. Yuting Tian, Mr. Khaleel O. Khadedah, Dr. Oluwafemi Ipinnimo, Mr. Saleh Almasabi, Mr. Atri Bera, and Mr. Fares Theyab Alharbi.

I want to thank my colleagues and friends, who kept helping and supporting me in my research in many ways even when they were not working in the same research area as mine, Dr. Hiep Nguyen, Dr. Yantao Song, Dr. Cuong Nguyen, Professor Phu Nguyen, Mr. Abhinav Gaur, Mr. Dinh Nguyen, and Mr. Ujjwal Karki. Your unconditional support and valuable friendship made my PhD program full of happiness and kindness.

Most of all, I would like to thank my parents, my sister, my husband and my little daughter for their unconditional love, support, and understanding. They were always there to encourage me at times of need.

TABLE OF CONTENTS

LIST OF TABLES

LIST OF FIGURES

Chapter 1

Introduction

With technological and economic growth, the need for energy has been on the rise worldwide. At present, the energy industry in the world relies heavily on coal, oil and natural gas. These fossil fuels come from finite resources which are gradually dwindling. Moreover, fossil fuels also cause environmental damage. In order to deal with these issues, renewable energy is being used to replace conventional sources of energy around the world. In contrast to fossil fuels, renewable energy resources are constantly replenished and their impact on the environment is considered to be less adverse. Another advantage of renewable energy resources is that unlike traditional sources of energy, renewable energy resources can exist over diverse geographical areas. The rapid growth of renewable energy is driven by the increasingly competitive cost of renewable energy, dedicated policy initiatives, environmental concerns, and the need for access to modern energy. As reported in [1], renewable energy provided 19.2% of global energy consumption in 2014, and kept growing in 2015. The global investment in new renewable power capacity was more than double the investment in new coal- and natural gas-fired power generation capacity in recent years [1].

With growing public awareness, promoting renewable sources is strongly supported. Around 30 nations already have more than 20% of energy supply being generated from renewable energy sources and this contribution is projected to continue to grow strongly in the coming years [2]. According to [3], renewable energy is expected to provide 40% of total electricity in the US by

2030, and half of that comes from wind power. In 2015, wind power was the leading source of new power generating capacity in the US [2]. Wind farms have been growing steadily throughout the US both in turbine size and in wind farm capacity. Furthermore, the cost of wind generators has decreased dramatically over the past decade. These have promoted wind power as a promising renewable energy technology.

1.1 Motivation and Challenges

Although rapid deployment of wind power results in pollution mitigation and economic benefits, the application of wind power into power system has been confronted with a host of technical and economical problems. The integration of wind power can negatively affect the stability and reliability of a power system if there are not enough appropriate measures to deal with the intermittency and low or zero inertia that characterize this resource. One of these undesirable effects is frequency disturbance. In normal operation, as system frequency deviation must be maintained within a specified range, a minimum inertial frequency response is vital for frequency stability. Therefore, by contributing to a reduction of the system's inertia response, high wind power penetration level can endanger the stable and reliable operation of the system. Once wind power sources are connected to the main grid and replace conventional generators, they will cause a larger and faster frequency deviation. If the main grid does not have sufficient regulation capability, frequency deviation might direct to load shedding or even cause the whole system to collapse. The North American Electric Reliability Corporation (NERC) as well as Electric Reliability Council of Texas (ERCOT) and Western Interconnect (WECC) have all reported a reduction in frequency response due to an increase of variable generation [4–8]. HydroQuébec TransÉnergie (HQT) is dealing with this problem by requiring their wind power plants to be equipped with an inertia emulation system [9]. Therefore, it is important to investigate not only the effects of different wind power penetration levels on frequency regulation capability of power systems but also the maximum acceptable level of wind power that can be integrated into the grid. Due to the limit of integrated wind power, the system reliability have to be re-evaluated to ensure the system security. As the result of the negative impacts of wind power on the grid, more advanced operating approaches to increase the wind penetration should be developed.

1.2 Contributions

The contributions of the work presented here can be summarized as follows:

- Modeling the effect of wind integration on the system frequency response characteristic.
- Modeling the effect of wind integration on the area control error (ACE) and on tie line interchanges in an interconnected system.
- Providing guidance on the wind penetration limit given a frequency deviation limit.
- Developing a mathematical model of wind power penetration limit based on frequency deviation using sensitivity analysis.
- Investigating the impacts of stochasticity and low inertia of wind on system reliability.
- Proposing an advanced method to coordinate the energy storage with the existing system to improve the wind-integrated system reliability while maintaining the system frequency security.
- Proposing an approach to utilize the "virtual energy storage" to increase the wind power penetration.

1.3 Organization of the Thesis

This thesis is organized as follows:

Chapter 2 examines the effects of intermittent and non-dispatchable features of wind power on the system frequency stability. The impacts of wind power on the inertia, frequency regulation constant, tie-line flows, and area control error are included. Some guidance on determining maximum wind power penetration level given a frequency deviation limit is presented.

Chapter 3 presents a method to estimate the maximum level of variable energy resources that can be integrated into the grid based on the frequency security constraint. The method described uses the approximation of the frequency deviation extremum based on the sensitivity analysis.

Chapter 4 presents a new method to evaluate the reliability of a power system with high penetration of wind generation, considering the impact of not only the intermittence but also the low inertia characteristic of wind power.

Chapter 5 proposes an advanced method to coordinate energy storage with an existing wind-integrated system to improve its reliability while maintaining system frequency security.

Chapter 6 presents a novel approach called "grid scale virtual energy storage", which addresses the challenges of the renewable energy in the power system at no cost. Reducing the reserve requirement, regulation capacity, transmission limit, and wear and tear on power system by functioning as normal energy storage, the grid scale virtual energy storage support greater penetration of renewable energy into the grid.

Chapter 7 provides concluding remarks and possible future work.

Chapter 2

Effects of Wind Power Penetration on System Frequency Regulation

2.1 Introduction

The substantial growth of technology and economy makes the need for energy on the rise worldwide. Because of the concerns about the reduction of fossil fuel reserve and the impact on the environment, renewable energy (RE) becomes an attractive resource in energy industry. RE is expected to provide 40% of total electricity in the US by 2030, and half of that comes from wind power [3]. However, the application of wind power has been confronted with a host of technical and economical problems. The integration of wind power can negatively affect the frequency stability of a power system because of the intermittency and low or zero inertia [10,11] characteristics. In normal operation, the system must maintain a minimum amount of inertia to ensure the system frequency deviation within a safe limit. Hence, high wind power penetration level with low or zero inertia can endanger the stable operation of the system by causing a larger and faster frequency deviation. This phenomenon is undesirable because a large frequency deviation might direct to

The content of this chapter has been reproduced with permission from *Nga Nguyen and Joydeep Mitra, An Analysis of the Effects and Dependency of Wind Power Penetration on System Frequency Regulation, IEEE Transactions on Sustainable Energy, vol. 7, no. 1, pp. 354–363, Jan. 2016.*

load shedding or even cause the whole system to collapse. Hence, it is important to investigate the impacts of wind power penetration on frequency regulation capability of power systems.

While examining the undesirable influence of wind power on the load frequency control (LFC) of power system, previous works mostly consider wind power output uncertainty (i.e. intermittency) and inertia reduction [6, 12–21], reserve requirement [22]. In [20] and [22], the effect of wind power on equivalent regulation constant was also investigated. Besides, several works have made an effort to identify the maximum penetration level of wind power based on thermal limit [23] or constraint on frequency deviation [24, 25]. The work presented in this chapter extends the prior art by adding the following contributions:

- Modeling the effect of wind integration on the system frequency response characteristic (β).
- Modeling the effect of wind integration on the area control error (ACE) and on tie line interchanges in an interconnected system.
- Providing guidance to the limit on wind penetration for a given limit on frequency deviation.

The load frequency control and the mathematical modeling of one control area in the presence of wind power are presented in the next section. The basis to define the limitation of wind penetration to the grid is also included. A simulation model and result are presented in section 2.3 to verify the computation obtained from the mathematical model. In this section, some observations and recommendations are also included to clarify the salient aspects of the contribution.

2.2 Mathematical LFC Modeling in the Presence of Wind

2.2.1 Load Frequency Control

The main objective of LFC is to return frequency excursion to the nominal value whenever a mismatch between generation and demand appears. Frequency disturbance is immediately inhibited by inertia, governor action, load and other damping mechanisms. Motor loads resist disturbance by adjusting their speed in direct proportion to frequency deviation while governor regulates generator output by changing prime mover input. These actions are attributed to the furthest frequency deviation point and a part of frequency recovery duration. They stabilize system frequency rather than restore frequency to its nominal value. To remove the remaining frequency error, it is required to have the Automatic Generation Control (AGC) change the generator set point.

When wind generators are installed into the main grid and replace conventional generators, the governor response will be less effective due to the decline of inertia and of ability to regulate the generation output of the entire system. As a result, the frequency deviates at a larger magnitude and the recovery is prolonged. These effects are considered in the mathematical model in the next sub-section.

2.2.2 LFC Mechanism of One Control Area in the Presence of Wind Power

Traditionally, mechanical power, which is created from rotational energy, is fed to the conventional generator via turbine to produce electrical power. Once an imbalance occurs between input and output, rotor speed will experience a deviation. The governor plays the role of sensing the disturbance that causes unbalance and sends a control signal to recover frequency by adjusting the turbine input. The combination of governor, turbine, rotating mass and load damping control model is represented in the load frequency control model as shown in Fig. 2.1 [26]. The disturbance caused by wind power is captured in the control model by $\Delta P_L(s)$ based on the assumption that wind power is considered to be a negative load. In Fig. 2.1, the notations used are as follows:

ΔP_C = supplementary control action

$K(s)$ = LFC controller

$$K(s) = \frac{K}{s}$$

ΔP_{wind} = disturbance caused by wind power

ΔP_{load} = non-frequency-sensitive load change

ΔP_L = disturbance

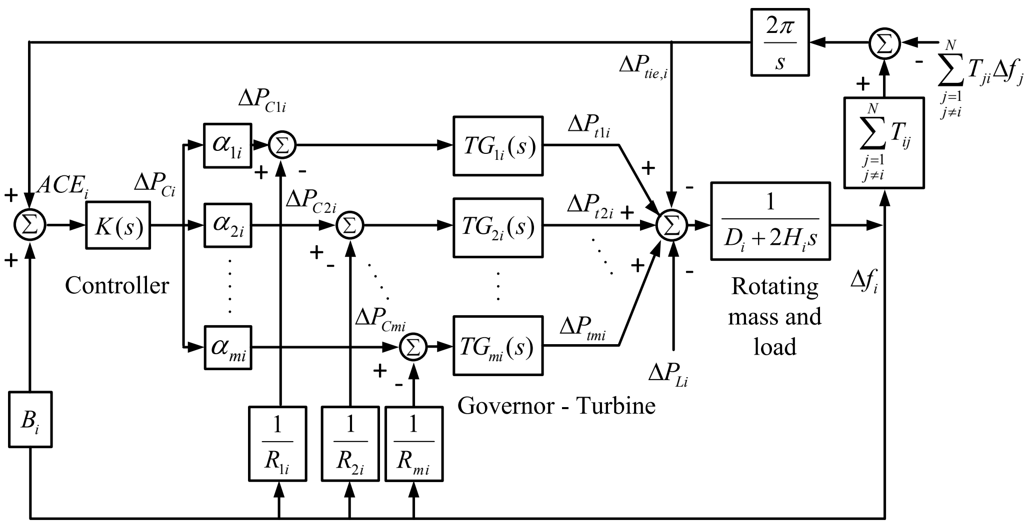

Figure 2.1: Control area i in an interconnected system in the presence of wind power.

$$\Delta P_L = \Delta P_{load} - \Delta P_{wind} \tag{2.1}$$

T_{ij} = synchronizing torque coefficient

H = equivalent inertia constant

Δf = frequency deviation

D = load damping constant

$TG_{ki}(s)$ = turbine-governor transfer function

$\Delta P_{tie,i}$ = tie-line power exchange between area i and other areas [26]

$$\Delta P_{tie,i} = \sum_{\substack{j=1 \\ j\neq i}}^{N} \Delta P_{tie,ij} = \frac{2\pi}{s}\Big(\sum_{\substack{j=1 \\ j\neq i}}^{N} T_{ij}\Delta f_i - \sum_{\substack{j=1 \\ j\neq i}}^{N} T_{ji}\Delta f_j\Big) \tag{2.2}$$

B_i = frequency bias factor which is calculated as below [27]:

$$B_i = \beta_i = \frac{1}{R_i} + D_i \tag{2.3}$$

Although the nature of wind power is intermittent, fixed-speed wind turbines can sometimes contribute to LFC by its spinning inertia [28–30]. On the other hand, variable speed wind turbines cannot provide spinning inertia because they are decoupled from the grid by power electronic converters. The reason for this decoupling is the control system of variable speed wind turbines operates to apply a restraining torque to the rotor following the predetermined torque - rotor speed curve [31]. However, with improved control strategies, some variable speed wind turbines such as DFIG turbines are able to provide partial inertia to support the grid by performing some operations similar to these in conventional generators [20,32–39]. As stated in [40–42], wind turbine can also have a droop characteristic with speed up/down averaging control. In another point of view, the application of synchronverters [38] can make wind generators mimic the behavior of synchronous generators. However, the wind inertia is limited by the available output of wind generators and the type of wind turbines. Once wind generators gradually replace conventional generators, the total inertia of the system decreases while the equivalent regulation constant increases. This effect yields a reduction of the area frequency response characteristic. Assuming that the fraction of inertia that wind power contributes to the grid is r_w (which is determined based on wind generation output [43]), the fraction of conventional generation inertia that is reduced in the presence of wind is r_r, the new inertia constant of the system can be calculated as follows:

$$H_{new,i} = H_{old,i}(1 + r_w - r_r) \tag{2.4}$$

The term r_w includes both the actual inertia provided by fixed-speed wind turbines as well as any artificial inertia that may be synthetically emulated at other wind turbines. It should also be noted that r_r is not always the fraction of wind power that takes the place of conventional power. The following example will illustrate the difference between these two definitions (power replacement and inertia replacement):

Consider a small power system with three conventional generators of 50 MW output and 0.02 pu.s inertia each. Assuming that the system has a total output of 150 MW, let us consider three possibilities as below:

- If the total integrated wind power is 40 MW (which is smaller than output of one conventional generator) and constitutes approximately 26.7% total power, the total power output of the conventional generators will reduce. However, the total inertia constant of the integrated system does not change because none of the conventional generators is decommitted.

- If the total integrated wind power is 50 MW (which equals to the output of one conventional generator) and constitutes approximately 33.3% total power, both the total power output of the conventional generators and the total inertia of the integrated system reduce because one of the conventional generators will be completely decommitted. The inertia constant reduction in this case equals 0.02 pu.s. The fraction of replaced power and the fraction of inertia reduction are the same.

- If the total integrated wind power is 60 MW (which is larger than the output of one conventional generator) and constitutes 40% total power, both the total power output of the conventional generators and the total inertia of the integrated system reduce. However, the inertia constant reduction in this case equals 0.02 pu.s which is approximately 33.3% total inertia.

Besides the change in the inertia constant, the equivalent regulation constant is also modified:

$$R_{new,i} = \frac{R_{old,i}}{1 + r_w - r_r} \tag{2.5}$$

Because of the change in equivalent regulation constant, the new area frequency response characteristic is determined as follows:

$$\beta_{new,i} = B_{new,i} = \frac{1}{R_{old,i}}(1 + r_w - r_r) + D_i \tag{2.6}$$

The change in R and β leads to the variation in the area control error in the interconnected system:

$$ACE_{new,i} = \Delta P_{tie,i} + \beta_{new,i}\Delta f_i \tag{2.7}$$

While investigating the effect of wind power on interconnected systems, three types of conventional turbine will be considered in LFC model: non-reheat turbine, reheat turbine and gas turbine. The dynamic models of turbine-governor systems for these three generators are shown in Fig. 2.2, Fig. 2.3 [27] and Fig. 2.4 [44,45].

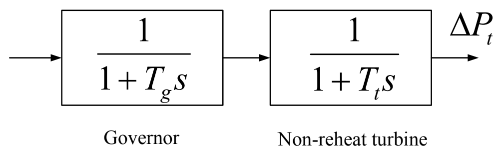

Figure 2.2: Block diagram of governor with non-reheat turbine.

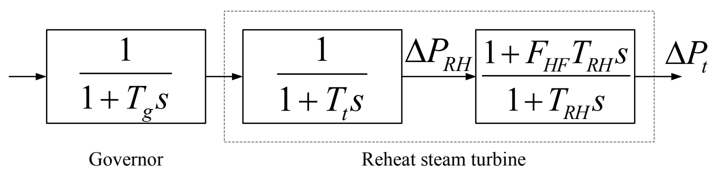

Figure 2.3: Block diagram of governor with reheat steam turbine.

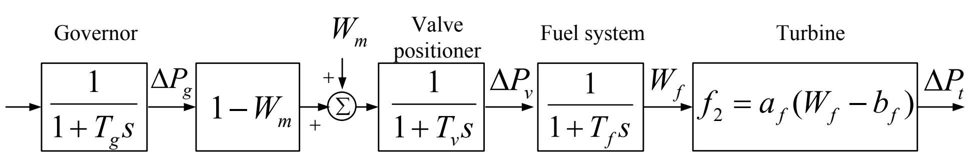

Figure 2.4: A simplified block diagram of single-shaft gas turbine.

In Fig. 2.2, Fig. 2.3 and Fig. 2.4, the notations used are as follows:

T_g = speed governor time constant

T_t = steam turbine time constant

T_{RH} = time constant of reheater

F_{HP} = fraction of turbine power generated by HP unit

ΔP_{RH} = intermediate (reheat) power signal

ΔP_v = intermediate valve positioner signal

T_v = valve positioner time constant

T_f = gas fuel time constant

W_m = minimum fuel flow

W_f = fuel flow

a_f, b_f = gas turbine constant

The state-space of LFC dynamic model for control area i that includes m reheat steam turbine generators in the presence of wind power can be presented as follows:

$$\dot{x_i} = \hat{A}_i x_i + \hat{B}_i u_i + \hat{C}_i n_i \tag{2.8}$$

$$y_i = \hat{D}_i x_i \tag{2.9}$$

where

$$\begin{aligned}
x_i &= \left[\Delta f_i \ \Delta P_{ti} \ \Delta P_{gi} \ \Delta P_{tie,i} \ \Delta P_{RHi}\right]^T \\
\Delta P_{ti} &= [\Delta P_{t1i} \ \Delta P_{t2i} \ \cdots \ \Delta P_{tmi}] \\
\Delta P_{gi} &= [\Delta P_{g1i} \ \Delta P_{g2i} \ \cdots \ \Delta P_{gmi}] \\
\Delta P_{RHi} &= [\Delta P_{RH1i} \ \Delta P_{RH2i} \ \cdots \ \Delta P_{RHmi}] \\
y_i &= [\Delta f_i \ ACE_i]^T \\
u_i &= [\Delta P_{C_{1i}} \ \Delta P_{C_{2i}} \ \ldots \ \Delta P_{C_{mi}}]^T \\
n_i &= [\Delta P_{Li} \ \sum_{\substack{j=1 \\ j\neq i}}^{N} T_{ji}\Delta f_j]^T
\end{aligned}$$

For simplicity, matrices $\hat{A}_i$, $\hat{B}_i$, $\hat{C}_i$ and $\hat{D}_i$ of a control area with one reheat steam turbine can be expressed as shown in (2.10):

$$\hat{A}_i = \begin{pmatrix} \frac{-D_i}{2H_i} & \frac{1}{2H_i} & 0 & \frac{-1}{2H_i} & 0 \\ 0 & \frac{-1}{T_{RHi}} & \frac{F_{HPi}T_{RHi}}{T_{ti}T_{RHi}} & 0 & \frac{T_{ti}-F_{HPi}T_{RHi}}{T_{ti}T_{RHi}} \\ \frac{-1}{R_iT_{gi}} & 0 & \frac{-1}{T_{gi}} & 0 & 0 \\ 2\pi\sum_{\substack{j=1 \\ j\neq i}}^{N} T_{ij} & 0 & 0 & 0 & 0 \\ 0 & 0 & \frac{1}{T_{ti}} & 0 & \frac{-1}{T_{ti}} \end{pmatrix} \tag{2.10}$$

$$\hat{B}_i = (0\ \ 0\ \ \frac{1}{T_{gi}}\ \ 0\ \ 0)^T$$

$$\hat{C}_i = \begin{pmatrix} \frac{-1}{2H_i} & 0 & 0 & 0 & 0 \\ 0 & 0 & 0 & -2\pi & 0 \end{pmatrix}^T$$

$$\hat{D}_i = \begin{pmatrix} 1 & 0 & 0 & 0 & 0 \\ \beta_i & 0 & 0 & 1 & 0 \end{pmatrix}$$

In case of non-reheat turbine, the state variables are similar to those in reheat turbine except that the entries corresponding to ΔP_{RH} are omitted and the entries corresponding to ΔP_t are modified. The state-space of the gas turbine is different from that of the reheat and non-reheat turbines and is shown as follows:

$$
\begin{aligned}
x_i &= [\Delta f_i \ \Delta P_{gi} \ \Delta P_{tie,i} \ \Delta P_{vi} \ \ W_{fi}]^T \\
\Delta P_{gi} &= [\Delta P_{g1i} \ \Delta P_{g2i} \ \cdots \ \Delta P_{gmi}] \\
\Delta P_v &= [\Delta P_{v1i} \ \Delta P_{v2i} \ \cdots \ \Delta P_{vmi}] \\
W_{fi} &= [W_{f1i} \ W_{f2i} \ \cdots \ W_{fmi}] \\
y_i &= [\Delta f_i \ ACE_i]^T \\
u_i &= [\Delta P_{C_{1i}} \ \Delta P_{C_{2i}} \ \cdots \ \Delta P_{C_{mi}}]^T \\
n_i &= [\Delta P_{Li} \ \sum_{\substack{j=1 \\ j \neq i}}^{N} T_{ji} \Delta f_j \ b_{fi} \ W_{mi}]^T
\end{aligned}
$$

Matrices $\hat{A}_i$, $\hat{B}_i$, $\hat{C}_i$ and $\hat{D}_i$ of a control area with one gas turbine are provided as follows:

$$\hat{A}_i = \begin{pmatrix} \frac{-D_i}{2H_i} & 0 & \frac{-1}{2H_i} & 0 & \frac{a_{fi}}{2H_i} \\ \frac{-1}{R_i T_{gi}} & \frac{-1}{T_{gi}} & 0 & 0 & 0 \\ 2\pi \sum_{\substack{j=1 \\ j\neq i}}^{N} T_{ij} & 0 & 0 & 0 & 0 \\ 0 & \frac{1-W_{mi}}{T_{vi}} & 0 & \frac{-1}{T_{vi}} & 0 \\ 0 & 0 & 0 & \frac{1}{T_{fi}} & \frac{-1}{T_{fi}} \end{pmatrix}$$

$$\hat{B}_i = [0 \;\; \frac{1}{T_{gi}} \;\; 0 \;\; 0 \;\; 0]^T$$

$$\hat{C}_i = \begin{pmatrix} \frac{-1}{2H_i} & 0 & 0 & 0 & 0 \\ 0 & 0 & -2\pi & 0 & 0 \\ \frac{-a_{fi}}{2H_i} & 0 & 0 & 0 & 0 \\ 0 & 0 & 0 & \frac{1}{T_{vi}} & 0 \end{pmatrix}^T$$

$$\hat{D}_i = \begin{pmatrix} 1 & 0 & 0 & 0 & 0 \\ \beta_i & 0 & 1 & 0 & 0 \end{pmatrix}$$

As is evident from Fig. 2.1, the frequency deviation can be expressed as follows:

$$\Delta f_i(s) = \frac{\sum_{k=1}^{m} TG_{ki}(s)\Delta P_{Cki}(s) - \Delta P_{tie,i}(s) - \Delta P_{L,i}(s)}{2H_{new,i}s + D_i + \frac{\sum_{k=1}^{m} TG_{ki}(s)}{R_{new,i}}} \tag{2.11}$$

Using the final value theorem to get the steady state value of the frequency deviation Δf_{iss}:

$$\Delta f_{iss} \;=\; \lim_{s\to 0} s\Delta f_i(s) \;=\; \lim_{s\to 0} s.\left(\frac{\sum_{k=1}^{m} TG_{ki}(s)\Delta P_{Cki}(s) - \Delta P_{tie,i}(s) - \Delta P_{L,i}(s)}{2H_{new,i}s + D_i + \frac{\sum_{k=1}^{m} TG_{ki}(s)}{R_{new,i}}}\right) \tag{2.12}$$

Following the assumption that $\Delta P_{tie,i}(s)$ approaches zero at steady state [26] and the system has enough reserve to match the disturbance $\Delta P_{Ci} = \Delta P_{Li}$, equation (2.12) gives the result:

$$\Delta f_{iss} = 0 \tag{2.13}$$

However, the frequency deviates farther from the scheduled value and the recovery duration is lengthened. Due to the change in frequency, the power flow on the tie line increases, which is a negative impact on each area. This can be inferred easily from equation (2.2).

When a stand-alone system is considered, power exchange in the tie-line between control areas does not exist and $\Delta P_{tie,i}(s)$ vanishes in equation (2.11).

From the above analysis, the maximum excursion of frequency can be identified. As a consequence, it is possible to evaluate the wind penetration limit. The maximum excursion is compared with the safe range of frequency deviation ± 0.2 Hz [46] to define how much wind power should be integrated into the main grid. Based on the theoretical examination in this section, a simulation model is implemented in the following section in order to verify the effect of wind power on frequency deviation, tie-line power flow, and area control error.

2.3 Simulation and Results

For the purpose of illustrating the aforementioned influence of integrating wind power into power system, the Matlab/Simulink model of the system explained in section 2.2 is developed. Three scenarios are evaluated, as described below. These scenarios examine the behavior of a single area, the interaction of two interconnected areas, and the impact of gas turbines that are being increasingly deployed to provide ramping capability. The test cases are constructed as follows:

- All generators in one area are chosen to be the same type and combined into one single unit.
- Only area 1 includes wind power.
- Load disturbance is simulated by a 0.04 pu step function.

- Only area 1 is subjected to a load disturbance in order to observe the assistance of area 2 to area 1.

- Wind penetration level will be adjusted with different values of inertia reduction: 0%, 10%, 20%, 30%, 40%, 50% and 60%.

- The effects of wind power on LFC with and without considering the change in frequency response characteristic and equivalent regulation constant will be compared.

Scenario 1: A stand-alone control area.

The simulation model of a stand-alone control area (area 1) is presented in Fig. 2.5. The parameters of the study system are derived from [26] and reported in Table 2.1. These parameters are the typical parameters for a small system and converted to per unit. Using initial values in Table 2.1 and applying equations (2.4), (2.5) and (2.6), simulation parameters are calculated and shown in Table 2.2.

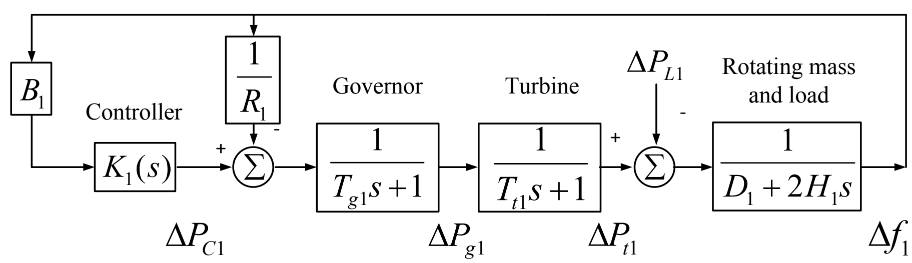

Figure 2.5: A stand-alone control area with non-reheat turbine unit.

Table 2.1: Simulation parameters of a stand-alone control area for scenario 1

K	D (pu/Hz)	$2H$ (pu.s)	R (Hz/pu)	T_g(s)	T_t(s)	B (pu/Hz)	T_{ij} (pu/Hz)
-0.3	0.015	0.1667	3.00	0.08	0.4	0.3483	0.2

Scenario 2: Two interconnected control areas.

In this scenario, parameters of control area 1 are kept the same as those in the first scenario. Parameters of area 2 are derived from [47] and reported in Table 2.3. The load disturbance is applied

Table 2.2: Simulation parameters for a stand-alone control area with wind effect on β and R

Inertia reduction (%)	K	D (pu/Hz)	$2H$ (pu.s)	R (Hz/pu)	T_g(s)	T_t(s)	B (pu/Hz)	T_{ij} (pu/Hz)
0	-0.3	0.015	0.1667	3.00	0.08	0.4	0.3483	0.2
10	-0.3	0.015	0.1500	3.333	0.08	0.4	0.315	0.2
20	-0.3	0.015	0.1334	3.75	0.08	0.4	0.2817	0.2
30	-0.3	0.015	0.1167	4.286	0.08	0.4	0.2483	0.2
40	-0.3	0.015	0.1000	5	0.08	0.4	0.215	0.2
50	-0.3	0.015	0.0834	6	0.08	0.4	0.1817	0.2
60	-0.3	0.015	0.0667	7.5	0.08	0.4	0.1483	0.2

only to area 1 to examine the mutual frequency assistance between the areas in an interconnected system and the change of ACE due to the adjusted R and β. The simulation model of the two interconnected control areas is presented in Fig. 2.6.

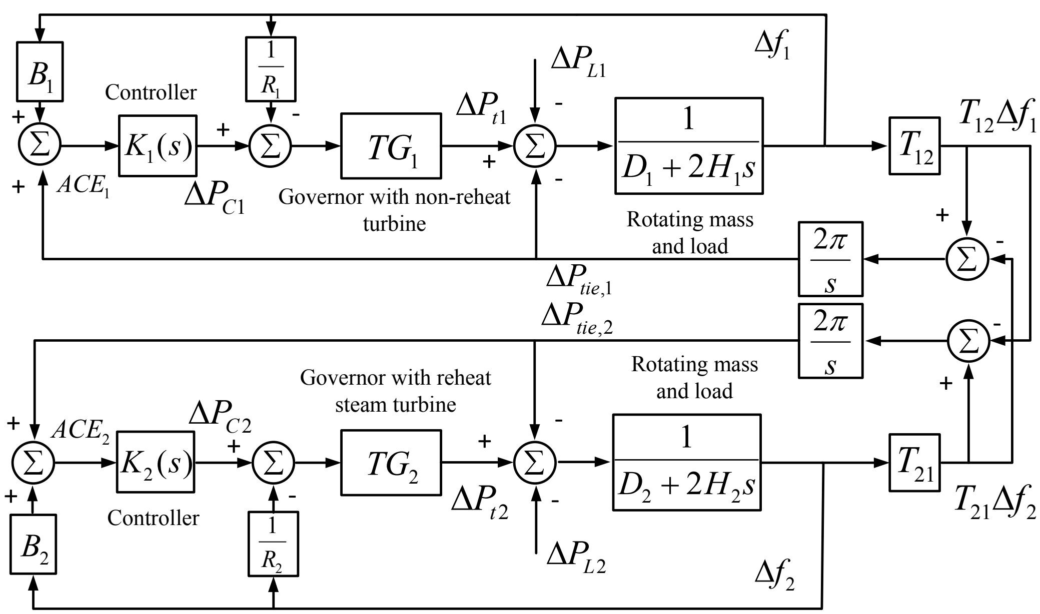

Figure 2.6: Simulation model of two interconnected control areas.

Scenario 3: A stand-alone control area with a combination of a gas turbine and a non-reheat turbine.

This scenario is similar to Scenario 1 except that it includes a gas turbine. This helps illustrate the impact of gas turbines, which are being increasingly integrated in systems with wind generation

Table 2.3: Simulation parameters of control area 2 for scenario 2

K	D (pu/Hz)	$2H$ (pu.s)	R (Hz/pu)	T_g(s)	T_t(s)	B (pu/Hz)	T_{ij} (pu/Hz)	T_{RH}(s)	F_{HP}
-0.4	0.008	0.167	2.4	0.08	0.3	0.42	0.087	10	0.5

to provide ramping capability. Without boiler and gas is burned to run the turbine, gas plants are easy to operate. They are efficient in following rapid and frequent changes in the system, hence supports wind integration. The parameters of the non-reheat turbine are kept the same as those in the first scenario. The parameters of the gas turbine are derived from [44] and reported in Table 2.4. Ramp rate limits are applied for all turbines with a higher ramp rate limit for the gas turbine. In particular, the ramp rate limit for the non-reheat turbine (RR_{nr}) is 0.029 while the ramp rate limit for the gas turbine (RR_g) is varied from 0.045 to 0.062 in order to observe the impact of the gas turbine. Due to the presence of wind, the 10% and 30% reduction of inertia are applied. The simulation model of this scenario is presented in Fig. 2.7.

Table 2.4: Simulation parameters of a gas turbine for scenario 3

K	D(pu/Hz)	T_g(s)	T_v(s)	T_f(s)	W_m	a_f	b_f
-0.3	0.015	0.05	0.05	0.4	0.23	1.3	0.23

In the first two scenarios, the simulation is implemented with and without the effect of wind on the frequency response characteristic and equivalent regulation constant to compare the differences between them. Frequency deviation obtained from scenario 1 and 2 with different wind penetration levels are shown in Figures 2.8, 2.10, 2.12 and 2.16. The rate of change of frequency (ROCOF) is presented in Fig. 2.9, Fig. 2.11, Fig. 2.13 and Fig. 2.17. Also, the power flows in the tie lines and the ACE in scenario 2 are illustrated in Fig. 2.14, Fig. 2.15 and Fig. 2.18, Fig. 2.19. The frequency deviations obtained from the third scenario are shown in Figures 2.20 and 2.21.

From the simulation results, several observations can be made:

1. The more wind power is integrated into the system, the larger the frequency deviation that occurs in case of disturbance. The reason is that when a greater amount of wind power

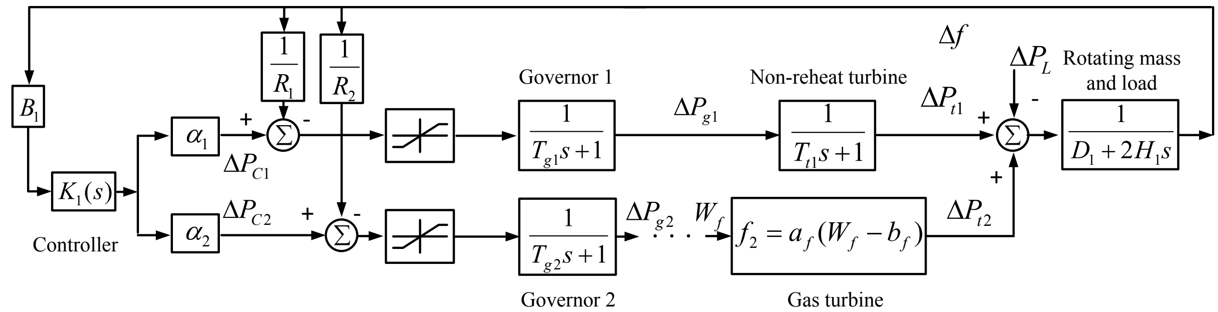

Figure 2.7: Simulation model of a control area including a gas turbine and a non-reheat turbine.

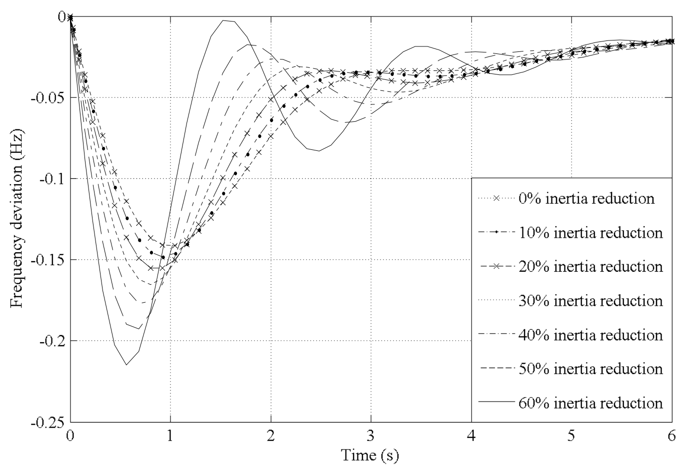

Figure 2.8: Scenario 1: Frequency deviations in the stand-alone control area 1 without considering the effect of wind on β and R.

substitutes conventional generators, a larger reduction in total system inertia and a higher increase in equivalent regulation constant occur. This leads to a deeper decrease in area frequency response characteristic. As a result, frequency deviates farther from the scheduled value. This is evident in Fig. 2.10 and Fig. 2.16: the largest frequency deviation increases from 0.14 Hz to 0.32 Hz (in the first scenario) and from 0.075 Hz to 0.125 Hz (in the second scenario) while inertia reduction augments from 0% to 60%. It is also obvious that if the effect of wind on frequency response characteristic and equivalent regulation constant is taken into account, frequency deviation gets worse value. From Fig. 2.8 to Fig. 2.16, these values fall into the range 0.14 to 0.32 Hz (in the first scenario) and 0.075 to 0.125 Hz (in the second scenario) instead of 0.14 to 0.22 Hz (in the first scenario) and 0.075 to 0.115 (in the second scenario) if these effects are not considered. In addition to the farther variation

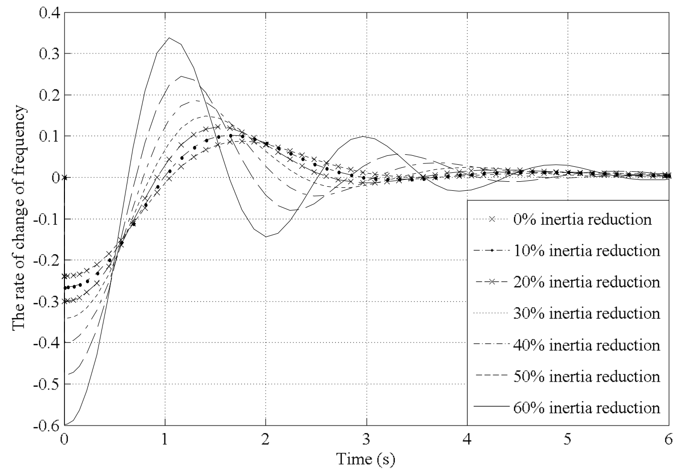

Figure 2.9: Scenario 1: ROCOF in the stand-alone control area 1 without considering the effect of wind on β and R.

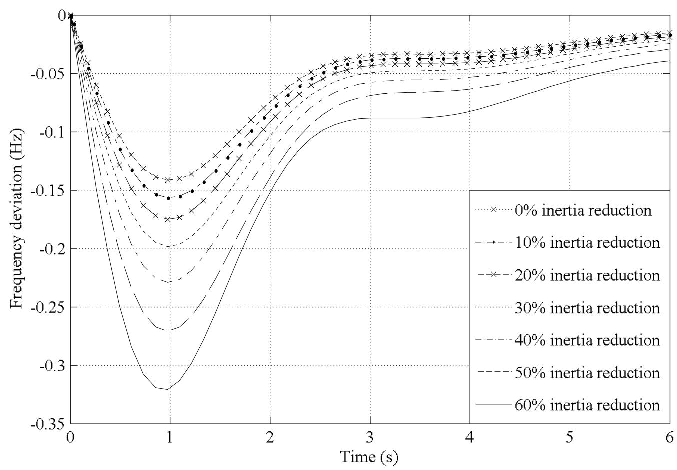

Figure 2.10: Scenario 1: Frequency deviations in the stand-alone control area 1 considering the effect of wind on β and R.

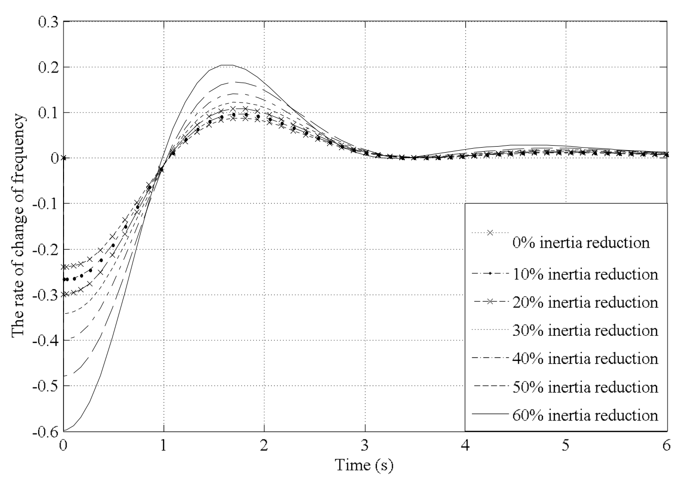

Figure 2.11: Scenario 1: ROCOF in the stand-alone control area 1 considering the effect of wind on β and R.

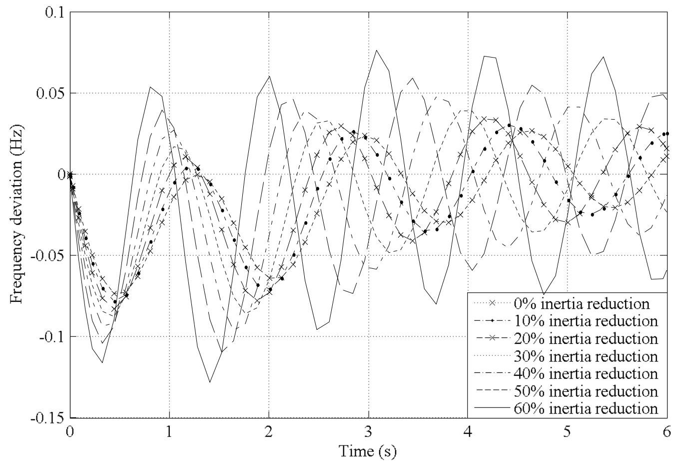

Figure 2.12: Scenario 2: Frequency deviations of area 1 in an interconnected system without considering the effect of wind on β and R.

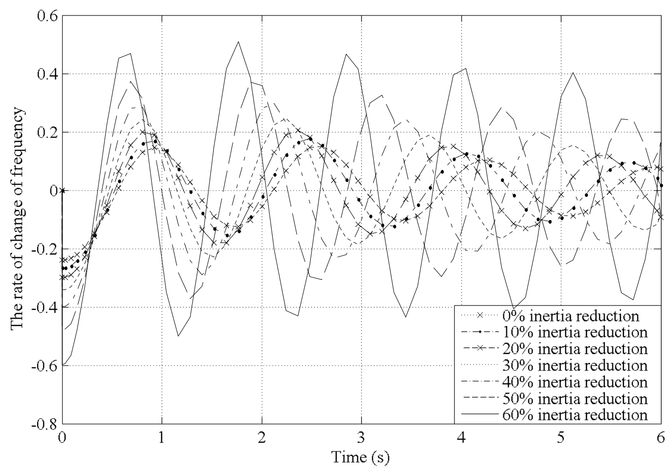

Figure 2.13: Scenario 2: ROCOF of area 1 in an interconnected system without considering the effect of wind on β and R.

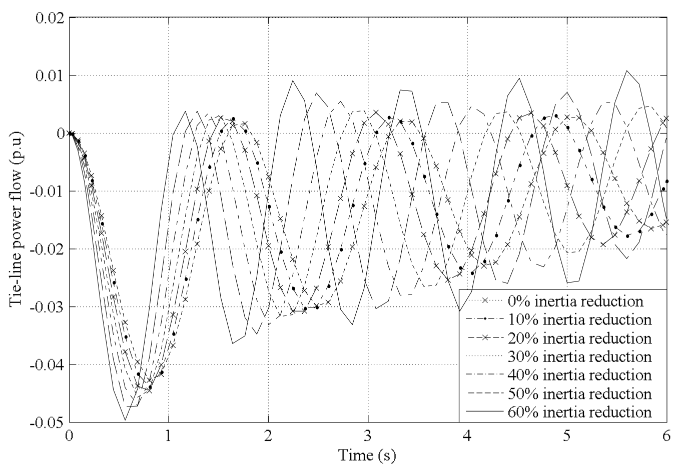

Figure 2.14: Scenario 2: The tie-line power flow of area 1 in an interconnected system without considering the effect of wind on β and R.

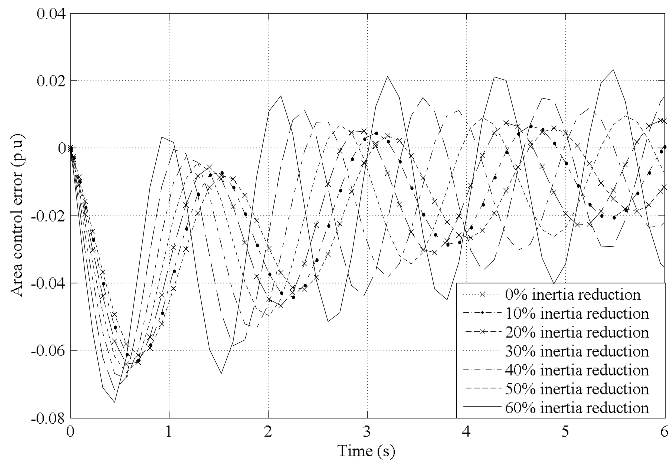

Figure 2.15: Scenario 2: Area control error of area 1 in the interconnected system without considering the effect of wind on β and R.

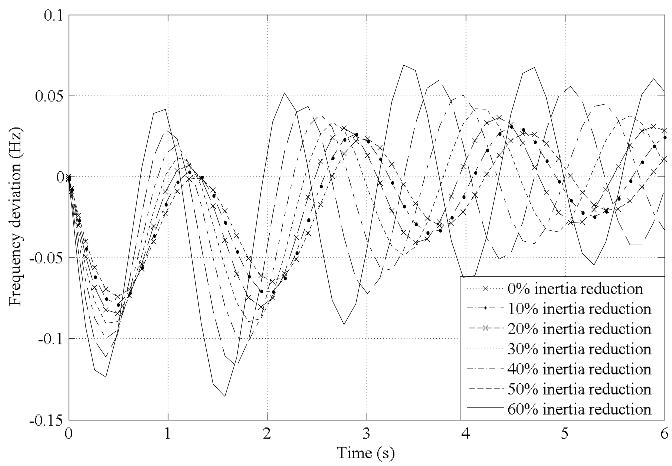

Figure 2.16: Scenario 2: Frequency deviations of area 1 in an interconnected system considering the effect of wind on β and R.

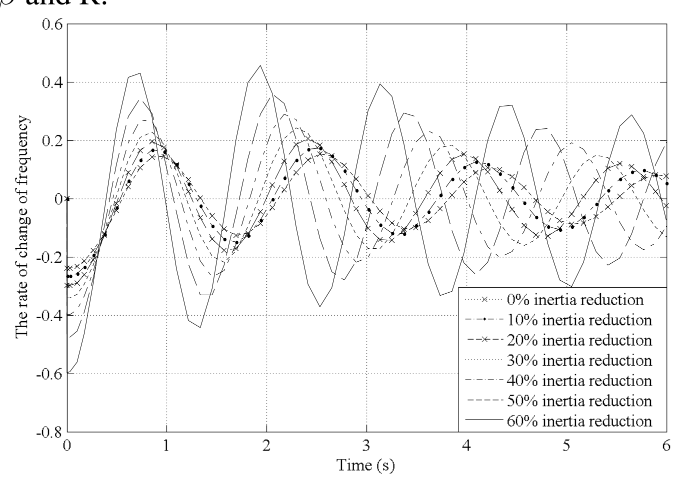

Figure 2.17: Scenario 2: ROCOF of area 1 in an interconnected system considering the effect of wind on β and R.

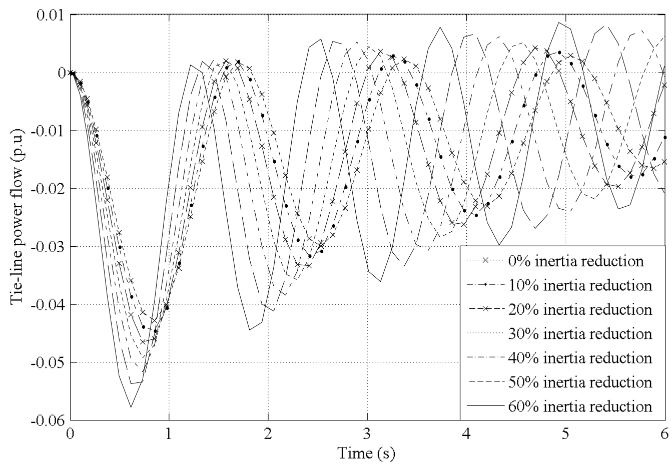

Figure 2.18: Scenario 2: The tie-line power flow of area 1 in an interconnected system considering the effect of wind on β and R.

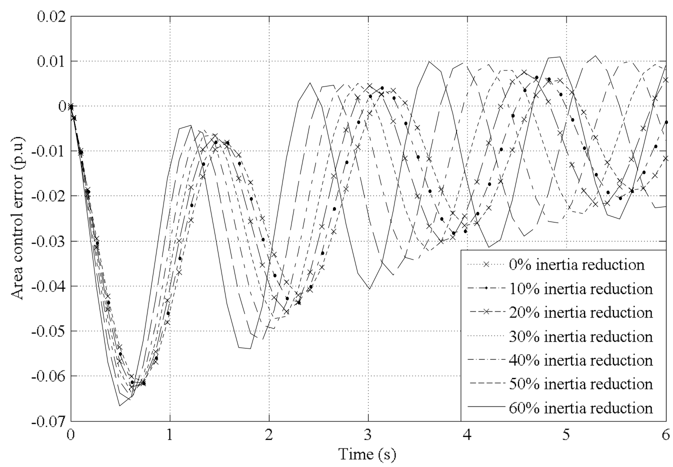

Figure 2.19: Scenario 2: Area control error of area 1 in the interconnected system considering the effect of wind on β and R.

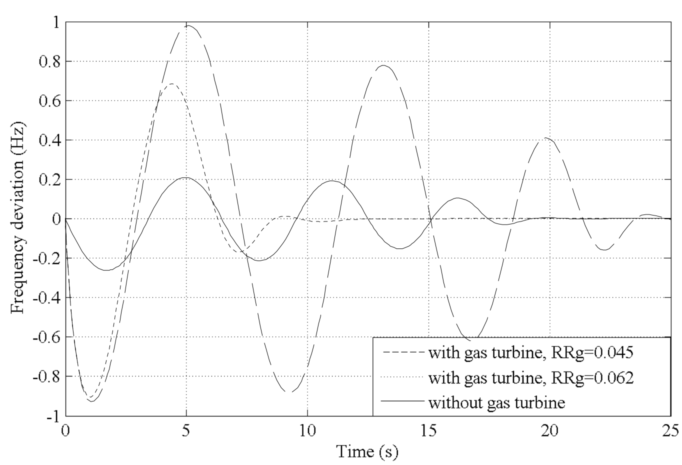

Figure 2.20: Scenario 3: Frequency deviations in the stand-alone control area considering the effect of gas turbine with 10% inertia reduction.

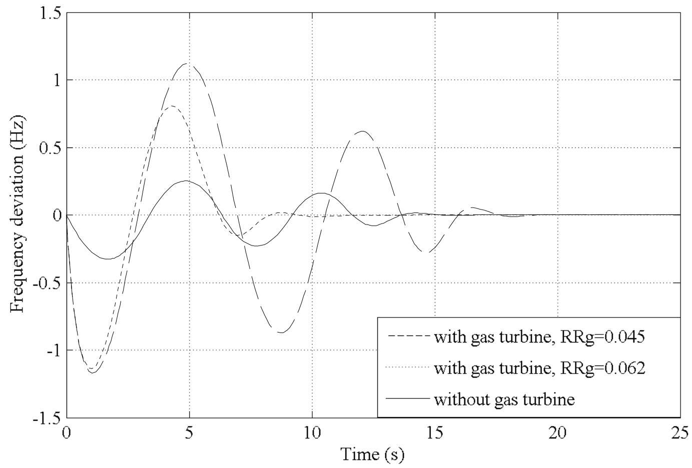

Figure 2.21: Scenario 3: Frequency deviations in the stand-alone control area considering the effect of gas turbine with 30% inertia reduction.

in the frequency, the rate of change of frequency as shown in Fig. 2.9, Fig. 2.11, Fig. 2.13 and Fig. 2.17 proves that the duration of frequency recovery has been extended due to the effect (the derivatives of frequency with respect to time change more slowly). Besides, the more wind power is integrated, the lower the ROCOF is. These changes can cause serious consequences if the system employs protective df/dt relays.

2. In an interconnected system, control areas are able to assist each other when the system is subject to disturbances. In simulation results, assistance from area 2 to area 1 has prevented frequency deviation from growing up. Frequency deviation is much smaller in the second scenario (0.075 to 0.125 Hz falling range) compared to the first scenario (0.14 to 0.32 Hz) as shown in Figures 2.10 and 2.16. For this reason, it is recommended that control areas collaborate to get the most benefit when wind generation is integrated into power system.

3. Following the increase of penetration levels, the tie-line power flow and the area control error get larger absolute values and longer time to recede as shown in Fig. 2.14, Fig. 2.15, Fig. 2.18 and Fig. 2.19. These are negative consequences due to the effect of wind power on β and on frequency which have been discussed in the foregoing section.

4. From the first two scenarios, by combining the mathematical model, the maximum pre-

dictable load disturbance, frequency stability standard, and simulation results, it is possible to estimate the penetration limit of wind generation into the main grid. This idea is illustrated in the simulation that has been presented: if the safe range of frequency deviation is ± 0.2 Hz [46], and if maximum predicted load disturbance is 0.04 pu, the penetration of wind power in a stand-alone control area should not be higher than the level that creates 30% reduction in inertia. This level can be higher than 30% of total generator inertia in the area if it has strong interconnections with neighboring control areas. However, planning and operation processes should take the following into account.

   (a) The effect of tie-line loading and congestion.

   (b) The effect of inadvertent islanding.

   (c) The proportion of inertia and regulating capability to the total system load.

5. Depending on the relationship between the ramp rate limits of two types of turbine, the gas turbine shows different impacts on frequency deviation. This is shown in Figures 2.20 and 2.21. If the ramp rate limit of the gas turbine is high (0.062), the system with gas turbine recovers faster. When this value decreases to 0.045, the system with gas turbine recovers slower. In the first case, the gas turbine benefits the frequency recovering speed clearly. However, the gas turbine makes the frequency nadir worse in both cases. This is consistent with the results reported in [48–50]. It is clear that while gas turbines benefit systems with wind generation through ramping capability, they are generally detrimental to frequency regulation.

2.4 Conclusion

In this chapter, the effect of wind power on load frequency control has been presented and examined at different penetration levels. The mathematical model and simulation results indicate that wind power leads to reduction in not only the overall system inertia but also frequency response characteristic due to an increase of regulation constant. As a consequence, the frequency deviation, the tie-line power flow and the area control error increase. This contribution of this research addresses a factor that is often overlooked when investigating load frequency control in the presence of wind generation. The analysis also provides guidelines toward estimating the allowable level of wind generation based on the configuration of system, maximum load disturbance and safe range of frequency excursion. The analyses presented here provide important information to the grid operator when considering wind power integration while ensuring the system stability. In the illustrations reported here, the control areas include gas turbine, reheat and non-reheat turbines. It is not difficult to extend this approach to include hydraulic turbine to more appropriately model the frequency response.

Chapter 3

Estimation of Penetration Limit of Wind Power Based on Frequency Deviation

3.1 Introduction

Over the last decade, regulatory, environmental, and technological forces have brought about a dramatic increase in the deployment of variable energy resources (VER) world-wide. As the costs associated with VER continues to decrease, VER is becoming both economically and environmentally competitive with conventional energy sources. VER has advantages of abundant supply, on-site generation and no greenhouse gases. Consequently, VER is considered by many to be a very promising source of energy in the future; some even estimate that VER penetration in the US will reach 40% by 2030 [3]. However, despite these advantages, the integration of most variable energy resources involves significant challenges, particularly on account of their variability and the fact that most of them possess little or no effective rotational inertia.

To ensure the stability and reliability of the power system, the balance between the demand and supply must be maintained. This balance is implemented through load frequency control (LFC).

The content of this chapter has been reproduced with permission from *Nga Nguyen, Saleh Almasabi and Joydeep Mitra, Estimation of Penetration Limit of Variable Resources Based on Frequency Deviation, North American Power Symposium 47th, IEEE, pp. 1–6, Oct. 2015.*

However, with high levels of VER, this objective becomes more difficult due to the inability to handle the fluctuations of both demand and supply. Moreover, the replacement of conventional generators with VER decreases the inertia of the system and increases the equivalent regulation constant, causing a higher variance in frequency. Accordingly, the high frequency deviation could trigger the under-frequency load shedding and protective df/dt relay. Hence, the maximum frequency deviation (frequency nadir point) plays an important role in defining system stability and reliability. In normal operation, the quality of power supplied must satisfy several conditions as required by the balancing authority. One of these conditions is the limit of frequency deviation or security constraint. To keep the frequency deviation in a safe limit, the penetration level of VER must be restricted.

To define the maximum penetration of VER, some previous works proposed ideas based on the stability power quality criteria: system minimum reserve requirement, the network congestions, voltage stability, system capacity, frequency stability, thermal violations [23, 51–58], transient stability limit and frequency security constraint [21, 59–62], harmonic limit considerations [63], wind-thermal coordination scheduling [64]. However, none of them provide a general mathematical formulation to estimate the maximum penetration level of VER for a multi-machine system. To further improve the previous work, this chapter presents a mathematical formulation for the maximum penetration of VER based on the frequency deviation limit. A mathematical model to define the maximum frequency deviation in the presence of VER is developed. Approximation based on sensitivity analysis is then used to estimate the change of frequency nadir due to the change of VER penetration. From the approximation results, the VER integration limit will be defined based on the frequency security.

The remainder of this chapter is organized as follows. Section 3.2 explains the mathematical model of the load frequency control and maximum frequency deviation. The maximum frequency deviation in the presence of VER and the formulation of maximum penetration of VER based on frequency security are included in Section 3.3. The calculation and simulation results, as well as the comparison and conclusion, are covered in Sections 3.4 and 3.5, respectively.

3.2 Load Frequency Control of Multi-machine System

3.2.1 Load Frequency Control

During normal operation, the balance between the power supplied and consumed is maintained by load frequency control (LFC). When there is a mismatch between load and generation, the frequency of the system experiences a disturbance. LFC restores the system frequency to its nominal value via four stages [64]: inertial, primary, secondary and tertiary response. In the first stage, load and other damping mechanisms restrain the deviation of frequency in the first few seconds after the disturbance. In the second stage, governor action prevents frequency from further deviation by changing the prime mover input. These two stages are attributed to the maximum frequency deviation and part of the frequency recovery duration. The third stage employs reserves to bring the frequency back to its nominal value by the Automatic Generation Control (AGC) and the last stage reschedules system reserves to prepare for the future mismatch. Since the scope of this chapter is frequency security, which is related to maximum frequency deviation, the first two stages will be the main interest.

3.2.2 The Mathematical Model of Frequency Deviation and Nadir Point for the Multi-machine System

To analyze the effects of VER on frequency nadir, it is necessary to understand the mathematical model of the system frequency. Fig. 3.1 is the model of LFC for the multi-machine system proposed in [25, 65]. This model is derived based on the sensitivity of the frequency deviation to the governor parameters for the low-order LFC model proposed in [66] using linear curve-fitting. The sensitivity of the maximum frequency deviation to governor parameters in [25] is shown in Table 3.1 and will be used later in this chapter.

The sensitivity results show that the frequency nadir is highly sensitive to regulation constant R and fraction of total power generated by the HP turbine F_H. Conversely, the sensitivity of frequency nadir to the governor time constant T_R, inertia H and load damping D is low. However,

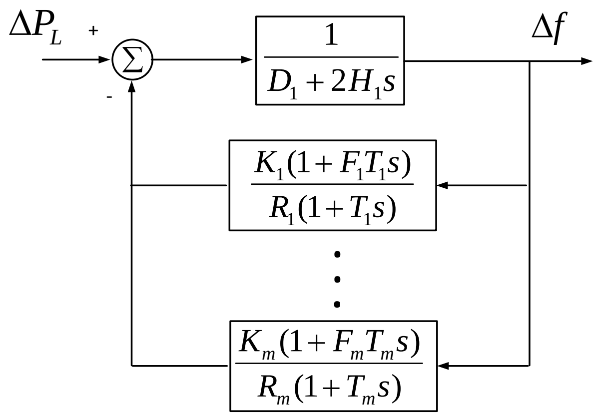

Figure 3.1: Multi-machine LFC model

Table 3.1: Sensitivity of frequency nadir to governor parameters

Parameters	K	T_R	H	F_H	D	R
Min	0.8	4	3	0.1	0	0.03
Max	1.2	11	9	0.35	2	0.08
Sensitivity	0.49	-0.01	0.03	1.35	0.05	-9.14

the time of frequency nadir is strongly sensitive to inertia. From these results, it is assumed in [25] that all of the values of governor time constant for the system governors are identical without losing sufficient accuracy.

Using LFC for the multi-machine system model and assuming that load disturbance is a step function, the frequency deviation can be shown in following equation [25]:

$$\Delta f = \frac{\frac{\Delta P_L}{s}}{D + 2Hs + \sum_{i=1}^{m} \frac{K_i(1+F_iT_Rs)}{R_i(1+T_Rs)}} \tag{3.1}$$

With identical values of T_R for all the system governors, equation (3.1) can be written as [25]:

$$\Delta f = \frac{\Delta P_L}{2HT_Rs} \frac{1 + T_Rs}{s^2 + 2\zeta\omega_n s + \omega_n^2} \tag{3.2}$$

where

$$\omega_n = \sqrt{\frac{1}{2HT}(D + R_T)} \tag{3.3}$$

$$\zeta = \frac{1}{2}\frac{2H + T_R(D + F_T)}{\sqrt{2HT_R(D + R_T)}} \tag{3.4}$$

$$F_T = \sum_{i=1}^{m} \frac{K_i F_i}{R_i} \tag{3.5}$$

$$R_T = \sum_{i=1}^{m} \frac{K_i}{R_i} \tag{3.6}$$

From equation (3.2), the frequency deviation can be expressed as a combination of two terms:

$$\Delta f = \frac{\Delta P_L}{2HT_R s}\frac{1}{s^2 + 2\zeta\omega_n s + \omega_n^2} + \frac{\Delta P_L}{2H(s^2 + 2\zeta\omega_n s + \omega_n^2)} \tag{3.7}$$

Taking the inverse Laplace transform, the time-domain of frequency deviation can be given as:

$$\Delta f = \frac{\Delta P_L}{2HT_R\omega_n^2}(1 - \frac{1}{\sqrt{1-\zeta^2}}e^{-\zeta\omega_n t}\cos(\omega_n\sqrt{1-\zeta^2}t - \phi)) + \frac{\Delta P_L}{2H\omega_n\sqrt{1-\zeta^2}}e^{-\zeta\omega_n t}\sin(\omega_n\sqrt{1-\zeta^2}t) \tag{3.8}$$

where

$$\phi = \tan^{-1}(\frac{\zeta}{\sqrt{1-\zeta^2}}) \tag{3.9}$$

At the frequency nadir, the derivative of frequency deviation equals zero. Hence, the time of frequency nadir and frequency nadir can be derived as [25]:

$$t_{max} = \frac{1}{\omega_n\sqrt{1-\zeta^2}}\tan^{-1}(\frac{\omega_n\sqrt{1-\zeta^2}}{\zeta\omega_n - 1/T}) \tag{3.10}$$

$$\Delta f_{max} = \frac{\Delta P}{R_T + D}(1 + e^{-\zeta\omega_n t_{max}}\sqrt{\frac{T_R(R_T - F_T)}{2H}}) \tag{3.11}$$

From above analysis, the equation of maximum penetration of VER is constructed in the following section.

3.3 The Limit of VER Penetration based on Frequency Security

As indicated in equation (3.11), frequency nadir is a function of inertia and the equivalent regulation constant, which is changed in the presence of VER. In the presence of VER, the system inertia decreases and the equivalent regulation constant increases. Assuming that the reduction in the system inertia when VER replaces the conventional generators is α_{conv}, the inertia that VER contributes to the system is α_{VER} (which can be derived from the output of VER [43]), the new values of system inertia and equivalent regulation constant can be expressed by:

$$H^{new} = H^{old}(1 - \alpha_{conv} + \alpha_{VER}) = \alpha H^{old} \tag{3.12}$$

$$R^{new} = R^{old}/(1 - \alpha_{conv} + \alpha_{VER}) = R^{old}/\alpha \tag{3.13}$$

The new values of H and R are applied to equation (3.11) to get the new value of frequency nadir in the presence of VER:

$$\Delta f_{max} = \frac{\Delta P}{\alpha R_T + D}(1 + e^{-\zeta^{new}\omega_n^{new}t_{max}^{new}}\sqrt{\frac{T(R_T - F_T)}{2H}}) \tag{3.14}$$

where

$$F_T^{new} = \sum_{i=1}^{m} n\frac{K_i F_i}{R_i} = \alpha F_T \tag{3.15}$$

$$R_T^{new} = \sum_{i=1}^{m} \alpha\frac{K_i}{R_i} = \alpha R_T \tag{3.16}$$

$$\omega_n^{new} = \sqrt{\frac{1}{2\alpha H T_R}(D + \alpha R_T)} \tag{3.17}$$

$$\zeta^{new} = \frac{1}{2}\frac{2\alpha H + T_R(D + \alpha F_T)}{\sqrt{2\alpha H T_R(D + \alpha R_T)}} \tag{3.18}$$

To ensure system security, the maximum frequency deviation should not pass the safe limit:

$$\Delta f_{max} \leq \Delta f_s \tag{3.19}$$

With a fixed system configuration, Δf_{max} is a function of only two variables α and ΔP_L. However, it is too complicated to withdraw the allowable maximum changing level of inertia (which shows penetration level of VER) directly based on security condition in equation (3.19). Hence, to examine the change of frequency nadir due to the change in penetration of VER, the approximation technique based on sensitivity analysis is utilized. Let's consider two cases:

Case 1: The load damping equals zero:

When $D = 0$, the new values of w_n and ζ in the presence of VER can be shown as:

$$\omega_n^{new} = \sqrt{\frac{1}{2\alpha H T_R}(\alpha R_T)} = \sqrt{\frac{R_T}{2 H T_R}} \tag{3.20}$$

$$\zeta^{new} = \frac{1}{2}\frac{2\alpha H + \alpha T_R F_T}{\sqrt{2\alpha H T_R \alpha R_T)}} = \frac{1}{2}\frac{2H + T_R F_T}{\sqrt{2 H T_R R_T}} \tag{3.21}$$

As can be seen from equations (3.20) and (3.21), values of ω_n^{new} and ζ^{new} do not change following the change of n and they keep the same values as those without VER. Therefore, the time at frequency nadir t_{max} does not change with α. This makes the change in frequency nadir depend only on the variables n and ΔP_L in the fraction $\frac{\Delta P_L}{\alpha R_T + D}$. Accordingly, the limit of n can be inferred from the frequency deviation limit Δf_s:

$$\alpha_{max} = \frac{\Delta P_L}{\Delta f_s R_T}(1 + e^{-\zeta^{new}\omega_n^{new} t_{max}^{new}}\sqrt{\frac{T_R(R_T - F_T)}{2H}}) \tag{3.22}$$

Case 2: The load damping is different from zero:

Although D is different from zero, the value of D is often much smaller than R_T and F_T when consider equations (3.17) and (3.18). It means that the values of ω_n^{new} and ζ^{new} do not have notable change when changing D. Also, as can be seen from the sensitivity analysis in Table 3.1, the sensitivity of maximum frequency deviation to D (0.05) is much less than that to R (-9.14) and F_H (1.35). Hence, it is possible to ignore load damping without losing significant accuracy. This approximation is more reasonable when consider the exponential term in equation (3.14). Due to the disposition of this exponential function (e^{-x}), its maximum value is 1 and the function approaches zero when the exponential variable x increases. The change in load damping does not have a remarkable impact on the exponential term. Therefore, it is reasonable to approximate the values of ω_n^{new} and ζ^{new} and the limit α_{max} as the case when D equals zero as in equations (3.20), (3.21), and (3.22).

Based on the above theoretical examination, the calculation of the approximation technique and the simulation model of the system are implemented in the following section in order to verify the proposed idea. The results of the simulation are then compared with the results from the approximation technique to evaluate the effectiveness of the method.

3.4 Results from Simulation and Model Approximation

In this section, two test systems - six-bus and IEEE 118-bus are utilized to show the application of the proposed method. The approximation and simulation are implemented to compare the results. The change in VER penetration is expressed by changing the variable α. The disturbance is presented by an increase of load. Assuming that the safe limit of frequency deviation is ± 0.1 Hz [46]. The variable α is reduced by a step size of 0.01 and the application only considers the maximum reduction of 70% ($\alpha = 0.7$) due to reality. Matlab is used as the simulation environment.

3.4.1 Six-bus test system

The six-bus test system is shown in Fig. 3.2 [67]. The system has 3 conventional generators and 2 VER generators. VER generators are installed at buses 4 and 5. The dynamic data of the system is given in Table 3.2 [25]. The load damping value is assumed a value of 0.5. The load disturbance is a step function $u = 2$. The calculation results for VER penetration limit based on the approximation technique and those based on simulation with different levels of VER penetration are shown in Fig. 3.3. The error of the proposed method compared to the simulation results is shown in Fig. 3.4.

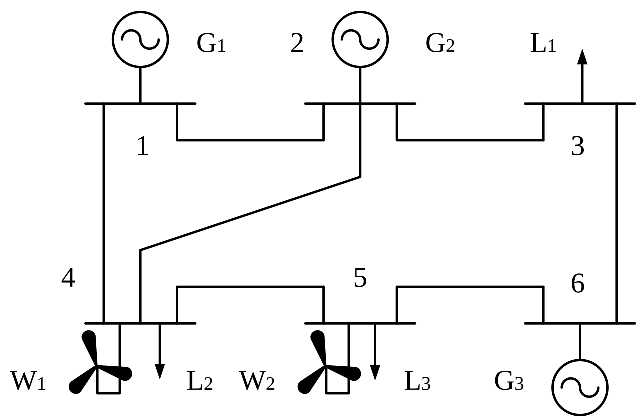

Figure 3.2: Six-bus test system

Table 3.2: Dynamic parameters for six-bus test system

Gen. No.	K	T_R	H	F_H	R
1	0.9	8	7	0.15	0.04
2	0.95	7	5.5	0.35	0.03
3	0.98	9	3.5	0.25	0.03
W1	-	-	0.5	-	-
W2	-	-	0.5	-	-

3.4.2 IEEE 118-bus test system

The IEEE 118-bus test system includes 54 conventional generators and 3 VER generators. The dynamic data of the system is chosen by random numbers within appropriate ranges. The load

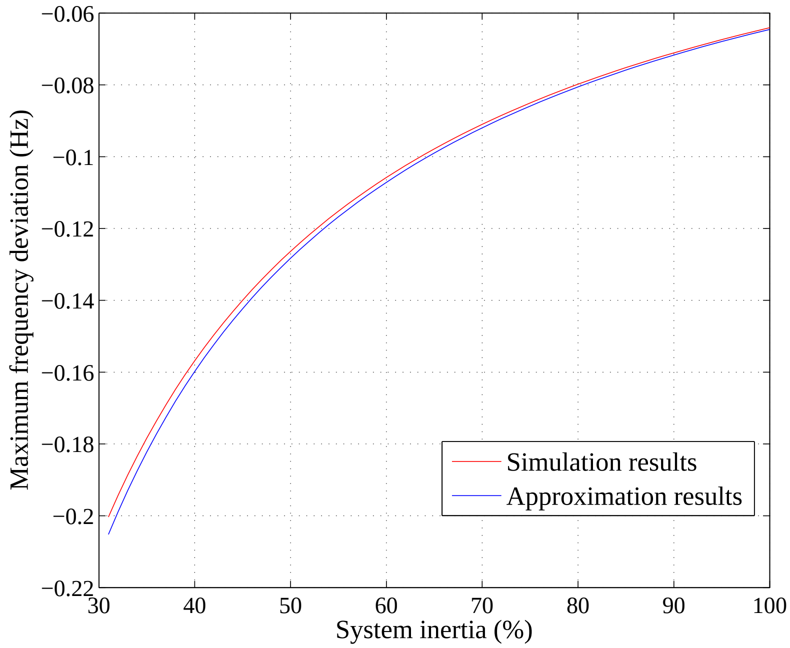

Figure 3.3: Approximation and simulation results of Δf_{max} with the change of system inertia for 6-bus test system

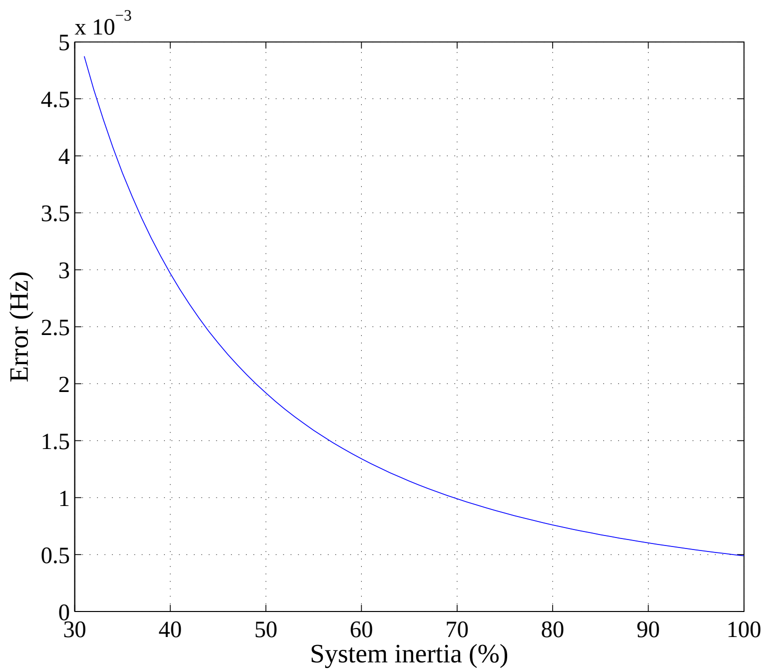

Figure 3.4: Error of the approximation results of Δf_{max} with the change of system inertia for 6-bus test system

damping value is assumed a value of 2. The load disturbance is a step function $u = 35$. The calculation results for VER penetration limit based on the approximation technique and those based on simulation with different levels of VER penetration are shown in Fig. 3.5. The error of the proposed method is shown in Fig. 3.6.

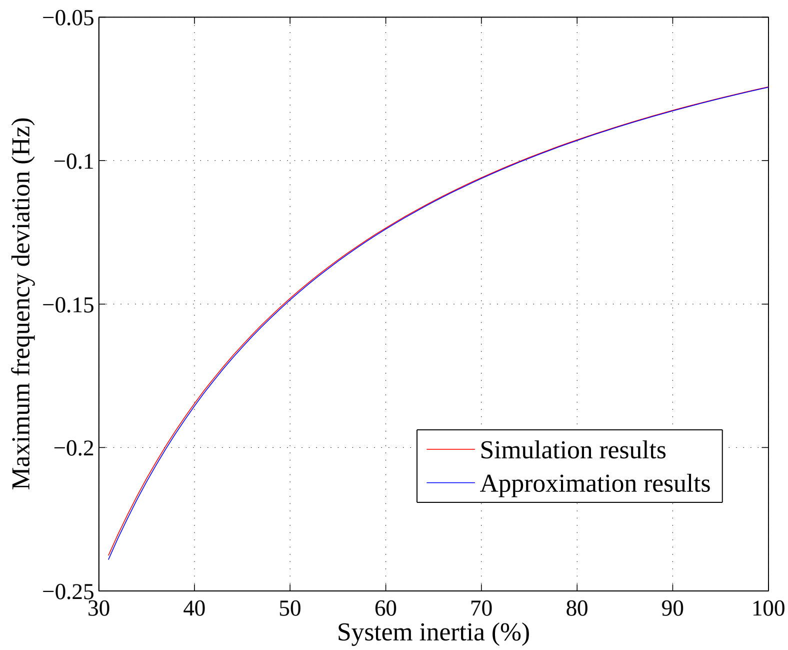

Figure 3.5: Approximation and simulation results of Δf_{max} with the change of system inertia for 118-bus test system

From the results, a few observations can be made:

1. From the frequency nadir results for two test systems, it can be seen that the results of the proposed method are close to the results obtained from the simulation, which are shown in Fig. 3.3 and Fig. 3.5. The error of the approximation and simulation shown in Fig. 3.4 and Fig. 3.6 is relatively small. Although the results are approximated, the calculation and simulation shows that the results are reliable. This confirms the effectiveness of the approximation used in the proposed method.

2. As can be seen in figures 3.3, 3.4, 3.5, and 3.6, when the inertia decreases (the VER penetration level increases), the error increases. The reason for this is when VER penetration

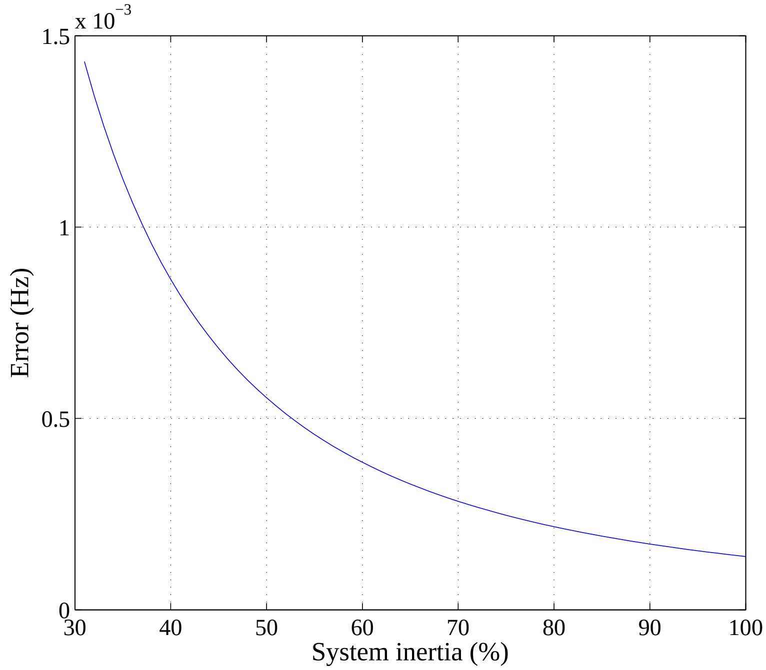

Figure 3.6: Error of the approximation results of Δf_{max} with the change of system inertia for 118-bus test system

increases, the regulation constant increases which reduces R_T and F_T. When R_T and F_T decrease, the domination of them to load damping factor decreases, which in turn increases the error.

3. The simulation results for the 6-bus test system show that if the maximum load disturbance of the system is 2 MW, the maximum system inertia reduction which ensures frequency security is 37% while the approximation gives the results of 36%. The error in this case is small (1%) and the accuracy of the proposed method is acceptable.

4. The simulation results for the IEEE 118-bus test system show that if the maximum load disturbance of the system is 35 MW, the maximum system inertia reduction which ensures frequency security is 27% while the approximation also gives the results of 27%. The error in this case is very small ($\approx 0.025\%$) compared to the 6-bus test system due to the high number of conventional generations (which increases system inertia H and constant R_T).

5. From the inertia reduction and maximum load disturbance, it is possible to determine the maximum penetration level of VER. Although the proposed method provides conservative results, it still has a relatively high accuracy with the advantage of fast calculation. Unlike the previous methods in the literature, this method has advantage of avoiding the linearization.

The maximum penetration level of VER obtained from the security criterion should be combined with other criteria such as voltage stability, thermal limit, network congestion, fault-ride through capability, etc. to determine the final penetration level of VER while ensuring the safe operation of the system. Supporting technologies such as energy storage can enable more VER to be integrated into the grid.

3.5 Conclusion

This chapter presents the approximation method to estimate the maximum penetration level of variable energy resources to the power system based on the system frequency security criterion. Although the method does not provide completely precise results, the approximated results are relatively close to the simulation results with a small error. This method is helpful in providing a fast technique for system operators to decide the maximum penetration level of VER, which is useful in generation dispatch. The proposed method's validity has been investigated and supported with a detailed mathematical analysis and simulation. Approximation and simulation results confirm the proposed model's effectiveness. The prediction of the maximum load disturbance and the total inertia that VER can provide to the grid based on its output should be examined carefully to increase the effectiveness of the proposed method.

Chapter 4

Reliability of Wind Generation Considering the Impacts of Uncertainty and Low Inertia

4.1 Introduction

Modeling of wind generation in power system reliability has been amply addressed in previous works, using both analytical and state sampling methods. In [68–70], the probabilistic models for wind power and their use in reliability studies of wind-integrated systems were investigated. In prior work, detailed probabilistic models of wind farms or wind turbines have been developed, which have considered different wind regimes, spatial wind speed correlation, wake effects [71–73], the correlation between turbine outputs [74, 75], and a large number of wind turbines [76]. A method to determine the equivalent capacity of a wind farm using Monte Carlo simulation is presented in [77]. State sampling has also been used to evaluate the reliability indexes of a wind farm [78, 79], and of the integrated system [80, 81]. Transmission constraints have also been taken into account when evaluating the reliability of a system with large-scale wind power [82].

However, the research reported in the literature does not simultaneously capture the effects

The content of this chapter has been reproduced with permission from *Nga Nguyen and Joydeep Mitra, Reliability of Power System with High Wind Penetration under Frequency Stability Constraint, IEEE Transactions on Power System, May 2017.*

of intermittency and low inertia on system reliability. As a variable and low inertia source of power, wind generation causes technical challenges such as the generation reserve requirement [83], frequency deviation [84, 85], transmission violation [12, 86] and voltage instability [87, 88]. The reduction in frequency response due to the increase of variable generation has been reported by the North American Electric Reliability Corporation (NERC), Electric Reliability Council of Texas (ERCOT) and Western Interconnect (WECC) [5,7,8]. These challenges limit the penetration level of wind generation. Only as much wind power should be injected as can be tolerated by the system while preserving stability. Therefore, the availability of wind generation in power system reliability modeling must be evaluated considering stability requirements.

The work presented in this chapter extends the prior art by adding the following contributions: (i) it proposes an improved reliability modeling of wind generation which considers the impacts of wind intermittence and low inertia; (ii) it presents a direct, analytical method, based on discrete convolution, to evaluate the system reliability in the presence of wind generation.

Due to the system stability requirement, the traditional reliability model of wind farms is modified. The improved reliability model is developed based on the following two criteria:

- The wind generators are required to operate below their available output power to ensure that they have the ability to provide reserve for frequency regulation [89, 90].
- Wind generation has low inertia, which negatively affects the stability of the system [43, 84]. Therefore, wind penetration is limited to ensure system frequency stability.

Since all of the available output power of wind generation cannot be accepted by the system, the reliability of the grid is affected.

The proposed approach is tested on the modified IEEE-RTS 79 system. The reliability indexes are calculated with and without the frequency stability constraint. The results show how the inclusion of the stability constraint impacts the system reliability.

The remainder of this chapter is organized as follows. Section 4.2 explains the reliability model of a wind farm with impacts of the intermittence and low inertia characteristics of wind generation.

The discrete convolution model for evaluating the reliability of power system with wind farms is also included. Simulation results that compare the models with and without considering the effects of wind intermittence and low inertia are presented in section 4.3. In this section, some observations are also included to clarify the salient aspects of the contribution. Finally, section 4.4 provides some concluding remarks on the work presented.

4.2 Reliability of the Integrated System Considering the Impacts of Intermittence and Low Inertia

The integrated system is modeled as a combination of multiple conventional generators and wind farms. The reliability of an integrated system is evaluated using the following 3 steps:

- Calculating the individual probabilities and frequency of all power outage states for each wind farm.
- Modeling the impacts of intermittence and low inertia of wind generation on the system frequency stability to modify the reliability indexes of wind farms.
- Calculating the reliability of the integrated system using discrete convolution under the stability constraints.

The details of each step are presented below.

4.2.1 Modeling of Wind Farm

4.2.1.1 Modeling of wind speed

To estimate the system reliability, wind speed is approximated by the discrete Markov process (Markov chains) with a finite number of states [71, 73]. An exemplar of wind speed model with n states is shown in Fig. 4.1. This model reflects the probability, the frequency and the duration attributes of wind speed. It is assumed that the wind speed is statistically stationary. The transitions between wind speed states and wind turbine states are independent and the transitions between all states are considered. To estimate the wind model parameters, the exponential distribution or the sample adjustment can be used [71]. In this project, a realization or a sample path of the wind speed is used to estimate the probability, the frequency and transition rate of each wind state. Since the total number of samples is very large (long realization), the probability can be estimated as follows [71]:

$$p_{c,i} = \frac{\sum_{j=1}^{N} n_{ij}}{\sum_{k=1}^{N} \sum_{j=1}^{N} n_{kj}} \tag{4.1}$$

where $p_{c,i}$ is the probability of wind being in state i, n_{ij} is the number of transitions from state i to state j, and N is the number of states.

The transition rate between any two states is calculated based on frequency balance between them as follows [71]:

$$\rho_{i,j} = \frac{N_{ij}}{D_i} \tag{4.2}$$

where N_{ij} is the number of transitions from state i to state j and D_i is the duration of state i.

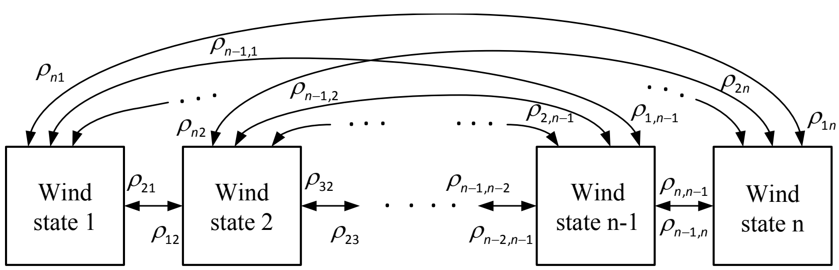

Figure 4.1: Wind speed model with n states.

4.2.1.2 Modeling of wind turbine output

The output power of a wind turbine depends on two factors: wind speed and turbine availability. The non-linear relationship between wind power output and wind speed is shown in Fig. 4.2 and equation (4.3) [91].

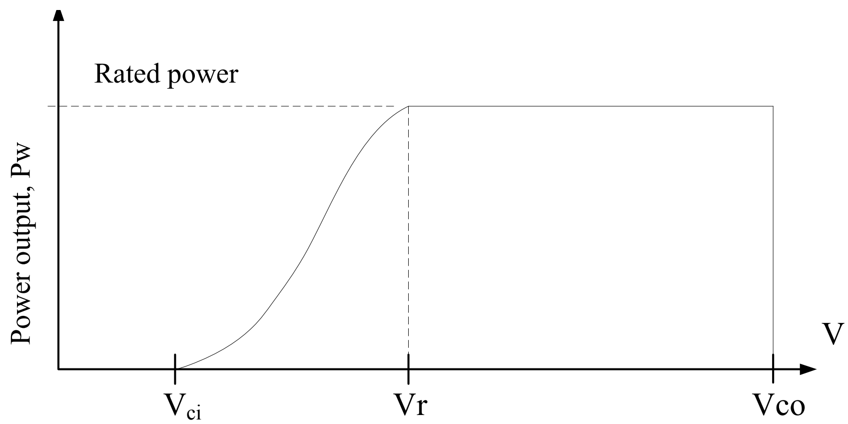

Figure 4.2: Wind power output and wind speed relationship.

$$P_w = \begin{cases} 0 & 0 \leq V \leq V_{ci} \\ (A + B \times V + C \times V^2)P_r & V_{ci} < V \leq V_r \\ P_r & V_r < V \leq V_{co} \\ 0 & V_{co} < V \end{cases} \tag{4.3}$$

where V_{ci}, V_{co}, V_r, P_r are the cut-in, cut-out, rated speed, and rated power of the wind turbine, respectively. The constants A, B, and C are as follows [75]:

$$A = \frac{1}{(V_{ci} - V_r)^2}[V_{ci}(V_{ci} + V_r) - 4(V_{ci}V_r)\frac{(V_{ci} + V_r)^3}{2V_r}]$$
$$B = \frac{1}{(V_{ci} - V_r)^2}[4(V_{ci} + V_r)\frac{(V_{ci} + V_r)^3}{2V_r} - (3V_{ci} + V_r)]$$
$$C = \frac{1}{(V_{ci} - V_r)^2}[2 - 4\frac{(V_{ci} + V_r)^3}{2V_r}]$$

4.2.1.3 Modeling of wind farm capacity outage

The model of wind farm output is the combination of wind speed model and wind turbine model. In the wind turbine model, the wind turbine availability is represented by a binary state component (the turbine is in service or out of service) which is similar to the conventional generators. While considering the wind farm output model, some assumptions have been made:

- All the turbines in a wind farm are approximately subject to the same wind speed. Because of the consistent behavior of wind turbines with the wind speed variation on the entire wind farm, similar wind turbines have similar outputs with some deviation [92] and their average outputs are approximately equal.
- All the turbines have the same failure rate λ_t and repair rate μ_t.
- All the states with the same output power are combined into one state.

As discrete convolution will be used later to calculate reliability of the integrated system, the model of wind farm output only considers the individual probability for each outage power state of the wind farm and its frequency to the lower outage capacity states. Also, all the transitions among wind states are considered, which is more appropriate than the birth and death Markov chain. This method is more convenient than previous methods as this method reduces the computational burden of calculating the transition frequencies of states to higher outage capacity states, since the required frequencies can be obtained just by considering transitions to lower outage capacity states. The model of wind farm outage is shown in matrix form in Fig. 4.3. In this figure, the capacity outage corresponding to each state is shown; these will be duly used in performing the discrete convolution. It should be noted that only the transitions from one state to other states with lower capacity outages are shown. The reason is that only these transitions are necessary when calculating the individual probability and frequency of wind farm states to other states with lower capacity outages.

In Fig. 4.3, m is number of wind turbines, G_j is the output of a single turbine at wind state j, and the transitions between non-adjacent states are not shown for the sake of clarity.

The capacity outage of each state can be represented as:

$$C_{i,j} = mG_N - (m - i + 1)G_j \tag{4.4}$$

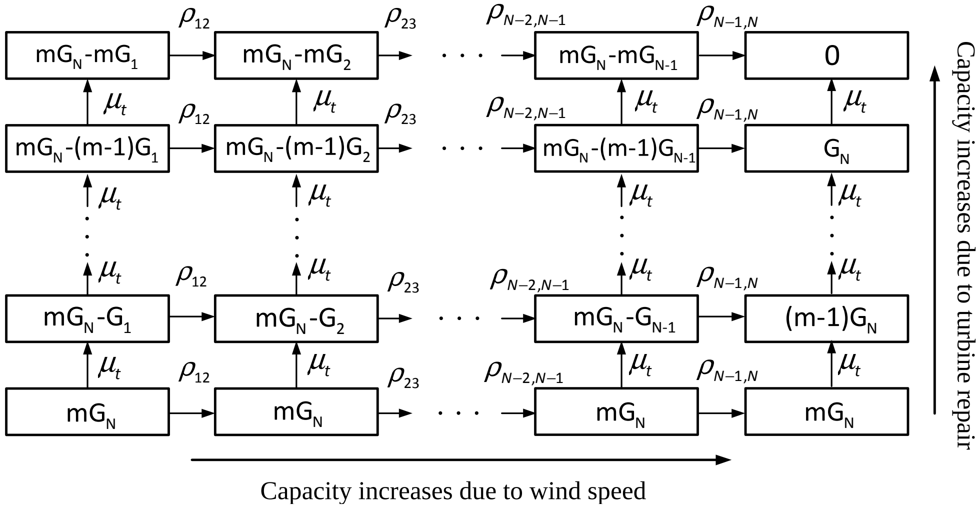

Figure 4.3: State transition diagram for wind farm (transitions between non-adjacent states are not shown in order to reduce clutter).

The individual probability of each outage state in Fig. 4.3 is calculated as follows:

$$p_{i,j} = p_{tb,i} p_{c,j} \tag{4.5}$$

where $p_{tb,i}$ is the probability of all wind turbines at state (i, j) and is calculated as follows:

$$p_{tb,i} = C_m^{m-i+1} p_u^{m-i+1} p_d^{i-1} \tag{4.6}$$

where p_u and p_d are the probabilities of a wind turbine being up and down, respectively. C_m^{m-i+1} is the combination of m turbines taken $m - i + 1$ at a time.

The individual jumping frequency to the lower capacity outage states of each outage state in Fig. 4.3 is calculated as follows:

$$f_{i,j} = p_{i,j} \sum \rho_{i,j}^{+} \tag{4.7}$$

where $\rho_{i,j}^{+}$ is the transition rate of state (i, j) to other states with lower capacity outages.

After grouping all states with the same capacity outages into one state, the probability of a capacity outage X and its frequency to the lower outage capacity is calculated as follows:

$$P_r(X) = \sum_{i,j} p_{i,j}(X) \tag{4.8}$$

$$\beta^{+}(X) = \frac{\sum_{i,j} f_{i,j}(X)}{P_r(X)} \tag{4.9}$$

If the impact of wind intermittence and low inertia is not considered, the results of wind farm probability and frequency can be used to combine with conventional generators to estimate the reliability of the system. However, this method is only appropriate when the level of wind penetration is low. When wind integration is high, the frequency stability of the system is negatively affected. Hence, it is necessary to consider the impact of wind intermittence and low inertia to ensure the system stability while system reliability is calculated.

4.2.2 Modeling the Impact of Wind Intermittence and Low Inertia

Due to its well-known uncertainty characteristics, wind power causes problems in maintaining the system frequency. In the presence of wind, the frequency disturbance gets worse in both density and magnitude. As required by power system standards, the frequency deviation must remain within the safe limits. To ensure the frequency security, several methods have been proposed. As described in [89, 90], the reserve requirement is mandatory for the wind turbine to support frequency regulation. The wind generators have to operate below their available output power to ensure that they have the ability to provide reserve for frequency regulation. The reserve requirement is implemented in wind generators by Delta control. The idea behind this control is to maintain a certain amount of power reserve so that the wind generators have the ability to respond and alter their outputs quickly both with positive and negative power ramps. As a result, the total available wind power might not be absorbed completely into the system. Because of the reserve requirement, the contribution of wind power to the reliability of the system reduces due to the decrease in injected wind power.

Besides the uncertainty, one of the drawbacks of wind is that wind turbines have very low inertia compared to that of conventional generators. This property of wind also introduces negative effects on the frequency regulation when wind generators replace conventional generators—larger frequency deviation and longer restoration time [43]. These negative effects become more adverse if the penetration of wind power increases [7, 8]. Due to the negative effect of wind on system frequency, the amount of wind that can be injected into the system is limited to ensure system stability.

The method to estimate the penetration limit of wind power has been presented in chapter 3. The most two important equations are repeated here for convenience.

The equation of maximum frequency deviation in the presence of VER is shown as follows:

$$\Delta f_{max} = \frac{\Delta P}{nR_T + D}(1 + e^{-\zeta^{new}\omega_n^{new}t_{max}^{new}}\sqrt{\frac{T(R_T - F_T)}{2H}}) \tag{4.10}$$

To ensure system security, the maximum frequency deviation should not pass the safe limit:

$$\Delta f_{max} \leq \Delta f_s \tag{4.11}$$

The limit of inertia reduction is as follows:

$$\alpha_{max} = \frac{\Delta P_L}{\Delta f_s R_T}(1 + e^{-\zeta\omega_n t_{max}}\sqrt{\frac{T_R(R_T - F_T)}{2H}}) \tag{4.12}$$

Based on the limit of inertia reduction, the maximum amount of wind integrated into the system is defined.

Previous work evaluating the reliability of a power system in the presence of wind considers all of the available wind output in the reliability model. However, in view of the two problems mentioned before that affect the amount of integrated wind power, the traditional reliability model of the system with wind power should be re-evaluated. The real amount of wind power injected into the system is lower than the available wind output, which means that the reliability of the system is negatively affected.

4.2.3 Capacity Outage Probability and Frequency Table

While combining the wind turbine model with the wind speed model, wind generation is treated as a generator with multiple derated states. The Unit Addition Algorithm with discrete convolution is utilized to build a Capacity Outage Probability and Frequency Table (COPAFT) [93]. The COPAFT of the integrated system which includes conventional generators and wind generators is built as follows:

4.2.3.1 Build COPAFT for all conventional generators

Each conventional generator is modeled as a two-state unit. The cumulative probability of a capacity outage stage of X MW after adding a unit of capacity C MW is as follows [93]:

$$P(X) = \sum_{i=1}^{2} P'(X - C_i)p_{cv,i} \tag{4.13}$$

where $P(X)$ is the "new" cumulative probability of the capacity outage state X MW and $P'(X - C_i)$ is the "old" cumulative probability of the capacity outage state $X - C_i$ MW. If $X \leq C_i$ then $P'(X - C_i) = 1$. $p_{cv,i}$ is the individual probability of the conventional generator with the capacity outage C_i.

The cumulative frequency $F(X)$ for a forced outage of X MW is given as follows [93]:

$$F(X) = \sum_{i=1}^{2} F'(X - C_i)p_{cv,i} + (P'(X - C_2) - P'(X))p_{cv,2}\mu_{cv} \tag{4.14}$$

where μ_{cv} is the repair rate of conventional generator. If $X \leq C_i$ then $F'(X - C_i) = 0$

4.2.3.2 Including wind farms

As mentioned in the previous section, wind farms are modeled as multi-state generators. Each capacity outage level is associated with a probability and frequencies of transitions to higher or lower outage levels; however in this analysis we consider only the transitions to lower outage levels for frequency calculation, since the system is considered to be frequency balanced.

The cumulative probability and frequency of the capacity outage state X MW is calculated as follows:

$$P(X) = \sum_{i=1}^{N} P'(X - C_{w,i}) P_{r,i} \tag{4.15}$$

$$\begin{aligned} F(X) = &\sum_{i=1}^{N} F'(X - C_{w,i}) P_{r,i} + \sum_{i=1}^{N-1} (P'(X - C_{w,i+1}) - P'(X - C_{w,i})) P_{r,i+1} \beta_{i+1}^{+} \\ &+ (P'(X - C_{w,N}) - P'(X - C_{w,1})) P_{r,N} \beta_{N}^{+} \end{aligned} \tag{4.16}$$

As can be seen from equations (4.15) and (4.16), the equations (4.13) and (4.14) are special cases of equations (4.15) and (4.16) with $N = 2$. This means that the conventional generator can be regarded as a special case of a multi-state unit where the number of states equals 2.

The probability calculations are easy to understand. The frequency calculations may be understood as follows. Consider adding a two-state unit of capacity C to an existing COPAFT with states $x_1, x_2, \cdots$. Fig. 4.4 shows the states created as a result of adding the two-state unit.

The first column shows the outage states prior to the addition of the new unit, and the second column shows the new outage states created. The set of states inside the polygon is described by $\{C_O \geq x_i\}$. In the steady state, the frequency of encountering the set is equal to the frequency of exiting the set [93]. This frequency can therefore be computed as:

$$F(C_O \geq x_i) = F_i P_{r,1} + F_j P_{r,2} + (P_j - P_i) f_{12} \tag{4.17}$$

where the first two terms result from the changes in states of units other than the unit being added, while the last term results from a change in the state of the unit being added.

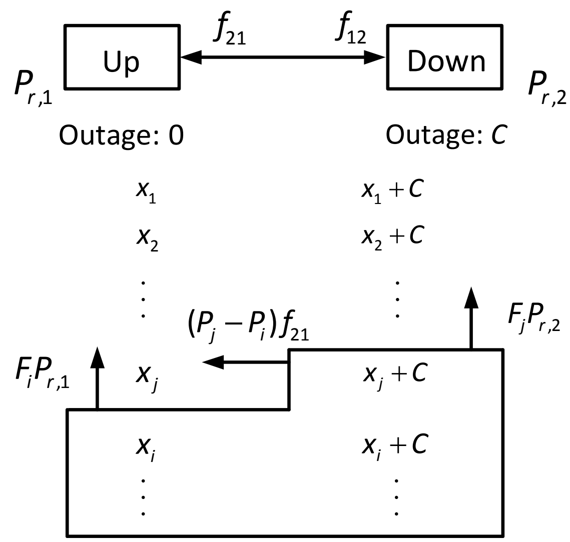

Figure 4.4: State frequency diagram for a two-state unit.

When this concept is extended to the addition of wind farms as multi-state units, the state frequency diagram assumes the form shown in Fig. 4.5, and the general form shown in (4.16) is used to calculate cumulative frequencies.

From above analysis, the COPAFT of the integrated system is constructed to estimate system reliability.

4.3 Results and Discussion

The proposed approach is tested on the modified IEEE-RTS system with 43 identical wind farms. The original system includes 32 conventional generators with a total capacity of 3405 MW. The modified IEEE-RTS system has 26 conventional generators and 43 identical wind farms. Each wind farm has 10 wind turbines, each with 8 MW rated power. The data for IEEE-RTS system can be found in [94]. The inertia data of IEEE-RTS system is shown in Table 4.1 [94]. The reliability of the system is evaluated for two cases: i) considering and ii) neglecting the impacts of wind intermittence and low inertia. The total rated power of the wind turbines is 3440 MW. This wind generation replaces six conventional generators with a total capacity of 860 MW. The replaced conventional generators include four 76 MW coal generators at bus 1 and 2, one 155

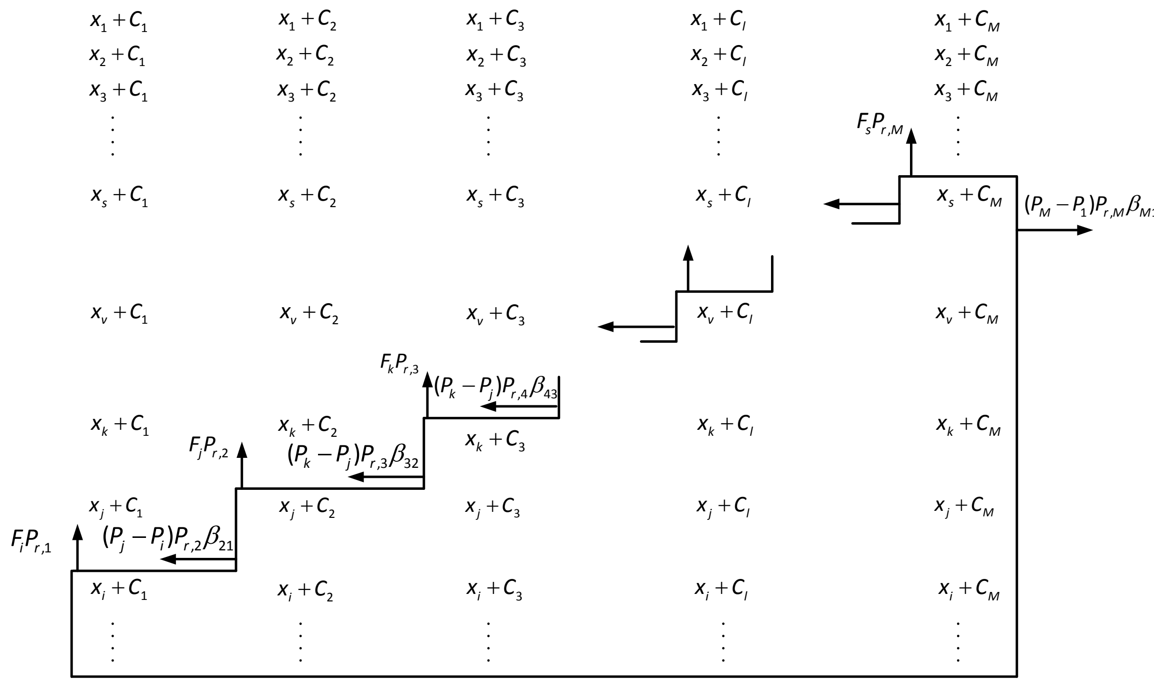

Figure 4.5: State frequency diagram for a multi-state unit.

MW coal generator at bus 15, and one 400 MW nuclear generator at bus 21. As wind generation does not always operate at its rated power, the total rated wind generation is chosen so that the amount of replaced conventional generation equals 25% of the total rated wind capacity. The wind data is extracted from [95] which is provided by National Renewable Energy Laboratory (NREL). Available data are collected over ten minutes periods. However, the data is clustered into one hour periods. The wind turbines are considered with the mean time to failure and the mean time to repair of 3600 hours and 150 hours, respectively. The cut-in, rated and cut-out speeds are 4, 12, and 25 m/s, respectively.

Considering one-hour intervals, the annual wind speed is represented by eight states with a step size equal to 1 m/s. This is because some of the states were combined together since they produce identical power (states 1– 6 produce 0 MW and states 12 – 25 produce 8 MW). Therefore, each wind turbine is treated as an eight-state unit. The transition rates among the eight states are shown in Table 4.2.

Four scenarios will be investigated to show the effect of the intermittence and low inertia of

Table 4.1: System inertia data

Unit group	U_{12}	U_{20}	U_{50}	U_{76}	U_{100}	U_{155}	U_{197}	U_{350}	U_{400}
Unit size (MW)	12	20	50	76	100	155	197	350	400
Inertia (MJ/MW)	0.34	0.56	1.75	2.28	2.80	4.65	5.52	10.5	20

Table 4.2: Transition rates between wind speed states

State	1	2	3	4	5	6	7	8
1	0.799	0.119	0.048	0.019	0.008	0.004	0.001	0.002
2	0.319	0.3	0.228	0.104	0.034	0.004	0.007	0.003
3	0.121	0.212	0.346	0.198	0.083	0.025	0.01	0.005
4	0.037	0.085	0.212	0.314	0.251	0.069	0.019	0.013
5	0.017	0.023	0.09	0.193	0.359	0.223	0.074	0.022
6	0.005	0.006	0.026	0.091	0.226	0.361	0.213	0.073
7	0.004	0.004	0.008	0.021	0.084	0.221	0.371	0.287
8	0.001	0.001	0.001	0.004	0.011	0.036	0.101	0.846

wind generation on system reliability:

Scenario 1: The effects of intermittence and low inertia of wind generation are not considered.

When the variability and inertia impacts are neglected, all the available wind output is integrated into the grid. The capacity outage of a wind turbine for each wind state and its probability are shown in Table 4.3. For simplicity, the output of wind turbine is approximated to the closest integer. Based on the data provided in Table 4.2, 4.3 and applying the proposed method, the COPAFT for a wind farm with 10 wind turbines is constructed and shown in Table 4.4. The reliability indexes of the integrated system are calculated and shown in Table 4.5 for comparison with other scenarios.

Scenario 2: In this case, the spinning reserve requirement is considered.

Considering the spinning reserve requirement, the wind generators have to operate at the lower level of its available power output. Assuming that the spinning reserve requirement of wind generation is 15% of wind available output, the wind power that integrates into the system reduces. As a result, the reliability of the system becomes worse. The comparison of available wind power and real wind power that integrates into the system for 100 hours can be seen in Fig. 4.6. The capacity outage of a wind turbine for each wind state and its probability are shown in Table 4.3. The COPAFT for a wind farm with reserve requirement is constructed and shown in Table 4.4. The reliability indexes of the integrated system are calculated and shown in Table 4.5.

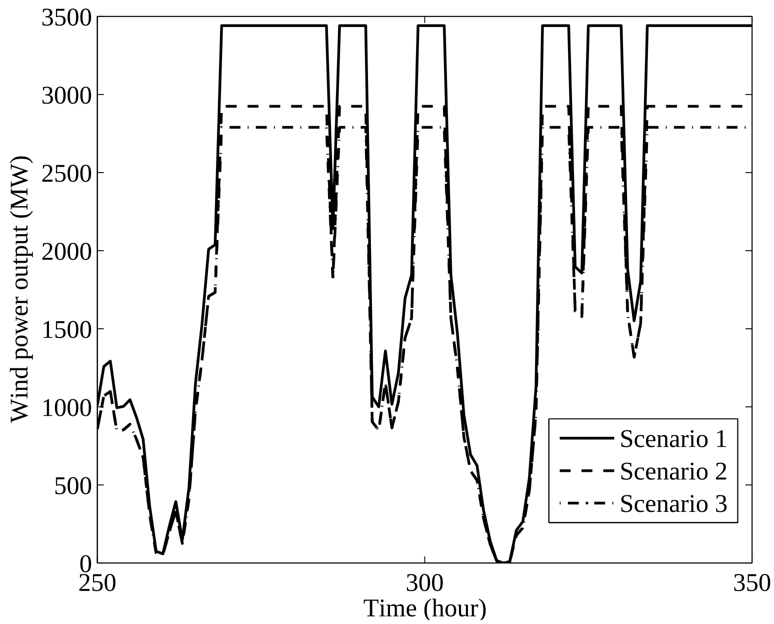

Figure 4.6: Available wind output and integrated wind output for the scenarios.

Scenario 3: In this case, both the spinning reserve requirement and the limit of wind penetration due to frequency security are considered.

Considering the impact of stochasticity and low inertia of wind on the frequency, the integrated wind power must be limited. This limit is implemented by the constraint of reduction of inertia as presented in the previous section. The dynamic parameters of the conventional generators are chosen within appropriate ranges which are shown in Table 3.1 [25]. The inertia of each wind farm is smaller than that of a conventional generator and can be chosen as 0.25 pu. The load damping value of the system is assumed a value of 2. Load disturbance is simulated by a 0.1 pu step function. The maximum frequency deviation is compared with the safe limit of frequency deviation ± 0.1 Hz [46] to define how much wind generation should be integrated into the main grid. Applying the data of the system dynamics to equation (4.12), the maximum reduction of inertia of the system is found to be 18.2%. As the inertia of wind power is considered, the maximum penetration limit of wind generation is 2792 MW to ensure the system frequency security. Therefore, only 705 MW of conventional generation can be replaced. This condition is combined with the spinning requirement of wind to give the real allowable integrated wind power. The comparison of available wind power with real wind power that integrates into system, considering both spinning reserve requirement and frequency security condition for 100 hours, can be seen in Fig. 4.6.

Scenario 4: In this case, large-scale energy storage is considered, to improve the reliability of the wind-integrated system. With large wind penetration, the operation of the wind generation and energy storage should be coordinated [96, 97]. The principle of this coordination is that the surplus hourly wind power, which has not been integrated into the main grid due to system stability requirement, will be stored. The work in this chapter will add to the method presented in [97] by considering frequency stability as the system stability requirement. The improved coordination is stated as follows.

If the available wind power is less than the wind integration limit, then the stored energy can be used to supply the load. However, the stored energy can be discharged if the available wind power is greater than the wind integration limit, and the power from conventional generation is less than the difference between the load and the wind integrated limit. In other words, the wind generation, the conventional generation, and the energy storage are all coordinated to meet the system demand. Assuming that the integration limit of wind is P_{li}, the time series representing the energy storage state is calculated as follows:

$$E_{t+1} = \begin{cases} E_t + (P_{w,t} - P_{li}) \times \Delta t & P_{w,t} \geq P_{li} \text{ and } P_{c,t} \geq P_L - P_{li} \\ E_t + (P_{c,t} - P_L + P_{li}) \times \Delta t & P_{w,t} \geq P_{li} \text{ and } P_{c,t} < P_L - P_{li} \\ E_t + (P_{w,t} - P_{li}) \times \Delta t & P_{w,t} < P_{li} \\ E_t & \text{otherwise} \end{cases}$$

where $P_{w,t}$ and $P_{c,t}$ are total power generation of the wind farms and the conventional generators at time t. The charging and discharging rate is considered linear using a 5-hour discharging period.

The maximum energy by which the storage can charge and discharge in a time interval Δt is $(E_{max} - E_{min})/5 \times \Delta t$ where E_{max} and E_{min} are the maximum and minimum capacity of the storage [97]. The minimum storage capacity is assumed to be 20% of the maximum capacity.

In this scenario, an energy storage system with maximum capacity of 30 MW each is installed at each wind farm to improve the system reliability. Both the spinning reserve requirement and the limit of wind penetration due to frequency security are included.

4.3.1 Results

The capacity outage of a wind turbine for each wind state and its probability are shown in Table 4.3. The COPAFT for a wind farm, considering the reserve requirement and the frequency security, is constructed and shown in Table 4.4. The reliability indexes of the original IEEE-RTS system and the augmented IEEE-RTS system considering the spinning reserve requirement, the limit of wind penetration due to frequency security, and the energy storage are calculated and shown in Table 4.5. It should be noticed that the capacity outages of three scenarios are different as shown in Table 4.4. The reason for this difference is that due to the frequency stability, some states with the high level of wind integration is removed (the system cannot absorb these high levels of wind generation and maintain stability). Because spinning reserve requirement and the limit of wind penetration due to frequency security are considered in both scenario 3 and 4, the results for scenario 3 in Table 4.4 will be utilized for scenario 4.

From the simulation results, it is clear that the operating conditions (spinning reserve requirement, frequency security) have a negative effect on the reliability of the integrated system. In the presence of these conditions, all the reliability indexes deteriorate. When wind power replaces the conventional generators, the Loss of Load Probability (LOLP) increases from 0.0012 to 0.002. The LOLP gets worse when considering spinning reserve requirement (0.0055) and frequency security (0.0084). As LOLP increases, the Loss of Load Expectation (LOLE = LOLP $\times$ 8760) also increases (from 9.369 to 17.52, 48.18, and 73.584 hours/year (h/y)). Due to the integration of wind, the Loss of Load Frequency (LOLF) increases from 2.016 failures/year (f/y) in the base case to

Table 4.3: The capacity outages and probabilities of a wind turbine for the first three scenarios

Scenario 1		Scenario 2		Scenario 3	
C_{O1}	$P_{r,i}$	C_{O2}	$P_{r,i}$	C_{O3}	$P_{r,i}$
8	0.212	8	0.212	8	0.212
6.8945	0.08	7.1156	0.08	7.1156	0.08
6.0977	0.092	6.47816	0.092	6.47816	0.092
5.082	0.09	5.6656	0.09	5.6656	0.09
3.899	0.104	4.7192	0.104	4.7192	0.104
2.4794	0.096	3.58352	0.096	3.58352	0.096
0.8758	0.0882	2.30064	0.0882	2.45	0.326
0	0.2378	1.6	0.2378		

9.636 f/y. In scenarios 2 and 3, LOLF is even worse with 26.28 and 37.668 f/y, respectively. A similar situation occurs when investigating Expected Demand not Severed (EDNS) and Loss of Energy Expectation (LOEE). EDNS increases from 0.1641 MW/year (MW/y) to 0.2190, 0.5840, 0.9125 MW/y in scenarios 1, 2, and 3, respectively. Due to the degradation of EDNS, LOEE increases accordingly. In scenario 4, the system reliability is improved due to the assistance from the energy storage as shown in Table 4.5. The reason for the deterioration is as follows.

- In the first scenario, the integration of wind power with a lower reliability level compared to the conventional generators causes the decrease of the integrated system reliability. The more wind power with a low reliability level, the worse the reliability.

- In the second scenario, the spinning reserve requirement makes the available wind power, which will dispatch to the main grid, to decrease (15%). This reduction in turn causes decrease in the system reliability. Since the idea behind this requirement is to maintain a certain amount of power reserve so that the wind generators have the ability to respond and alter their outputs quickly with power ramps, an increase in the reserve requirement causes the injected wind power and the system reliability to decrease further and vice versa.

- When both spinning reserve requirement and frequency security are considered in the third scenario, the amount of wind power accepted by the system is limited due to the violation of

Table 4.4: The probability and frequency of a wind farm with 10 wind turbines

State	Scenario 1			Scenario 2			Scenario 3		
	C_{O1}	$P_{r,i1}$	β_1^+	C_{O2}	$P_{r,i2}$	β_2^+	C_{O3}	$P_{r,i3}$	β_3^+
1	0	0.1581	0	12	0.1581	0	16	0.1581	0
2	8	0.0659	0.0067	19	0.1245	0.1388	22	0.0659	0.0067
3	9	0.0586	0.2872	25	0.0244	0.2939	23	0.0586	0.2872
4	16	0.0368	0.1974	26	0.0124	0.0067	29	0.0368	0.1974
5	23	0.0046	0.2939	32	0.006	0.2277	34	0.0046	0.2939
6	24	0.0014	0.0067	33	0.0635	0.2856	35	0.0014	0.0067
7	25	0.0635	0.2856	38	0.027	0.2923	36	0.0635	0.2856
8	30	0.027	0.2923	39	0.0001	0.0067	40	0.027	0.2923
9	32	0.0001	0.0067	42	0.005	0.2923	42	0.0001	0.0067
10	36	0.005	0.2923	45	0.0689	0.3183	45	0.005	0.2923
11	39	0.0689	0.3183	47	0.0006	0.2923	47	0.0689	0.3183
12	41	0.0006	0.2923	49	0.0287	0.325	49	0.0006	0.2923
13	43	0.0287	0.325	52	0.0054	0.3247	50	0.0287	0.325
14	47	0.0054	0.3247	55	0.0601	0.3522	54	0.0054	0.3247
15	51	0.0607	0.3519	56	0.0006	0.325	57	0.0607	0.3519
16	54	0.025	0.3589	58	0.025	0.3589	59	0.025	0.3589
17	57	0.0047	0.3589	60	0.0047	0.3589	61	0.0047	0.3589
18	60	0.0005	0.3589	63	0.0005	0.3587	64	0.0005	0.3587
19	61	0.0612	0.321	64	0.0612	0.321	65	0.0612	0.321
20	63	0.0255	0.3277	65	0.0256	0.3277	66	0.0256	0.3277
21	65	0.0048	0.3277	67	0.0048	0.3277	68	0.0048	0.3277
22	67	0.0005	0.3277	69	0.0005	0.3277	69	0.0005	0.3277
23	69	0.0531	0.3806	71	0.0531	0.3806	71	0.0531	0.3806
24	70	0.0221	0.3873	72	0.0263	0.3862	72	0.0221	0.3873
25	71	0.0041	0.3873	73	0.0005	0.3873	73	0.0041	0.3873
26	72	0.0005	0.3873	80	0.2124	0.2005	74	0.0005	0.3873
27	80	0.2124	0.2005				80	0.2124	0.2005

Table 4.5: The reliability indexes of the augmented IEEE-RTS system for four scenarios

Index	LOLE h/y	LOLF f/y	LOLP	EDNS MW/y	LOEE MWh/y
Base case	9.369	2.016	0.0012	0.1641	1433.75
Scenario 1	17.52	9.636	0.002	0.2190	1918.44
Scenario 2	48.18	26.28	0.0055	0.5840	5115.84
Scenario 3	73.584	37.668	0.0084	0.9125	7993.50
Scenario 4	64.531	34.660	0.0074	0.7956	6969.50

frequency deviation. This limit creates a further decline of reliability indexes compared to the second scenario, which shows that the limit of wind penetration is more sensitive to the reliability indexes than to the spinning reserve requirement.

- In the presence of energy storage, the reliability of the system is improved. By storing the surplus wind power, the energy storage assists the system when demand is not satisfied by wind farms and conventional generators.

The system reliability can be enhanced by incorporating improved forecast of wind speed, increasing inertia of wind via advanced control strategies. In addition to the above mentioned methods, demand response is also another way of mitigating some of the reliability issues brought about by high penetration of renewable generation.

4.3.2 Discussion

The work in this chapter presents an improved method to evaluate the adequacy of wind integrated systems. Future work will consider the inclusion of the transmission lines in system reliability investigation. When the transmission lines are considered, the reliability of supply at any load bus in the system depends on both generation and transmission adequacy. In this case, the power flows must be modeled appropriately. The method presented herein can accommodate any power flow model in power systems. The reliability model can generally be stated as follows.

$$\text{Min } C_T = \sum_{i=1}^{NB} C_i \tag{4.18}$$

Subject to:

- Power balance conditions. These conditions can be represented by means of a capacity flow model [98], a DC power flow model [99], or an AC power flow model [100], depending on the required accuracy and on the availability of system data.

- Equipment availability and capacity constraints.

Here, C_T is the power not served, C_i is the power curtailed at bus i_{th}, and N_B is the number of buses. For any encountered scenario, power will be routed through the network in such a manner as to minimize the power outage.

4.4 Conclusion

This chapter has presented the effects of stochasticity and low inertia characteristics of wind power on the reliability of the system. This work has shown that the reliability of the integrated system decreases when system security has to be ensured. This is one of the important aspects that has not been investigated in depth in prior research. The validity of the proposed method has been investigated and supported by a mathematical analysis and simulation. The effect of the energy storage on improving the integrated system reliability was also examined. The technique presented here will assist the system operator in better dispatch to maintain system stability and reliability as increasing amounts of renewable resources are integrated into the power grid. The technique is also helpful for power system planning to ensure system stability.

Chapter 5

Energy Storage for Reliability Improvement of Wind Integrated Systems under Frequency Security Constraint

5.1 Introduction

With the advantages of being abundant and environment-friendly, wind power is gradually replacing conventional generation at an ever-increasing pace. Moreover, with the development of state-of-art wind turbine technologies, the levelized cost of wind power is becoming more competetive with conventional generation. In [101], the Department of Energy lays out a detailed, long-term goal to produce 35% of the U.S electric energy from wind power by 2050 using both land-based and offshore wind resources. According to a report by the European Wind Energy Association [102], the combined wind energy production of the EU is projected to meet 31% of their total electricity demand by 2030. In order to meet these targets, various technical problems associated with wind integration must be addressed. Among these are the negative effects of wind

The content of this chapter has been reproduced with permission from *Nga Nguyen, Atri Bera, and Joydeep Mitra, Energy Storage for Reliability Improvement of Wind Integrated Systems under Frequency Security Constraint, IEEE IAS Annual Meeting, pp. 1–8, Oct. 2017.*

integration on frequency stability [12, 84, 86, 103–105] and reliability [106]. Wind generation amplifies the problem of frequency fluctuation due to its intermittence since frequency fluctuation is aggravated by the imbalance between generation and load. In addition to its variable nature, wind turbines with low inertia cause a larger variation in frequency if they replace the conventional generators. These factors impact the stable operation of the power system. Often, wind production must be limited.

Numerous solutions have been proposed to improve system stability and reliability in the presence of wind power. Integration of energy storage [107–109], advanced control strategies [110–113], and accurate forecasting [114,115] have been investigated. Energy storage has emerged to be a very effective technology that can assist wind integration, improve system reliability and security due to its fast response and high storage capacity [116].

Even though energy storage systems (ESS) tend to be efficient, the operation of the energy storage must be optimized in a manner so as to maximize the benefits that can be provided to the grid. According to [117], the system obtains the maximum benefits from an ESS if wind generation, conventional generation and energy storage are coordinated. The control strategy of an ESS can be designed to cater to various needs, such as mitigation of the fluctuation of renewable power output [118–120], maximization of the economic benefits by minimizing energy cost [121], achievement of load management for deferral of system upgrades, and minimizing the system losses [122]. In other works, a utility-scale energy storage was used as a control measure in a corrective form of the security-constrained unit commitment problem [123], for improvement of corrective security [124], or just for planning of emergency backup resources [125]. Energy storage is also considered as an important component for improving the grid reliability [126]. In [97], the size of energy storage was determined by a specific percentage of demand while evaluating reliability of generating systems containing wind power and energy storage. In [127–132], an energy storage has been used to assist in the penetration of renewable energy resources to improve the reliability of the system. The control strategy used here is based on the fact that the amount of energy used in charging or generated during discharging of the energy storage is equal to the imbalance between the supply and demand.

However, none of the previous works addresses the issue of frequency stability while considering the operation of large-scale energy storage being used to support the integration of wind power into the grid. To overcome this drawback, this chapter proposes an improved methodology for incorporating an energy storage with wind and conventional generation to improve system reliability while securing the frequency stability of the system.

The remainder of this chapter is organized as follows. Section 5.2 proposes an improved method to cooperate the operation of wind, conventional generation and energy storage to ensure the system frequency stability. The reliability evaluation of wind generation is presented in section 5.3. Simulation results, discussions, and conclusion about the effectiveness of the new method are covered in Section 5.4 and 5.5, respectively.

5.2 Operating Strategy of Energy Storage and System Generation

An energy storage system is useful in mitigating the variation of the wind generation output. However, it also has to operate in a manner so as to ensure system stability. This chapter presents an advanced strategy to coordinate the energy storage, wind and conventional generation to avoid the violation of system frequency.

The main idea of this coordination is that the amount of wind generation, which can not be integrated into the system due to the frequency security constraint, will be used to charge the energy storage. The advanced control strategy of the energy storage is stated as follows.

If the available wind generation is less than the wind penetration limit, the energy storage will be utilized to provide the demand. However, the energy storage can be deployed if the available wind generation is more than the wind penetration limit, but the power from conventional generation is less than the surplus of the demand compared to the wind penetration limit. Hence, the energy storage, the wind and conventional generation are coordinated to satisfy the system demand. From the proposed idea, the energy storage state time series is calculated as follows:

$$E_{i+1} = \begin{cases} E_i + (P_{cv,i} - L_i + P_{lim}) \times t & \text{if } \begin{cases} P_{w,i} \geq P_{lim} \\ P_{cv,i} < L_i - P_{lim} \end{cases} \\ E_i + (P_{w,t} - P_{lim}) \times t & P_{w,i} < P_{lim} \\ E_i + (P_{w,i} - P_{lim}) \times t & \text{if } \begin{cases} P_{w,i} \geq P_{lim} \\ P_{cv,i} \geq L_i - P_{lim} \end{cases} \\ E_i & \text{otherwise} \end{cases}$$

where P_{lim} is the penetration limit of wind generation, which was developed in Chapter 3.

While operating within the system, the charging and discharging rates, the maximum and minimum storage capacities of the energy storage must be considered carefully. If these factors are taken into account, the detailed control strategy of the energy storage becomes more complicated and is developed as follows.

If the maximum and minimum capacities of the energy storage are E_{max} and E_{min}, and the charging and discharging rates are considered linear using a 5-hour discharging period, then the maximum energy that the storage can charge and discharge in a time interval t is given by $E_{lim} = (E_{max} - E_{min})/5 \times t$ [97]. The minimum storage capacity is considered to be 20% of the maximum capacity. Assuming that $P_{w,i}$, $P_{cv,i}$ and L_i represent the total power from wind, conventional generators and load respectively, at step i, the energy storage state time series E is calculated as follows:

Case 1: Discharge Let the available wind power be greater than the wind penetration limit, and the power from conventional generation is less than the surplus of the demand compared to the wind penetration limit. The energy storage capacity is considered to be not lower than its minimum capacity. ($P_{w,i} \geq P_{lim}$, $\Delta P_i = L_i - P_{cv,i} - P_{lim} > 0$, and $E_i \geq E_{min}$).

- When $E_i - E_{min} \geq \Delta P_i$:

$$E_{i+1} = \begin{cases} E_i - \Delta P_i \times t & \text{if } \Delta P_i \leq E_{lim} \\ E_i - E_{lim} \times t & \text{if } \Delta P_i > E_{lim} \end{cases} \tag{5.1}$$

- When $E_i - E_{min} < \Delta P_i$:

$$E_{i+1} = \begin{cases} E_i - (E_i - E_{min}) \times t & \text{if } E_i - E_{min} \leq E_{lim} \\ E_i - E_{lim} \times t & \text{if } E_i - E_{min} > E_{lim} \end{cases} \tag{5.2}$$

Case 2: Discharge Let the available wind power be less than the wind penetration limit and the energy storage capacity is not lower than its minimum capacity ($\Delta P_{w,i} = P_{lim} - P_{w,i} > 0$ and $E_i \geq E_{min}$).

$$E_{i+1} = \begin{cases} E_i - \Delta P_{w,i} \times t & \text{if } \begin{cases} \Delta P_{w,i} \leq E_{lim} \\ E_i - E_{min} \geq \Delta P_{w,i} \end{cases} \\ E_i - (E_i - E_{min}) \times t & \text{if } \begin{cases} E_i - E_{min} < \Delta P_{w,i} \\ E_i - E_{min} \leq E_{lim} \end{cases} \\ E_i - E_{lim} \times t & \text{otherwise} \end{cases} \tag{5.3}$$

Case 3: Charge It is assumed that the wind power limit and the conventional generation meet the demand and the energy storage is not fully charged ($E_i < E_{max}$ and $P_{w,i} - P_{lim} \geq 0$, and $P_{cv,i} + P_{lim} - L_i \geq 0$).

- When $P_{w,i} - P_{lim} \geq E_{max} - E_i$:

$$E_{i+1} = \begin{cases} E_i + (E_{max} - E_i) \times t & \text{if } E_{max} - E_i \leq E_{lim} \\ E_i + E_{lim} \times t & \text{if } E_{max} - E_i > E_{lim} \end{cases} \tag{5.4}$$

- When $P_{w,i} - P_{lim} < E_{max} - E_i$:

$$E_{i+1} = \begin{cases} E_i + (P_{w,i} - P_{lim}) \times t & \text{if } P_{w,i} - P_{lim} \leq E_{lim} \\ E_i + E_{lim} \times t & \text{if } P_{w,i} - P_{lim} > E_{lim} \end{cases} \tag{5.5}$$

Case 4: No change Other than the three mentioned cases, the energy storage status stays the same.

In summary, the four cases can be represented as follows:

$$E_{i+1} = \begin{cases} E_i - \min(\Delta P_i, E_{lim}, E_i - E_{min}) \times t & \text{case 1} \\ E_i - \min(\Delta P_{w,i}, E_{lim}, E_i - E_{min}) \times t & \text{case 2} \\ E_i + \min(E_{max} - E_i, E_{lim}, P_{w,i} - P_{lim}) \times t & \text{case 3} \\ E_i & \text{case 4} \end{cases} \tag{5.6}$$

5.3 Reliability Evaluation of a Wind Farm Using Monte Carlo Simulation

While evaluating reliability of a wind-integrated system, a conventional generator can be modeled as a two-state unit. However, a wind farm should be modeled as a multi-state generator due to the variation of wind speed and the reliability of wind turbines. Due to the application of sequential Monte Carlo simulation, only transition rate between states and the wind power output of each state are necessary. The reliability model of a wind farm is shown as follows.

5.3.1 Wind farm output modeling

Wind farm output model is the combination of two models: wind speed and wind turbine. For simplification, it is assumed that the turbines in a wind farm are subject to the same wind speed and they have the same failure rate λ_t and repair rate μ_t. In this model, all the transitions among wind classes are considered, which is more appropriate than the birth and death Markov chain. The model of wind farm output is shown in a matrix form in Fig. 5.1 where each value in each state shows its capacity output. It should be noted that the transitions between non-adjacent states and the transition from one state to other states with lower capacity outputs are shown for the sake of clarity.

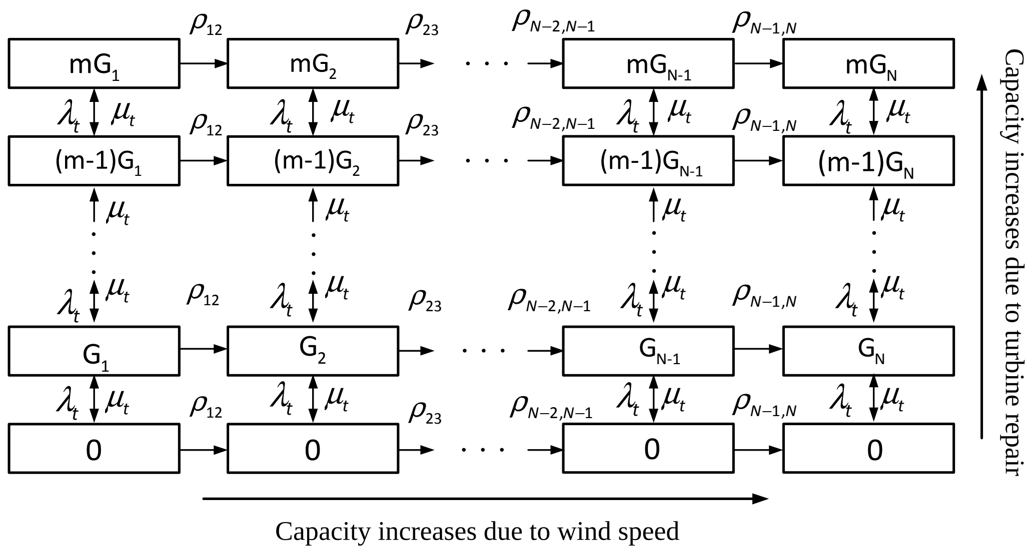

Figure 5.1: State transition diagram for a wind farm (transitions between non-adjacent states are not shown in order to reduce clutter).

In Fig. 5.1, the notations used are as follows:

m = number of wind turbine.

N = number of wind class.

G_j = output of a single turbine at wind class j.

The reliability of the system in the presence of wind is estimated using sequential Monte Carlo simulation as follows.

5.3.2 Sequential Monte Carlo simulation for a wind farm

Monte Carlo method is applied for stochastic simulation using random numbers. In power system reliability, Monte Carlo can be used to replace analytical methods when time-dependent issues are considered or a large set of states is involved [133]. In Monte Carlo simulation, a system can be divided into many components. The behavior of these components can be deterministic or probability distributions. All components are then combined to estimate system reliability. Monte Carlo simulation performs multiple sampling and gets results while meeting the sampling time limit or the convergence condition.

In this chapter, the wind-integrated system reliability is estimated using Monte Carlo - State duration sampling method due to the presence of energy storage. All components are assumed to be up in the initial state. Then, the duration of each component in its present state is calculated. The value of the state duration of component i is calculated using an exponential distribution as follows:

$$T_i = -\frac{1}{\lambda_i} \ln(U_i) \tag{5.7}$$

where U_i is a uniformly distributed random number; λ is the failure rate at the up state and the repair rate at the down state of the i_{th} equipment.

However, equation (5.7) must be modified when it is applied for a wind farm with multi-state. A derated state model can be utilized for a wind farm and each state of wind farm can be considered a derated state. Assuming that the present state of a wind farm is state j, k is the states that state j can transit to, the value of the state j duration is given by:

$$T_j = \min(T_{up,k}) \quad k = 1, .., l \tag{5.8}$$

where

$$T_{up,k} = -\frac{1}{\lambda_{jk}} \ln(U_k) \tag{5.9}$$

For each duration of a state, the imbalance between load and generation is determined. This process is repeated for a given time span and then the reliability indexes are calculated. The Loss of Load Expectation (LOLE) and Loss of Load Probability (LOLP) can be obtained from the duration for which the load is higher than the generation. The Energy Demand Not Supplied (EDSi) is determined from the amount of load that is greater than the generation and also for the duration for which this is true. The Loss of Load Frequency (LOLF) is determined from the number of times that the imbalance moves from a positive value to a negative value. The reliability indices in S sampling years can be estimated as follows [133]:

Loss Of Load Expectation (hour/year):

$$LOLE = \frac{\sum_{i=1}^{S} (\text{Loss of Load Duration } i)}{S} \tag{5.10}$$

Loss Of Load Probability:

$$LOLP = LOLE \times 8760 \tag{5.11}$$

Loss Of Energy Expectation (MWh/year):

$$LOEE = \frac{\sum_{i=1}^{S} (\text{Energy Not Supply } i)}{S} \tag{5.12}$$

Loss Of Load Frequency (failures/year):

$$LOLF = \frac{\sum_{i=1}^{S} (\text{Loss of Load Occurance } i)}{S} \tag{5.13}$$

The algorithm of Monte Carlo-State duration sampling method is presented in Fig. 5.2.

5.4 Simulation and results

The improved approach is simulated on the modified IEEE-RTS system. The original IEEE-RTS system includes 32 conventional generators. Total capacity of these generators is 3405 MW. In the modified IEEE-RTS system, 43 identical wind farms replace 6 conventional generators with a total capacity of 860 MW (four 76 MW coal generators at bus 1 and 2, one 155 MW coal generator at bus 15, and one 400 MW nuclear generator at bus 21). Each wind farm has 80 MW rated power with 10 identical wind turbines. The data for IEEE-RTS system reliability evaluation can be found in [94]. The inertia data of IEEE-RTS system is shown in Table 4.1 in Chapter 4 [94]. Since wind

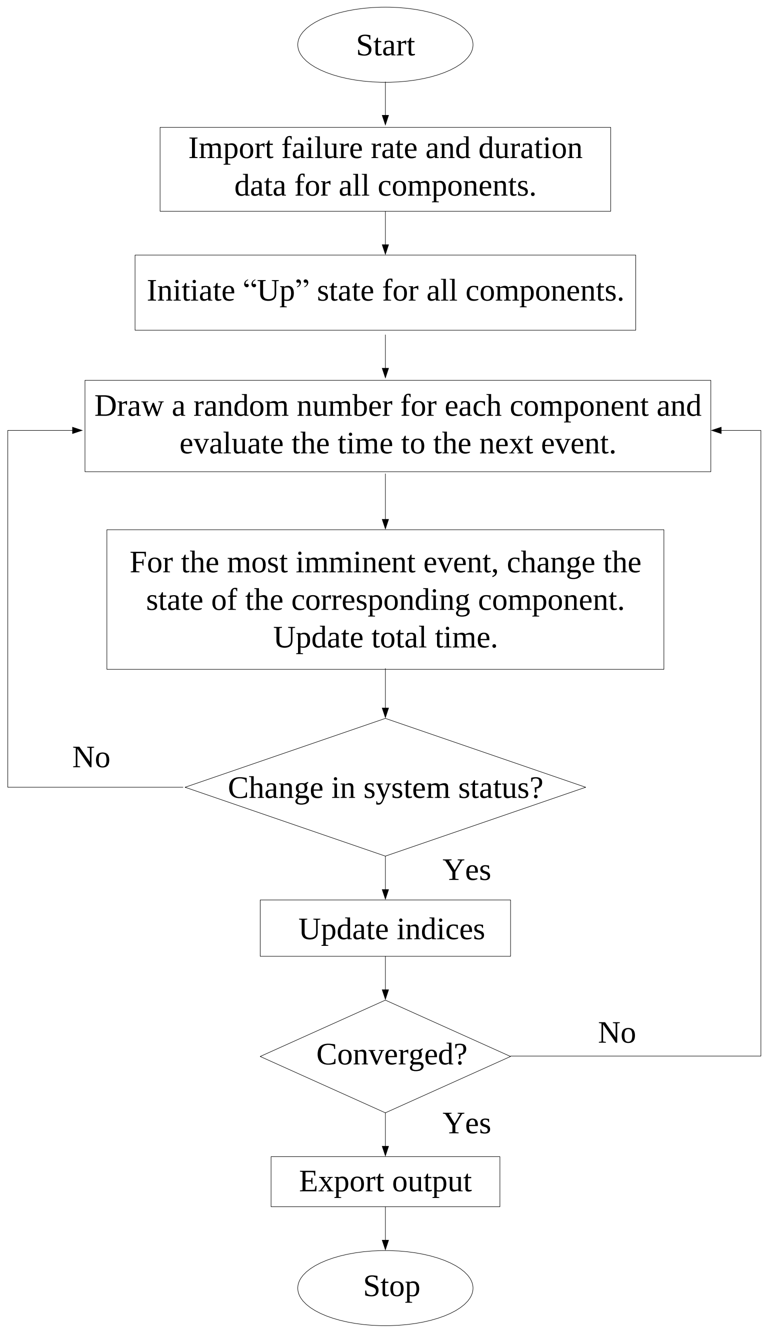

Figure 5.2: Algorithm of Monte Carlo simulation method.

power output is a random value, wind power capacity is chosen much higher (4 times) than the capacity of the replaced conventional generation to secure system reliability. The wind data used in the simulation is extracted from [95]. The data is clustered into one hour periods based on ten minutes periods of wind data provided.

The mean time to failure and the mean time to repair of wind turbines are 3600 and 150 hours, respectively. The cut-in, rated and cut-out speeds of wind turbines are 4, 12, and 25 m/s, respectively. After clustering wind data, the annual wind speed is represented by eight states from 0 to 8 m/s since some of the states, which produce identical power, are combined into one state (states 1–6 produce 0 MW and states 12–25 produce 8 MW). Hence, one wind generator is treated as a generator with 8 derated states. An energy storage system with maximum capacity of 30 MW each is installed at each wind farm to improve the system reliability. The transition rates of each output state of a wind farm are shown in Table 4.2 in Chapter 4. Four scenarios will be investigated to show the effect of proposed operating manner on the reliability of wind-integrated system:

Scenario 1: In the first scenario, reliability evaluation of the modified IEEE-RTS system with wind integration is implemented without frequency security constraint or energy storage. The effect of wind on frequency is neglected. All the available wind power output will be included in evaluating system reliability. Based on the data provided in Table 4.2, the reliability indexes of the modified system are calculated and shown in Table 5.1 for comparison with other scenarios.

Scenario 2: In the second scenario, reliability of the wind-integrated system is evaluated in the presence of energy storage but without the frequency security constraint. In this scenario, the operation of energy storage follows the manner proposed in [97]: if the available wind power is less than a specific percent (X%) of load, the stored energy can discharge to supply the load. The total of wind power and the storage power used cannot exceed that limit. The stored energy also serve the load if the available wind power is greater than the limit, and the power from conventional generators is less than (1 – X)% of load. In this chapter, the limit is chosen to be 30% of the maximum load. Then the system reliability is calculated.

Scenario 3: In this scenario, reliability evaluation of modified IEEE-RTS system with wind integration is implemented with frequency security constraint but without energy storage. Based on the developed model of the frequency security constraint in Chapter 4, the limit of inerita reduction is defined. The dynamic parameters of the conventional generators are chosen within appropriate ranges shown in Table 3.1. The inertia of each wind farm can be chosen as 0.25 pu. Load disturbance is modeled by a 0.1 pu step function and load damping is is assumed a value of 2. The safe limit of frequency deviation is -0.1 Hz [46]. Applying the data of the system dynamics to equation (4.12), the maximum reduction of system inertia is found to be 18.2%. Therefore, the maximum penetration of wind generation is 2792 MW to ensure the system frequency security and only 705 MW of conventional generation can be replaced. The system reliability then is evaluated and shown in Table 5.1.

Scenario 4: In this case, the operation of energy storage follows the proposed method in section 5.2. When the wind penetration limit is higher than the available wind generation, the energy storage will discharge to assist the demand. When the available wind generation is more than the wind penetration limit, but the power from conventional generation is less than the surplus of the demand compared to the wind penetration limit, the energy storage will also discharge. When wind power is higher than the penetration limit and the total generation in the system meets the expectation of the demand, energy storage will charge. The results for this scenario are shown in Table 5.1.

Table 5.1: The reliability indexes of the augmented IEEE-RTS system for four scenarios

Index	LOLE (h/y)	LOLF (f/y)	LOLP	EDNS (MW/y)	LOEE (MWh/y)
Scenario 1	53.9153	17.2032	0.0062	0.5255	4603.2
Scenario 2	30.8117	10.8648	0.0035	0.2776	2431.6
Scenario 3	65.3270	25.3656	0.0075	0.7801	6834.1
Scenario 4	35.2342	13.5783	0.0042	0.3479	3047.6

From the simulation results, some observations can be made:

1. The energy storage has a positive effect on system reliability in both scenarios: with or without frequency security constraint. All the indexes LOLP, LOLE, LOLF, LOLE, and EDNS reduce in the presence of energy storage in scenarios 2 and 4 – system reliability is improved.
2. Considering the frequency security constraint, the wind power that can be integrated into the system is limited. Hence, the reliability of the system decreases in both scenarios 3 and 4 compared to scenarios 1 and 2.
3. By comparing scenarios 2 and 4, it is clear that the reliability of the system is much worse when considering the frequency security even in the presence of energy storage.

The analysis and simulation results show that it is important to consider the frequency security of the system when estimating the reliability of the system with the application of energy storage. Otherwise, it is possible that the operators overestimate the ability to improve system reliability by application of energy storage system.

5.5 Conclusion

This chapter presents a new operating method for energy storage systems in a wind-integrated grid. This new method coordinates the operation of wind, conventional generators and energy storage to improve reliability while ensuring system frequency security. A mathematical model for the energy storage operation is developed and is then validated using Monte Carlo simulation. This method would benefit the system operators in both planning and operation of power systems with a high penetration of renewable energy. Besides energy storage, incorporating improved forecast of wind speed, increasing inertia of wind turbine, using demand response can be another way of improving the reliability of power system in the presence of renewable generation.

Chapter 6

Application of Grid Scale Virtual Energy Storage in Assisting Renewable Energy Penetration

6.1 Introduction

For decades, researchers have been interested in renewable energy (RE) due to its environmental benefits and abundant supply. With recent technological advances in this area, the levelized cost of renewable energy production is becoming economically competitive with that of conventional technologies. According to PNNL's report [3], RE will contribute a significant portion to the total electricity generated in the coming years. For example, the United States established a target of 40% of the overall electricity production coming from RE by 2030, while the European Union set a goal of 20% penetration by 2020 [134]. However, there are problems associated with integrating RE into the grid that need to be addressed in order to meet these objectives. One problem lies in the intermittent nature of renewable resources which restricts the amount of electricity that can be obtained from such resources. Once RE is integrated into the main grid, a host of issues are introduced such as the generation reserve requirement, frequency deviation, transmission violation

[12, 13, 83, 84, 86, 103, 135] and voltage instability [87, 88, 136]. These issues could potentially distort the balanced operation of the power system.

To resolve the issues associated with RE, many solutions were applied such as energy storage [10, 11, 107–109, 116, 137], advanced RE control strategies and power electronic interfaces [110–113, 138, 139], collaboration among control areas [140], RE prediction improvement [114, 115] and the diversification of RE resources and locations [141]. Among these solutions, energy storage, which has a speedy response and high storage capacity [116], is strongly capable of alleviating power instability. This makes it well suited for assisting with integration of RE into the main grid. However, the installation of energy storage is expensive although energy storage devices are constantly improving. To counter this economic drawback while retaining favorable features of energy storage, [140] has introduced a novel concept called "virtual energy storage". This concept provides an innovative operation method for power systems by allowing period power to be freely exchanged among balancing authorities. Period power, which is the difference between the scheduled interchange and the constant schedule of control areas, is omitted from area control errors to create a reduction in regulation of the whole system. Hence, period power is considered "virtual energy" and each balancing authority is called "virtual energy storage". To further expand the idea of "virtual energy", this chapter proposes a new concept called "grid scale virtual energy storage", which is based on the regulation of system frequency and the collaboration of control areas. The fundamental concept is the combination of frequency drift within a safe specified limit and the diversity of area control error (ACE) in order to create virtual storages among control areas. This method does not require capital investment in storage devices and implementation. Moreover, as will be presented later in the chapter, this method effectively reduces the amount of regulation for all control areas when the system is subject to disturbances. The main difference between the concept of "virtual energy" in this chapter and the one in paper [140] is the nature of "virtual energy". In [140] "virtual energy" is period power (which is related to the first term of ACE), while in this chapter, "virtual energy" is created by the deviation of actual frequency from its nominal value (which is related to the second term of ACE).

The remainder of this chapter is organized as follows. Section 6.2 explains the fundamentals of grid scale virtual energy storage and its mathematical formulation. Section 6.3 presents a fully-constituted control model with grid scale virtual energy storage of one-area power generating unit. Simulation results and conclusion, potential challenges in realizing grid scale virtual energy storage are covered in Section 6.4 and 6.5, respectively.

6.2 Grid Scale Virtual Energy Storage

Frequency is considered one of the principal indicators of stability in power systems. Frequency is maintained at a scheduled value (60 Hz in the US for example) in the long term by balancing generation and load. This nominal frequency has been accepted and enacted strictly since the 1930s. The NERC has prescribed bounds and established standards for frequency deviation and area control error and these are still in effect. However, the increasing of renewable resources penetration with low inertia challenges the frequency stability. To assist the RE penetration, consolidation of balancing authorities, which increases the system rotational storage capacity, has been implemented increasingly in recent years. An alternative approach to support RE is to mitigate its variability. As proposed in [142] a few years ago, the NERC had considered relaxing the frequency deviation standards. Although this has not been implemented, it is shown in this work that this could enable increased penetration of renewable resources. This is due to the fact that permitting frequency deviation over a period of time translates to absorption or depletion of rotational kinetic energy in conventional generators, and this would help mitigate the variability of RE. The relaxation in frequency regulation is important to the establishment of grid scale virtual energy storage. By allowing the frequency to deviate *slightly* from 60 Hz and by taking advantage of ACE diversity in different control areas, each control area can act as a virtual energy storage for the others. An example depicted in Fig. 6.1 is used to illustrate the idea.

When control area 1 experiences a decrease (or increase) in load, the frequency of the interconnected system increases (or decreases). While the traditional regulation would restore the frequency precisely to the nominal value (60 Hz) in all areas, the new concept of slightly drifted

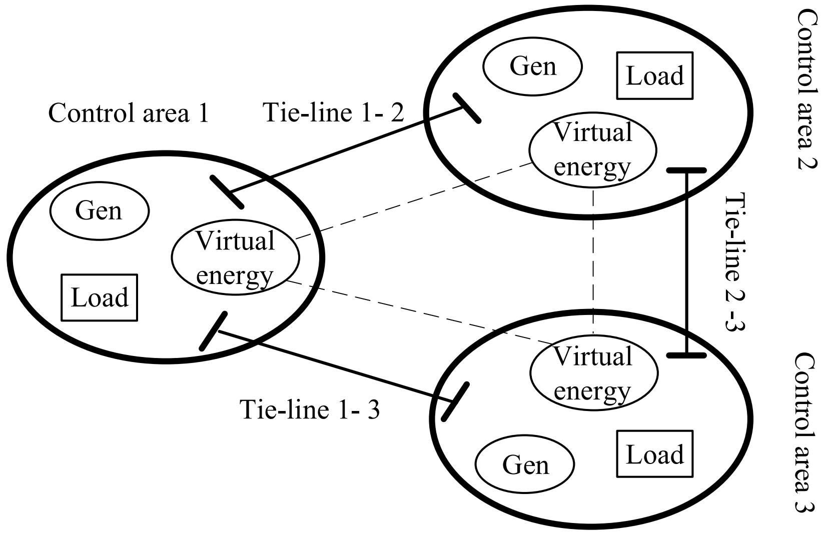

Figure 6.1: Grid scale virtual storage in a multi-area system.

frequency suggests that the implemented regulation should only bring the frequency back to a value within the allowed drift range. At the upward (or downward) drifted frequency, all areas will consume more (or less) energy than they do at nominal frequency. The difference between the amount of energy consumed at drifted frequency and at nominal frequency in each area is called the virtual energy area 1 stored in that area. Hence, it is said that the areas other than area 1 charge (or discharge) virtual energy. Such charged (or discharged) energy can be paid back to area 1 during the time when area 1 charges (or discharges) virtual energy for other areas or when other areas discharge (or charge) virtual energy for area 1. Because the difference between generation and demand in one control area can be positive or negative, other control areas that connect to it can charge or discharge virtual energy. This flexibility makes grid scale virtual energy storage in the interconnected system operate in a more efficient manner.

The new method offers great economical and technical benefits because of the reduction in regulation, transmission, installation cost, ACE and of no cost in virtual energy storage.

In preparing for the analysis and simulation of grid scale virtual energy storage in the system, the mathematical model of virtual energy storage and ACE in one control area is presented below.

Defining ϵ as the frequency drift limit of the system, ACE and virtual energy storage of control area i can be expressed as:

If $f_{i,a} - f_{i,s} > \epsilon$:

$$ACE_i = (P_{i,a}^{tie} - P_{i,s}^{tie}) - B_i(f_{i,a} - f_{i,s} - \epsilon) \tag{6.1}$$

$$E_i^{virt} = \int B_i \epsilon dt \tag{6.2}$$

If $f_{i,a} - f_{i,s} < -\epsilon$:

$$ACE_i = (P_{i,a}^{tie} - P_{i,s}^{tie}) - B_i(f_{i,a} - f_{i,s} + \epsilon) \tag{6.3}$$

$$E_i^{virt} = -\int B_i \epsilon dt \tag{6.4}$$

If $\left| f_{i,a} - f_{i,s} \right| \leq \epsilon$:

$$ACE_i = (P_{i,a}^{tie} - P_{i,s}^{tie}) \tag{6.5}$$

$$E_i^{virt} = \int B_i (f_{i,a} - f_{i,s}) dt \tag{6.6}$$

where

$f_{i,a}$ = the actual frequency of area i

$f_{i,s}$ = the scheduled (nominal) frequency

B_i = the frequency bias constant of area i, in MW/ 0.1 Hz

E_i^{virt} = virtual energy storage of control area i

ACE_i = area control error of control area i

These equations indicate that when control area i's actual frequency $f_{i,a}$ is lower (or higher) than the scheduled frequency $f_{i,s}$, control area i discharges (or charges) virtual energy.

Based on the above concept of grid scale virtual energy storage and its mathematical model, the following section of the chapter describes the implementation of load frequency control (LFC) with grid scale virtual energy storage.

6.3 LFC Model of one Control Area with Grid Scale Virtual Energy Storage

6.3.1 Frequency Regulation Procedure

As stated earlier, if there is a difference between generation and demand, the frequency of the power system will experience a disturbance. Once this disturbance happens, the load frequency control will take action to bring the frequency back to the nominal value with the assistance of various resources. The LFC action consists of three main stages [110]: Inertial response, Primary control and Secondary control.

1. Inertial response: in this stage, the kinetic energy of rotating mass is immediately discharged or absorbed by synchronous generators to resist the change in frequency.

2. Primary control: this stage, which is invoked in the first few seconds following the disturbance, relies on governor action and load damping to stabilize the frequency. Once the governors sense the frequency deviation, they regulate the generators' output accordingly by adjusting the prime movers' input. On the other hand, load damping, which is the resultant speed change of motor loads in direct proportion to frequency excursion, helps to resist the frequency disturbance by changing the motor loads' power consumption.

3. Secondary control: the purpose of this stage is to further stabilize the frequency after primary control to the nominal value by means of Automatic Generation Control (AGC). AGC consults ACE and economic dispatch in order to determine the most practical output for each generator, then changes governor set points accordingly. This third stage is employed in minutes.

Traditionally, LFC manages to regulate frequency deviation to zero at the end. However, in the new method with grid scale virtual energy storage, the difference between frequency deviation and frequency drift limit would be controlled to zero instead.

6.3.2 LFC Mechanism of one Control Area with Grid Scale Virtual Energy Storage

The combination of turbine-governor, rotating mass and load damping with virtual energy storage is represented in the load frequency control model as shown in Fig. 6.2 below [26]. The effect of renewable energy is taken into account by ΔP_L based on the assumption that renewable energy is a negative load. Also, a dead zone is embedded in the model to allow the frequency to drift. The parameters of the described LFC model are as follows:

ΔP_C = supplementary control
ΔP_P = primary control
$K(s)$ = LFC controller
ΔP_{load} = non-frequency-sensitive load change
ΔP_L = disturbance

$$\Delta P_L = \Delta P_{load} - \Delta P_{RE} \tag{6.7}$$

T_{ij} = synchronizing torque coefficient between area i and area j
H = equivalent inertia constant
Δf = frequency deviation
D = load damping constant
GT_{ki} = turbine-governor
β_i = frequency response characteristic of area i
T_g = time constant of the governor
T_t = time delay of turbine model
$\Delta P_{tie,i}$ = total tie-line power exchange between area i and other areas

B_i = frequency bias factor in area i. Its suitable value can be calculated as follows [27]:

$$B_i = \beta_i = \frac{1}{R_i} + D_i \tag{6.8}$$

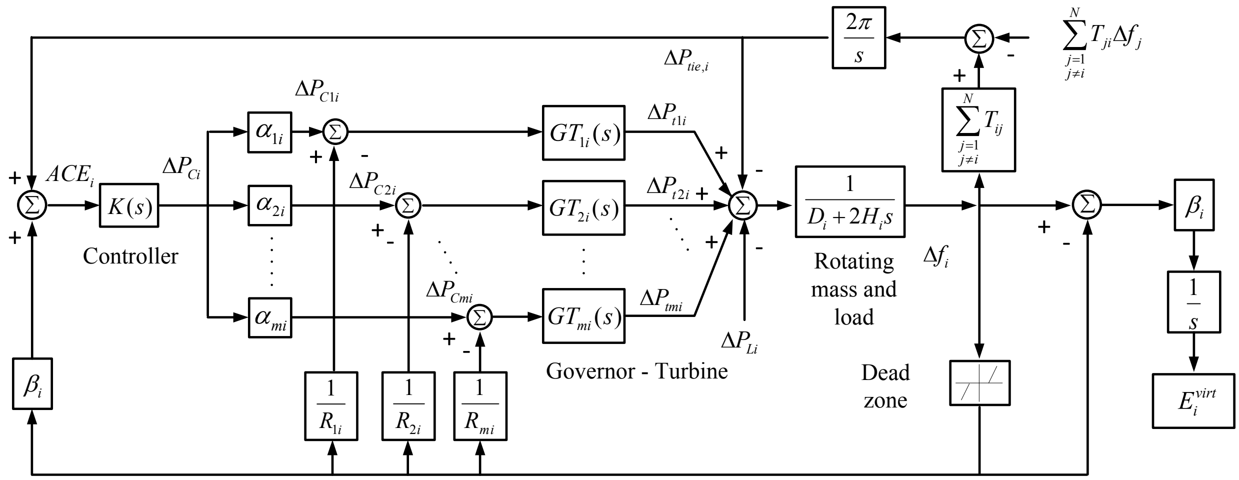

Figure 6.2: Control area i in an interconnected system with grid scale virtual energy storage.

Assuming that the generators consist of non-reheat turbines and reheat turbines, the turbine-governor dynamic models are represented in equation (6.9) and (6.10), respectively [27]:

$$GT_{i_{non-reheat}}(s) = \frac{1}{1+T_{t,i}s}\frac{1}{1+T_{g,i}s} \tag{6.9}$$

$$GT_{i_{reheat}}(s) = \frac{1}{1+T_{t,i}s}\frac{1}{1+T_{g,i}s}\frac{1+F_{HF,i}T_{RH,i}s}{1+T_{RH,i}s} \tag{6.10}$$

where T_{RH} is time constant of reheater and F_{HF} is the fraction of turbine power generated by HP unit.

When a load disturbance occurs, the resultant frequency deviation will be filtered by the dead zone. That filtered frequency deviation and the tie-line power signal are captured as feedback in control system to generate ACE.

The filtered frequency deviation is determined according to the below Matlab mathematical model for the dead zone [143]:

$$u = \begin{cases} 0 & \text{if } -\epsilon \leq \Delta f \leq \epsilon \\ \Delta f - (-\epsilon) & \text{if } \Delta f < -\epsilon \\ \Delta f - \epsilon & \text{if } \Delta f > \epsilon \end{cases} \tag{6.11}$$

where

$-\epsilon$ $=$ the start of the dead zone (lower limit)

ϵ $=$ the end of the dead zone (upper limit)

u $=$ filtered frequency deviation, which is the output signal of the dead zone.

The three cases of filtered frequency deviation u could be accordingly divided into the following three case studies.

Case 1: When $-\epsilon \leq \Delta f \leq \epsilon$, the frequency deviation is within the drift limit and the control signal u equals zero. Therefore, the primary control and part of secondary control have no effect on the system. The diagram of control system turns into Fig. 6.3 and the frequency deviation can be obtained as:

$$\Delta f_i(s) = \frac{1}{2H_i s + D_i}\left(\sum_{k=1}^{m} GT_{ki}(s)\Delta P_{Cki}(s) - \Delta P_{tie,i}(s) - \Delta P_{L,i}(s)\right) \tag{6.12}$$

where

$$\begin{aligned} \Delta P_{Cki}(s) &= K(s)\Delta P_{tie,i}(s)\alpha_{ki} \\ K(s) &= \frac{K}{s} \end{aligned} \tag{6.13}$$

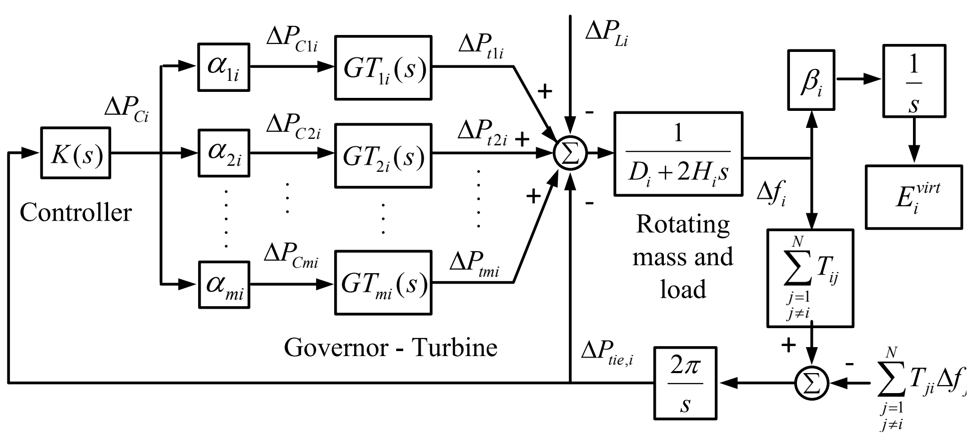

Figure 6.3: Control area i in an interconnected system with grid scale virtual energy storage for case 1.

After applying equation (6.13) into (6.5) and moving Δf to the left hand side, the frequency deviation is given by:

$$\Delta f_i(s) = \frac{\sum_{k=1}^{m} GT_{ki}(s)K(s)\Delta P_{tie,i}(s)\alpha_{ki} - \Delta P_{tie,i}(s) - \Delta P_{L,i}(s)}{2H_i s + D_i} \tag{6.14}$$

Final value theorem is employed to yield the steady state value of the frequency deviation $\Delta f_{i,ss}$ as in equation (6.15):

$$\Delta f_{iss} = \lim_{s\to 0} s\Delta f(s) = \lim_{s\to 0} s.\frac{\sum_{k=1}^{m} GT_{ki}(s)K(s)\Delta P_{tie,i}(s)\alpha_{ki} - \Delta P_{tie,i}(s) - \Delta P_{L,i}(s)}{2H_i s + D_i} \tag{6.15}$$

From the assumption that $\Delta P_{tie,i}(s)$ moves toward zero as the system reaches the steady state, equation (6.15) turns out to be:

$$\Delta f_{iss} = -\frac{\Delta P_{L,i}}{D_i} \tag{6.16}$$

Equation (6.16) indicates that for the case when the frequency deviation is within the drift limit, it will be eventually settled to the value $-\frac{\Delta P_{L,i}}{D_i}$. The value of virtual energy storage in this case has already been shown in equation (6.6).

Case 2: When $\Delta f > \epsilon$, frequency deviation raises above the drift limit, the control signal u equals $\Delta f - \epsilon$. All three LFC stages are engaged in the frequency control procedure. The system frequency deviation is given by:

$$\Delta f_i(s) = \frac{1}{2H_i s + D_i}(\sum_{k=1}^{m} GT_{ki}(s)[\Delta P_{Cki}(s) - \Delta P_{Pki}(s)] - \Delta P_{tie,i}(s) - \Delta P_{L,i}(s)) \tag{6.17}$$

where

$$\Delta P_{Cki}(s) = K(s)(\Delta P_{tie,i}(s) + B_i(\Delta f_i(s) - \epsilon))\alpha_{ki} \tag{6.18}$$

$$\Delta P_{Pki}(s) = \frac{\Delta f_i(s) - \epsilon}{R_{ki}} \tag{6.19}$$

Substituting $\Delta P_{Cki}(s)$ and $\Delta P_{Pki}(s)$ by their corresponding right-hand side in (6.18) and (6.19), equation (6.17) can be rewritten into the following form:

$$\Delta f_i(s) - \epsilon = \frac{\sum_{k=1}^{m} GT_{ki}(s)K(s)\Delta P_{tie,i}(s)\alpha_{ki}}{2H_is + D_i - \sum_{k=1}^{m} GT_{ki}(s)K(s)B_i\alpha_{ki} + \frac{\sum_{k=1}^{m} GT_{ki}(s)}{R_i}} - \frac{\Delta P_{tie,i}(s) + \Delta P_{L,i}(s) + \epsilon(2H_is + D_i)}{2H_is + D_i - \sum_{k=1}^{m} GT_{ki}(s)K(s)B_i\alpha_{ki} + \frac{\sum_{k=1}^{m} GT_{ki}(s)}{R_i}} \tag{6.20}$$

Applying final value theorem as in case 1 to find the steady state value yields the result:

$$(\Delta f_i - \epsilon)_{ss} = \lim_{s\to 0} s(\Delta f(s) - \epsilon) \tag{6.21}$$

As stated in case 1, $\Delta P_{tie,i}(s)$ disappears at steady state, so equation (6.21) is equivalent to:

$$(\Delta f_i - \epsilon)_{ss} = 0 \tag{6.22}$$

Therefore:

$$\Delta f_{i,ss} = \epsilon \tag{6.23}$$

Equation (6.23) obviously shows that for the case when the frequency deviation exceeds the upper drift limit ϵ, it will be finally regulated to that upper drift limit at steady state. The value of virtual energy storage in this case has already been shown in equation (6.2).

Case 3: When $\Delta f < -\epsilon$, the frequency deviation falls below the lower drift limit, the control signal u equals $\Delta f + \epsilon$. This case is symmetric to case 2. A calculation similar to that in case 2 yields the frequency deviation at steady state:

$$\Delta f_{i,ss} = -\epsilon \tag{6.24}$$

The value of virtual energy storage in this case has already been shown in equation (6.4).

In short, equation (6.25) summarizes the value of the system frequency at steady state under the regulation of the LFC model with grid scale virtual energy storage:

$$\Delta f_{i,ss} = \begin{cases} -\dfrac{\Delta P_{L,i}}{D_i} & \text{if } -\epsilon \leq \Delta f \leq \epsilon \\ -\epsilon & \text{if } \Delta f < -\epsilon \\ \epsilon & \text{if } \Delta f > \epsilon \end{cases} \tag{6.25}$$

Based on the above theoretical analysis, a simulation model is implemented in section 6.4 to evaluate the effectiveness of the proposed grid scale virtual energy storage idea.

6.4 Simulation and Results

In order to observe the quantitative benefit of grid scale virtual energy storage to frequency control in multi-area power system, a simulation model that includes two interconnected control areas is developed under the following settings and assumptions:

- The two areas are strongly connected; transmission constraints and losses are ignored.
- One non-reheat turbine and one reheat turbine configuration is employed for area 1 and 2.
- The LFC model of the studied system is developed as in Fig. 6.4, where Δf_1 and Δf_2 are respectively the frequency deviations in area 1 and area 2, in Hz.
- Load disturbance is simulated by a step function. Area 1 is subject to the load disturbance in order to observe the operation of virtual energy storage in control area 2.
- The parameters of the investigated systems are given in Table 6.1 [26,47]. It is assumed that these parameters have already taken into account the change in inertia, equivalent regulation constant and frequency response characteristic due to the impact of renewable energy integration.

- Matlab/Simulink is used as the simulation environment.

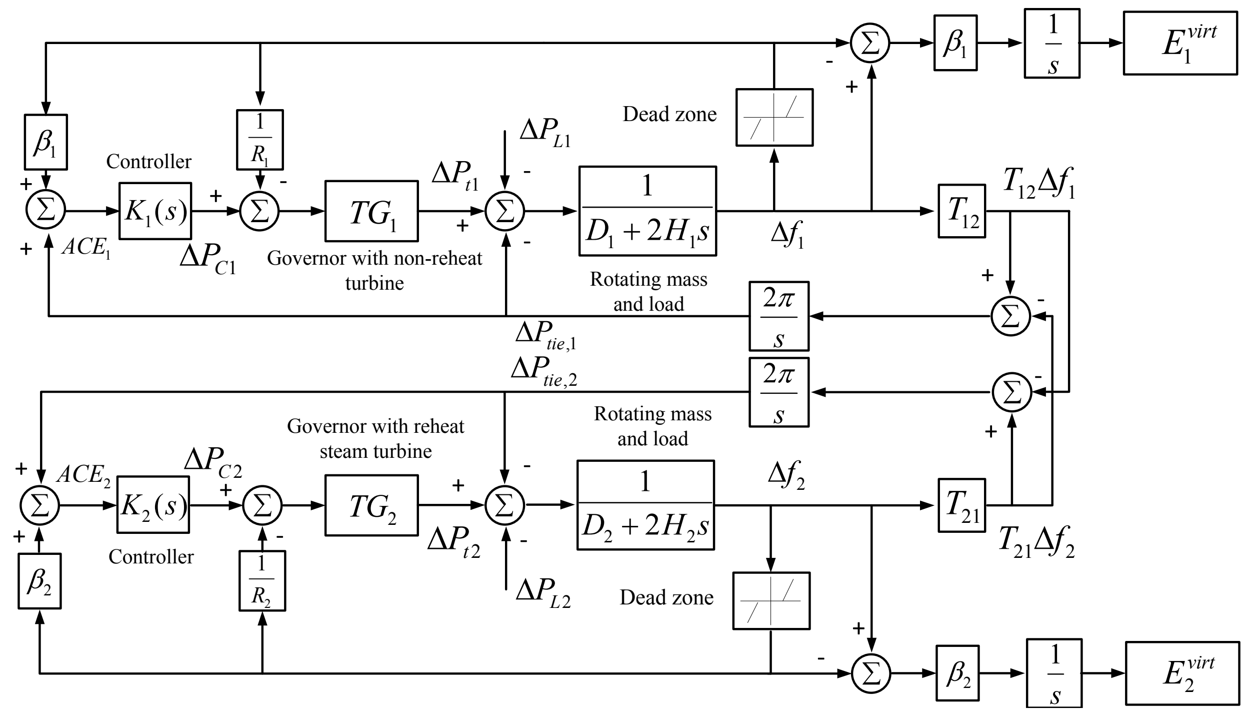

Figure 6.4: Two control areas with one non-reheat turbine and one reheat turbine unit.

Table 6.1: Simulation parameters for two interconnected control areas

K	D (pu/Hz)	$2H$ (pu.s)	R (Hz/pu)	T_g (s)	T_t (s)	B (pu/Hz)	T_{ij} (pu/Hz)	T_{RH} (s)	F_{HP}
-0.3	0.015	0.167	3.00	0.08	0.4	0.348	0.2	0	0
-0.4	0.008	0.167	2.4	0.08	0.3	0.42	0.2	10	0.5

A dead zone is employed to specify the frequency drift limit between -0.05 Hz and 0.05 Hz. This frequency drift limit follows the recommended safe range $\pm$ 0.2 Hz for frequency deviation under normal condition without event disturbance [46, 144].

Three simulation scenarios are developed based on the three case studies described in section 6.3. A fourth scenario that doesn't employ grid scale virtual energy storage is also included in the simulation in order to highlight the difference introduced by grid scale virtual energy storage.

In the first scenario, the load disturbance in control area 1 is set up in such a way that it yields a frequency deviation within the dead zone's drift limit. A 0.001 pu load disturbance is chosen to produce such outcome. This scenario observes a zero value in control signal u and no primary control. The frequency deviations, the virtual energy storage that area 1 stores in area 2, and the ACE following the disturbance are shown in Fig. 6.5, Fig. 6.6 and Fig. 6.7, respectively.

In the second scenario, the load disturbance is arranged so that the resultant frequency deviation is greater than the upper limit of the dead zone. The application of -0.03 pu load disturbance could meet that requirement. The control signal u is $\Delta f - \epsilon$ in this case. The frequency deviations, the virtual energy storage that area 1 stores in area 2, and the ACE following the disturbance are respectively depicted in Fig. 6.8, Fig. 6.9 and Fig. 6.10.

In the third scenario, the arrangement for the load disturbance in control area 1 is opposite to that in the second scenario. The resultant frequency deviation should be smaller than the lower limit of the dead zone and the value of control signal u is $\Delta f + \epsilon$. A load step disturbance of 0.03 pu is employed. The frequency deviations, virtual energy storage that area 1 stores in area 2, and ACE following the disturbance are respectively depicted in Fig. 6.11, Fig. 6.12, and Fig. 6.13.

In the fourth scenario, the dead zone is eliminated from the LFC model while the load disturbance arrangement is the same as in the third scenario. The frequency deviations and the ACE following the disturbance in control area 1 are shown in Fig. 6.14 and Fig. 6.15 respectively.

From the graphical simulation results, some observations can be made:

1. Following a load disturbance in the control area 1 in the three simulation scenarios with grid scale virtual energy storage, the frequency of the interconnected system experiences a transient instability and returns to the values within the drift limit under the regulation of LFC.

2. In the first simulation scenario, none of the control actions was invoked. The system frequency oscillated inside the drift limit until it reached a stable value. Area 2 discharged virtual energy.

3. In the second simulation scenario, the frequency of the interconnected system was stabilized at the upper boundary of the frequency drift limit which was above the nominal frequency.

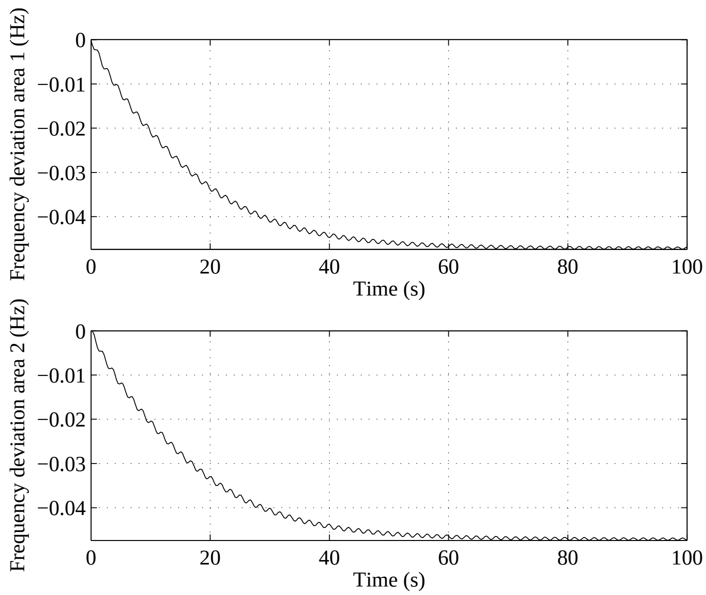

Figure 6.5: Frequency deviations in area 1 and 2 following a 0.001 pu load step disturbance in control area 1.

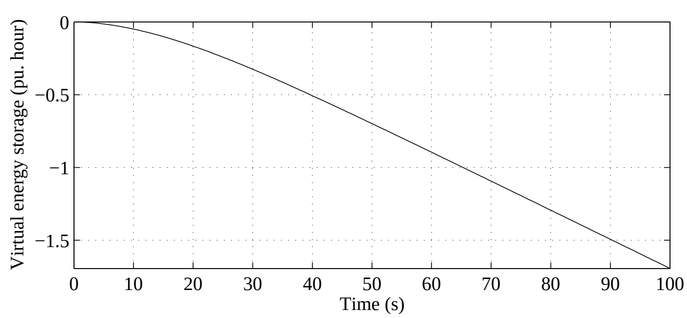

Figure 6.6: Virtual energy storage in area 2 following 0.001 pu load step disturbance in control area 1.

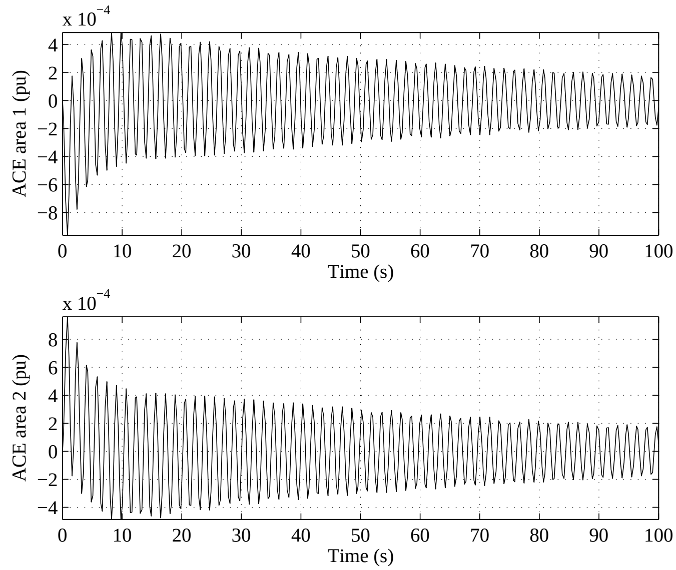

Figure 6.7: ACE in area 1 and 2 following a 0.001 pu load step disturbance in control area 1.

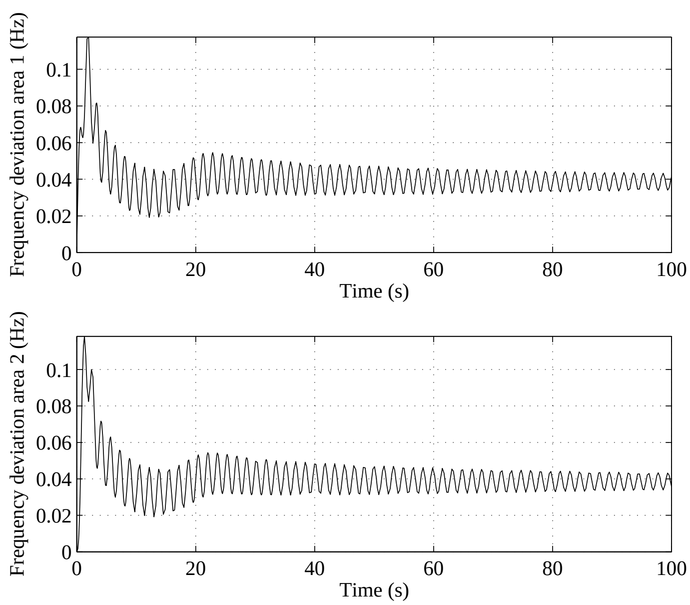

Figure 6.8: Frequency deviations following a –0.03 pu load step disturbance in control area 1.

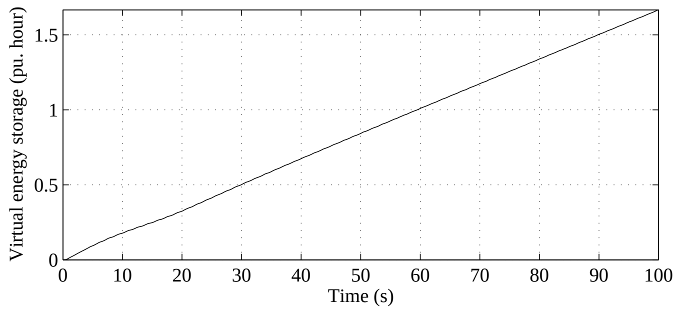

Figure 6.9: Virtual energy storage in area 2 following a –0.03 pu load step disturbance in control area 1.

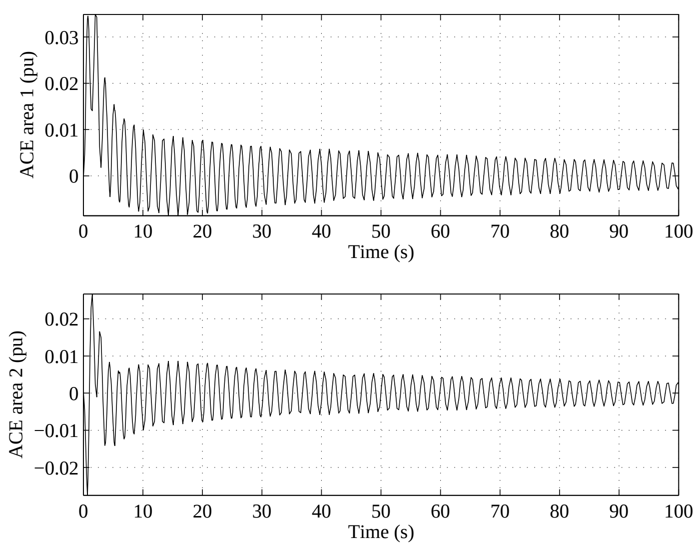

Figure 6.10: ACE in area 1 and 2 following a –0.03 pu load step disturbance in control area 1.

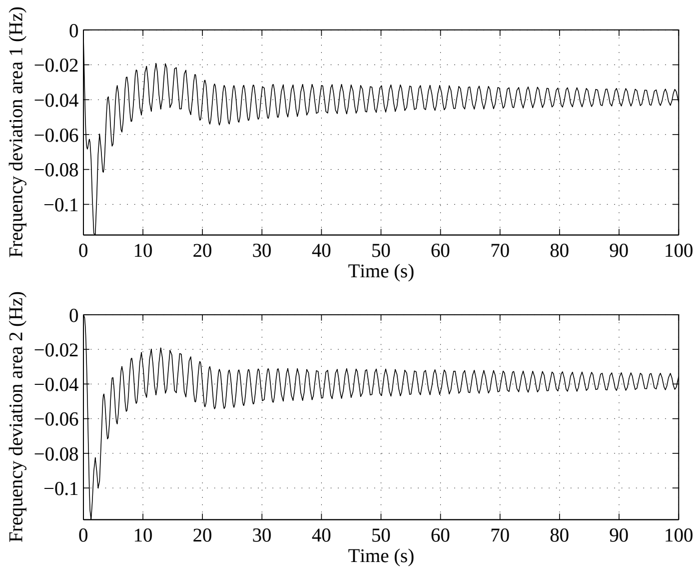

Figure 6.11: Frequency deviations following a 0.03 pu load step disturbance in control area 1.

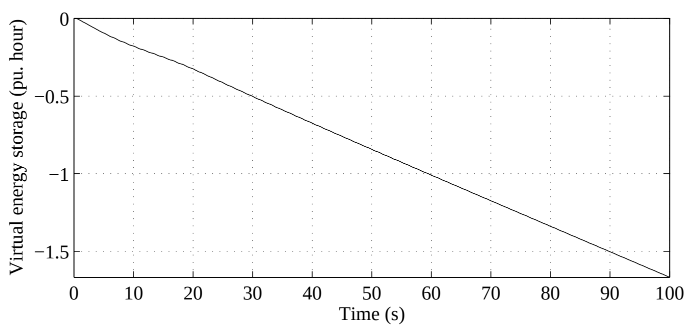

Figure 6.12: Virtual energy storage in area 2 following a 0.03 pu load step disturbance in control area 1.

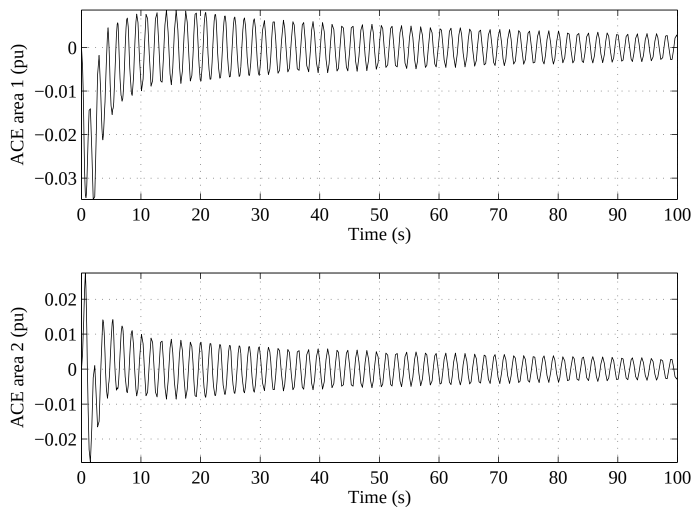

Figure 6.13: ACE in area 1 and 2 following a 0.03 pu load step disturbance in control area 1.

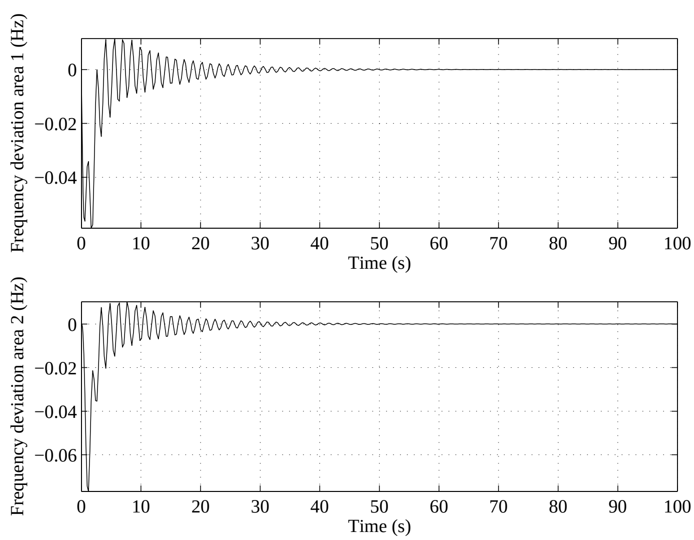

Figure 6.14: Frequency deviations following a 0.03 pu load step disturbance in control area 1 without virtual energy storage.

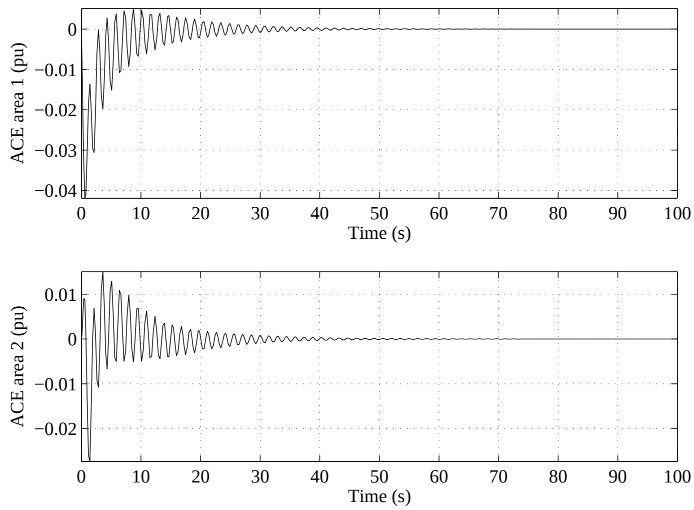

Figure 6.15: ACE in area 1 and 2 following a 0.03 pu load step disturbance in control area 1 without virtual energy storage.

As a result, the virtual energy storage in area 2 was positive, implying that area 2 charged virtual energy.

4. In the third simulation scenario, the frequency of the interconnected system at the steady state stayed at the lower boundary of the frequency drift limit which was below the nominal frequency. As a consequence, the virtual energy storage in area 2 was negative, indicating that area 2 discharged virtual energy.

5. In all three scenarios that utilized grid scale virtual energy storage, the ACE regulation requirement was markedly less stressful than that in the fourth scenario where the traditional LFC mechanism did not include grid scale virtual energy storage. This distinction is obvious when observing Figures 6.10, 6.13 and 6.15. The rapid vanishing of ACE signal to sharp zero value in Fig. 6.15 and the gradual attenuation of ACE signal in Fig. 6.10 and Fig. 6.13 verifies that the effort to settle down the ACE spent by the traditional LFC was more intensive than the effort spent by the LFC with grid scale virtual energy.

The flexibility in system frequency at steady state allows an area to borrow virtual energy (e.g. when its demand increases) from other control areas and pay the charged virtual energy back to other control areas (when its demand decreases). This flexibility and significant reduction in ACE regulation requirement explained above are advantages of grid scale virtual energy that enable power system operators to save a considerable investment in reserve, transmission, regulation, wear and tear facilities.

6.5 Conclusion

This chapter presents the concept of grid scale virtual energy, which is a novel broadening of the virtual energy concept, as a new promising feature to be integrated into the load frequency control model, and supports its validity with a detailed mathematical analysis and simulation. Simulation results confirm the proposed model's effectiveness at restoring the disturbed frequency as well as economical benefit in reducing regulation expense without introducing additional installation or implementation costs. However, one technical problem, which should be examined carefully during the realization of grid scale virtual energy storage, is how to determine a good frequency drift limit. The more flexibility in frequency drift limit facilitates the operation of grid scale virtual energy storage, but that may have an adverse impact on the service quality and the safety of the power system. The optimal frequency drift limit varies in each interconnected system, particularly that drift limit heavily depends on the individual system configuration and system's ability to resist disturbances. Once the technical subtleties have been properly resolved, the mechanism of grid scale virtual energy storage would enable the safe integration of renewable energy into the power grid.

Chapter 7

Contributions and Future Work

7.1 Contributions

This thesis examines the effect of wind generation on power system. The contributions include:

- The effects of the intermittent and non-dispatchable features of wind power on the system frequency stability was investigated. The impacts of wind power on the inertia, frequency regulation constant, tie-line flows, and area control error are included. The more accurate model of frequency deviation is developed.
- A mathematical model to estimate the maximum level of variable energy resources that can be integrated into the grid based on the frequency security constraint is developed. The method described uses the approximation of the frequency deviation extremum based on the sensitivity analysis. This model is very helpful in operation and planning in power system.
- A new method to evaluate the reliability of a power system with high penetration of wind generation, considering the impact of not only the intermittence but also the low inertia characteristic of wind power, is presented. This method helps the operator to avoid overestimating the reliability of the integrated system.
- A new operating method for energy storage systems in a wind-integrated grid is presented.

This new method coordinates the operation of wind, conventional generators and energy storage to improve reliability while ensuring system frequency security. This method would benefit the system operators in both planning and operation of power systems with a high penetration of renewable energy.

- A novel approach named "grid scale virtual energy storage", which addresses the challenges of the renewable energy in the power system at no cost is proposed. The grid scale virtual energy storage support greater penetration of renewable energy into the grid.

7.2 Future Work

1. Develop the mathematical model of wind penetration limit based on voltage stability requirement.
2. Re-consider the economic/environmental dispatch in the presence of both frequency stability and voltage stability constraints.
3. Examine the optimal power flow under voltage stability requirement.
4. Application of FACTS devices to improve the penetration of wind power.
5. Improve voltage stability by advanced operating approaches.

BIBLIOGRAPHY

BIBLIOGRAPHY

[1] REN steering committee, "Renewables 2016 – Global status report," 2016.

[2] C. Greenwood, A. Hohler, V. Sonntag-OBrien, *et al.*, "Global trends in sustainable energy investment 2007," 2007.

[3] Y. Diao, P. Etingov, S. Malhara, N. Zhou, R. Guttromson, J. Ma, P. Du, and N. S. C. Sastry, "Analysis methodology for balancing authority cooperation in high penetration of variable generation," *US Dep. Energy*, 2010.

[4] North American Electric Reliability Corporation, "Operating practices, procedures and tools, NERC IVGTF, Task 2.4 report," Mar. 2011.

[5] J. Conto, "Grid challenges on high penetration levels of wind power," in *IEEE Power and Energy Society General Meeting*, pp. 1–3, 2012.

[6] S. Sharma, S.-H. Huang, and N. Sarma, "System inertial frequency response estimation and impact of renewable resources in ERCOT interconnection," in *IEEE Power and Energy Society General Meeting*, pp. 1–6, 2011.

[7] S.-H. Huang, D. Maggio, K. McIntyre, V. Betanabhatla, J. Dumas, and J. Adams, "Impact of wind generation on system operations in the deregulated environment: ERCOT experience," in *IEEE Power and Energy Society General Meeting*, pp. 1–8, 2009.

[8] N. Miller, M. Shao, S. Venkataraman, C. Loutan, and M. Rothleder, "Frequency response of California and WECC under high wind and solar conditions," in *IEEE Power and Energy Society General Meeting*, pp. 1–8, 2012.

[9] J. Brisebois and N. Aubut, "Wind farm inertia emulation to fulfill Hydro-Québec's specific need," in *Power and Energy Society General Meeting, 2011 IEEE*, pp. 1–7, 2011.

[10] M. Benidris, S. Elsaiah, S. Sulaeman, and J. Mitra, "Transient stability of distributed generators in the presence of energy storage devices," in *North American Power Symposium (NAPS), 2012*, pp. 1–6, IEEE, 2012.

[11] M. Benidris and J. Mitra, "Enhancing stability performance of renewable energy generators by utilizing virtual inertia," in *2012 IEEE Power and Energy Society General Meeting*, pp. 1–6, 2012.

[12] H. Bevrani, A. Ghosh, and G. Ledwich, "Renewable energy sources and frequency regulation: survey and new perspectives," *Renewable Power Generation, IET*, vol. 4, no. 5, pp. 438–457, Sep. 2010.

[13] I. Erlich, K. Rensch, and F. Shewarega, "Impact of large wind power generation on frequency stability," in *IEEE Power Engineering Society General Meeting*, pp. 1–8, 2006.

[14] W. Li, G. Joós, and C. Abbey, "Wind power impact on system frequency deviation and an ESS based power filtering algorithm solution," in *2006 IEEE PES Power Systems Conference and Exposition*, pp. 2077–2084, 2006.

[15] E. Muljadi, V. Gevorgian, M. Singh, and S. Santoso, *Understanding inertial and frequency response of wind power plants*. IEEE, 2012.

[16] C. Luo and B.-T. Ooi, "Frequency deviation of thermal power plants due to wind farms," *IEEE Trans. Energy Conversion*, vol. 21, no. 3, pp. 708–716, Sept. 2006.

[17] H. Mathur, L. B. F. Leite, H. Siguerdidjane, and Y. Bhateshvar, "Study of impact of wind power penetration on frequency stabilization in multi-area power system," in *2013 8Th International Symposium on Advanced Topics in Electrical Engineering (Atee)*, pp. 1–6, IEEE, 2013.

[18] J. Morren, J. Pierik, and S. W. De Haan, "Inertial response of variable speed wind turbines," *Electric power systems research*, vol. 76, no. 11, pp. 980–987, Jul. 2006.

[19] L. Meegahapola and D. Flynn, "Impact on transient and frequency stability for a power system at very high wind penetration," in *IEEE PES General Meeting*, pp. 1–8, 2010.

[20] N. R. Ullah, T. Thiringer, and D. Karlsson, "Temporary primary frequency control support by variable speed wind turbines–Potential and applications," *IEEE Trans. Power Syst*, vol. 23, no. 2, pp. 601–612, May 2008.

[21] H. Ahmadi and H. Ghasemi, "Maximum penetration level of wind generation considering power system security limits," *Generation, Transmission & Distribution, IET*, vol. 6, no. 11, pp. 1164–1170, Nov. 2012.

[22] G. Strbac, A. Shakoor, M. Black, D. Pudjianto, and T. Bopp, "Impact of wind generation on the operation and development of the UK electricity systems," *Electric Power Systems Research*, vol. 77, no. 9, pp. 1214–1227, Jul. 2007.

[23] E. Vittal, J. McCalley, V. Ajjarapu, and T. Harbour, "Wind penetration limited by thermal constraints and frequency stability," in *Power Symposium, 2007. NAPS'07. 39th North American*, pp. 353–359, 2007.

[24] C. Luo, H. G. Far, H. Banakar, P.-K. Keung, and B.-T. Ooi, "Estimation of wind penetration as limited by frequency deviation," *IEEE Trans. Energy Convers.*, vol. 22, no. 3, p. 783, Sep. 2007.

[25] H. Ahmadi and H. Ghasemi, "Security-constrained unit commitment with linearized system frequency limit constraints," *IEEE Trans. Power Syst.*, vol. 29, no. 4, pp. 1536–1545, Jul. 2014.

[26] H. Bevrani, *Robust power system frequency control*. Springer, 2009.

[27] P. Kundur, N. J. Balu, and M. G. Lauby, *Power system stability and control*. New York: McGraw-Hill, 1994.

[28] J. Ekanayake and N. Jenkins, “Comparison of the response of doubly fed and fixed-speed induction generator wind turbines to changes in network frequency,” *IEEE Trans. Energy Convers.*, vol. 19, no. 4, pp. 800–802, Dec. 2004.

[29] J. M. Kennedy, B. Fox, T. Littler, and D. Flynn, “Validation of fixed speed induction generator models for inertial response using wind farm measurements,” *IEEE Trans. Power Syst*, vol. 26, no. 3, pp. 1454–1461, Aug. 2011.

[30] L. Holdsworth, J. B. Ekanayake, and N. Jenkins, “Power system frequency response from fixed speed and doubly fed induction generator-based wind turbines,” *Wind energy*, vol. 7, no. 1, pp. 21–35, 2004.

[31] J. Ekanayake, L. Holdsworth, and N. Jenkins, “Control of DFIG wind turbines,” *Power Engineer*, vol. 17, no. 1, pp. 28–32, 2003.

[32] N. Miller, K. Clark, and M. Shao, “Frequency responsive wind plant controls: Impacts on grid performance,” in *2011 IEEE Power and Energy Society General Meeting*, pp. 1–8, 2011.

[33] M. F. M. Arani and E. F. El-Saadany, “Implementing virtual inertia in DFIG-based wind power generation,” *IEEE Trans. Power Syst*, vol. 28, no. 2, pp. 1373–1384, Aug. 2013.

[34] J. Morren, S. W. De Haan, W. L. Kling, and J. Ferreira, “Wind turbines emulating inertia and supporting primary frequency control,” *IEEE Trans. Power Syst*, vol. 21, no. 1, pp. 433–434, Feb. 2006.

[35] R. G. De Almeida and J. P. Lopes, “Participation of doubly fed induction wind generators in system frequency regulation,” *IEEE Trans. Power Syst*, vol. 22, no. 3, pp. 944–950, Aug. 2007.

[36] X. Yingcheng and T. Nengling, “Review of contribution to frequency control through variable speed wind turbine,” *Renewable Energy*, vol. 36, no. 6, pp. 1671–1677, Jun. 2011.

[37] X. Zhang, H. Li, and Y. Wang, “Control of DFIG-based wind farms for power network frequency support,” in *Power System Technology (POWERCON), 2010 International Conference on*, pp. 1–6, IEEE, 2010.

[38] Q.-C. Zhong and G. Weiss, “Synchronverters: Inverters that mimic synchronous generators,” *IEEE Trans. Industrial Electronics*, vol. 58, no. 4, pp. 1259–1267, Mar. 2011.

[39] I. Gowaid, A. El-Zawawi, and M. El-Gammal, “Improved inertia and frequency support from grid-connected DFIG wind farms,” in *Power Systems Conference and Exposition (PSCE), 2011 IEEE/PES*, pp. 1–9, 2011.

[40] W. Yao and K. Y. Lee, “A control configuration of wind farm for load-following and frequency support by considering the inertia issue,” in *2011 IEEE Power and Energy Society General Meeting*, pp. 1–6, 2011.

[41] M. Wang-Hansen, R. Josefsson, and H. Mehmedovic, “Frequency controlling wind power modeling of control strategies,” *IEEE Trans. Sustainable Energy*, vol. 4, no. 4, pp. 954–959, Oct. 2013.

[42] L. Wu and D. Infield, “Investigation on the interaction between inertial response and droop control from variable speed wind turbines under changing wind conditions,” in *2012 47th International Universities Power Engineering Conference (UPEC)*, pp. 1–6, IEEE, 2012.

[43] R. Doherty, A. Mullane, G. Nolan, D. J. Burke, A. Bryson, and M. O’Malley, “An assessment of the impact of wind generation on system frequency control,” *IEEE Trans. Power Syst.*, vol. 25, no. 1, pp. 452–460, Feb. 2010.

[44] W. I. Rowen, “Simplified mathematical representations of heavy-duty gas turbines,” *Journal of engineering for power*, vol. 105, no. 4, pp. 865–869, 1983.

[45] S. K. Yee, J. V. Milanovic, and F. M. Hughes, “Overview and comparative analysis of gas turbine models for system stability studies,” *IEEE Trans. Power Syst*, vol. 23, no. 1, pp. 108–118, Jan. 2008.

[46] I. Erinmez, D. Bickers, G. Wood, and W. Hung, “NGC experience with frequency control in England and Wales-provision of frequency response by generators,” in *Power Engineering Society 1999 Winter Meeting, IEEE*, vol. 1, pp. 590–596, 1999.

[47] K. S. Parmar, S. Majhi, and D. Kothari, “Optimal load frequency control of an interconnected power system,” *MIT International Journal of Electrical and Instrumentation Engineering*, vol. 1, no. 1, pp. 1–5, 2011.

[48] M. Hanley, “Frequency instability problems in North American interconnections, DOE/NETL,” tech. rep., DOE/NETL-2011/1473, May 1, 2011.

[49] G. Lalor and M. O’Malley, “Frequency control on an island power system with increasing proportions of combined cycle gas turbines,” in *Power Tech Conference Proceedings, 2003 IEEE Bologna*, vol. 4, pp. 7–pp, 2003.

[50] G. Lalor, J. Ritchie, D. Flynn, and M. J. O’Malley, “The impact of combined-cycle gas turbine short-term dynamics on frequency control,” *IEEE Trans. Power Syst*, vol. 20, no. 3, pp. 1456–1464, Aug. 2005.

[51] H. Bayem, L. Capely, F. Dufourd, and M. Petit, “Probabilistic study of the maximum penetration rate of renewable energy in an island network,” in *PowerTech, 2009 IEEE Bucharest*, pp. 1–5, 2009.

[52] M. Knopp, “Study on maximum permissible intermittent electricity generators in an electricity supply network based on grid stability power quality criteria,” *Master’s Thesis, Fernuniversität Hagen*, 2012.

[53] C.-A. Chang, Y.-K. Wu, Z.-G. Peng, and B.-K. Chen, “Determination of maximum wind power penetration in a isolated island system by considering spinning reserve,” in *2014 IEEE/IAS 50th Industrial & Commercial Power Systems Technical Conference*, pp. 1–8, 2014.

[54] E. Vittal, "A static analysis of maximum wind penetration in iowa and a dynamic assessment of frequency response in wind turbine types," *Master's Thesis, Electrical Engineering, Iowa State University, Ames*, 2008.

[55] A. A. Tamimi, A. Pahwa, S. Starrett, and N. Williams, "Maximizing wind penetration using voltage stability based methods for sizing and locating new wind farms in power system," in *IEEE PES General Meeting*, pp. 1–7, 2010.

[56] H. Ayres, W. Freitas, M. De Almeida, and L. Da Silva, "Method for determining the maximum allowable penetration level of distributed generation without steady-state voltage violations," *IET generation, transmission & distribution*, vol. 4, no. 4, pp. 495–508, 2010.

[57] J. Kaldellis, K. Kavadias, and A. Filios, "A new computational algorithm for the calculation of maximum wind energy penetration in autonomous electrical generation systems," *Applied Energy*, vol. 86, no. 7, pp. 1011–1023, Aug. 2009.

[58] H. Yu, R. Bansal, and Z. Dong, "Fast computation of the maximum wind penetration based on frequency response in small isolated power systems," *Applied Energy*, vol. 113, pp. 648–659, 2014.

[59] A. Pitto, D. Cirio, A. Gatti, M. Benini, A. Gelmini, and V. Brignoli, "Wind power expansion and security assessment: A 2020 scenario in Sardinia," in *Power Generation, Transmission, Distribution and Energy Conversion (MEDPOWER 2012), 8th Mediterranean Conference on*, pp. 1–8, IET, 2012.

[60] N.-A. Masood, R. Yan, and T. K. Saha, "Estimation of maximum wind power penetration level to maintain an adequate frequency response in a power system," in *Electrical and Computer Engineering (ICECE), 2014 International Conference on*, pp. 587–590, IEEE, 2014.

[61] N. Farrokhseresht, H. C. Oréstica, and M. R. Hesamzadeh, "Determination of acceptable inertia limit for ensuring adequacy under high levels of wind integration," in *11th International Conference on the European Energy Market (EEM14)*, pp. 1–5, IEEE, 2014.

[62] Y.-Z. Wang, S.-Y. Ma, Q. Wang, S.-J. Ma, and Y.-L. Sun, "Estimation of wind penetration in a thermal dominated power system limited by frequency deviation,"

[63] A. Bhowmik, A. Maitra, S. M. Halpin, and J. E. Schatz, "Determination of allowable penetration levels of distributed generation resources based on harmonic limit considerations," *IEEE Trans. Power Delivery*, vol. 18, no. 2, pp. 619–624, Apr. 2003.

[64] C.-L. Chen, "Optimal wind–thermal generating unit commitment," *IEEE Trans. Energy Convers.*, vol. 23, no. 1, pp. 273–280, Mar. 2008.

[65] D. L. H. Aik, "A general-order system frequency response model incorporating load shedding: analytic modeling and applications," *IEEE Trans. Power Syst*, vol. 21, no. 2, pp. 709–717, May 2006.

[66] P. M. Anderson and M. Mirheydar, "A low-order system frequency response model," *IEEE Trans. Power Syst*, vol. 5, no. 3, pp. 720–729, Aug. 1990.

[67] Y. Fu, M. Shahidehpour, and Z. Li, "Security-constrained unit commitment with AC constraints," *IEEE Trans. Power Syst*, vol. 20, no. 2, pp. 1001–1013, Aug. 2005.

[68] R. Desmukh and R. Kumar, "Reliability analysis of combined wind-electric and conventional systems," *Solar Energy*, vol. 28, no. 4, pp. 345–352, Aug. 1982.

[69] R. Billinton and A. Chowdhury, "Incorporation of wind energy conversion systems in conventional generating capacity adequacy assessment," *IEE Proceedings C - Generation, Transmission and Distribution*, vol. 139, no. 1, pp. 47–56, Jan. 1992.

[70] C. Singh and A. Lago-Gonzalez, "Reliability modeling of generation systems including unconventional energy sources," *IEEE Trans. Power App. Syst.*, vol. PAS-104, no. 5, pp. 1049–1056, May 1985.

[71] F. C. Sayas and R. Allan, "Generation availability assessment of wind farms," *IEE Proceedings - Generation, Transmission and Distribution*, vol. 143, no. 5, pp. 507–518, Sep. 1996.

[72] A. P. Leite, C. L. Borges, and D. M. Falcao, "Probabilistic wind farms generation model for reliability studies applied to Brazilian sites," *IEEE Trans. Power Syst.*, vol. 21, no. 4, pp. 1493–1501, Nov. 2006.

[73] T. Manco and A. Testa, "A Markovian approach to model power availability of a wind turbine," in *Power Tech, 2007 IEEE*, pp. 1256–1261, Jul. 2007.

[74] S. Sulaeman, M. Benidris, J. Mitra, and C. Singh, "A wind farm reliability model considering both wind variability and turbine forced outages," *IEEE Trans. Sustain. Energy*, vol. 8, no. 2, pp. 629–637, Apr. 2017.

[75] P. Giorsetto and K. F. Utsurogi, "Development of a new procedure for reliability modeling of wind turbine generators," *IEEE Trans. Power App. Syst.*, vol. PAS-102, no. 1, pp. 134–143, Jan. 1983.

[76] A. S. Dobakhshari and M. Fotuhi-Firuzabad, "A reliability model of large wind farms for power system adequacy studies," *IEEE Trans. Energy Convers.*, vol. 24, no. 3, pp. 792–801, Aug. 2009.

[77] F. Vallee, J. Lobry, and O. Deblecker, "System reliability assessment method for wind power integration," *IEEE Trans. Power Syst.*, vol. 23, no. 3, pp. 1288–1297, Aug. 2008.

[78] N. B. Negra, O. Holmstrøm, B. Bak-Jensen, and P. Sorensen, "Aspects of relevance in offshore wind farm reliability assessment," *IEEE Trans. Energy Convers.*, vol. 22, no. 1, pp. 159–166, Mar. 2007.

[79] H. Kim, C. Singh, and A. Sprintson, "Simulation and estimation of reliability in a wind farm considering the wake effect," *IEEE Trans. Sustain. Energy*, vol. 3, no. 2, pp. 274–282, Mar. 2012.

[80] R. Billinton, H. Chen, and R. Ghajar, “A sequential simulation technique for adequacy evaluation of generating systems including wind energy,” *IEEE Trans. Energy Convers.*, vol. 11, no. 4, pp. 728–734, Dec. 1996.

[81] P. Wang and R. Billinton, “Reliability benefit analysis of adding WTG to a distribution system,” *IEEE Trans. Energy Convers.*, vol. 16, no. 2, pp. 134–139, Jun. 2001.

[82] W. Wangdee and R. Billinton, “Reliability assessment of bulk electric systems containing large wind farms,” *International Journal of Electrical Power & Energy Systems*, vol. 29, no. 10, pp. 759–766, Dec. 2007.

[83] D. Halamay, T. K. Brekken, A. Simmons, and S. McArthur, “Reserve requirement impacts of large-scale integration of wind, solar, and ocean wave power generation,” *IEEE Trans. Sustain. Energy*, vol. 2, no. 3, pp. 321–328, Jul. 2011.

[84] N. Nguyen and J. Mitra, “An analysis of the effects and dependency of wind power penetration on system frequency regulation,” *IEEE Trans. Sustain. Energy*, vol. 7, no. 1, pp. 354–363, Jan. 2016.

[85] N. Nguyen and J. Mitra, “Effect of wind power on load frequency control,” in *IEEE Power and Energy Society General Meeting*, pp. 1–5, Jul. 2016.

[86] H. Banakar, C. Luo, and B. T. Ooi, “Impacts of wind power minute-to-minute variations on power system operation,” *IEEE Trans. Power Syst.*, vol. 23, no. 1, pp. 150–160, Feb. 2008.

[87] M. J. Hossain, H. R. Pota, M. A. Mahmud, and R. Ramos, “Investigation of the impacts of large-scale wind power penetration on the angle and voltage stability of power systems,” *Systems Journal, IEEE*, vol. 6, no. 1, pp. 76–84, Mar. 2012.

[88] E. Vittal, M. O’Malley, and A. Keane, “A steady-state voltage stability analysis of power systems with high penetrations of wind,” *IEEE Trans. Power Syst.*, vol. 25, no. 1, pp. 433–442, Feb. 2010.

[89] R. Gonzales, R. Mukerji, M. Swider, D. Allen, R. Pike, D. Edelson, E. Nelson, and J. Adams, “Integration of wind into system dispatch,” *New York ISO White Paper*, Oct. 2008.

[90] E. Ela, V. Gevorgian, P. Fleming, Y. Zhang, M. Singh, E. Muljadi, A. Scholbrook, J. Aho, A. Buckspan, and L. Pao, *Active Power Controls from Wind Power: Bridging the Gap*. National Renewable Energy Laboratory, 2014.

[91] R. Billinton and G. Bai, “Generating capacity adequacy associated with wind energy,” *IEEE Trans. Energy Convers.*, vol. 19, no. 3, pp. 641–646, Sep. 2004.

[92] B. Hasche, “General statistics of geographically dispersed wind power,” *Wind Energy*, vol. 13, no. 8, pp. 773–784, Apr. 2010.

[93] B. S. Dhillon and C. Singh, *Engineering Reliability: New Techniques and Applications*. Wiley, New York, 1981.

[94] RTS Working Group, "The IEEE reliability test system—1996. a report prepared by the reliability test system task force of the application of probability methods subcommittee," *IEEE Trans. Power Syst.*, vol. 14, no. 3, pp. 1010–1020, Aug. 1999.

[95] National Renewable Energy Laboratory, "Eastern wind dataset," 2015.

[96] Tapbury Management Limited, Sustainable Energy Ireland, "VRB ESS energy storage and the development of dispatchable wind turbine output," 2006.

[97] P. Hu, R. Karki, and R. Billinton, "Reliability evaluation of generating systems containing wind power and energy storage," *IET Generation, Transmission Distribution*, vol. 3, pp. 783–791, August 2009.

[98] J. Mitra, M. R. Vallem, and C. Singh, "Optimal deployment of distributed generation using a reliability criterion," *IEEE Trans. Ind. Appl.*, vol. 52, no. 3, pp. 1989–1997, 2016.

[99] J. Mitra and C. Singh, "Incorporating the DC load flow model in the decomposition-simulation method of multi-area reliability evaluation," *IEEE Trans. Power Syst.*, vol. 11, no. 3, pp. 1245–1254, Aug. 1996.

[100] S. Sulaeman, Y. Tian, M. Benidris, and J. Mitra, "Quantification of storage necessary to firm up wind generation," *IEEE Trans. Ind. Appl.*, vol. 53, no. 4, 2017.

[101] R. Wiser, E. Lantz, T. Mai, J. Zayas, E. DeMeo, E. Eugeni, J. Lin-Powers, and R. Tusing, "Wind vision: A new era for wind power in the united states," *The Electricity Journal*, vol. 28, pp. 120–132, Mar. 2015.

[102] European Wind Energy Association, "Wind energy scenarios for 2030," 2015.

[103] N. Nguyen and J. Mitra, "Effect of wind power on load frequency control," in *Power and Energy Society General Meeting (PESGM), 2016*, pp. 1–5, IEEE, 2016.

[104] N. Nguyen, V. Johnson, and J. Mitra, "Environmental-economic dispatch of power system in the presence of wind generation," in *North American Power Symposium (NAPS), 2015*, pp. 1–6, IEEE, 2015.

[105] N. Nguyen, V. Johnson, and J. Mitra, "Environmental-economic dispatch of power system based on frequency stability constraint," in *North American Power Symposium (NAPS), 2016*, pp. 1–6, IEEE, 2016.

[106] N. Nguyen, M. Benidris, and J. Mitra, "A unified analysis of the impacts of stochasticity and low inertia of wind generation," in *Probabilistic Methods Applied to Power Systems (PMAPS), 2016 International Conference on*, pp. 1–7, 2016.

[107] C.-F. Lu, C.-C. Liu, and C.-J. Wu, "Effect of battery energy storage system on load frequency control considering governor deadband and generation rate constraint," *IEEE Trans. Energy Convers.*, vol. 10, no. 3, pp. 555–561, Sep. 1995.

[108] S. Teleke, M. E. Baran, A. Q. Huang, S. Bhattacharya, and L. Anderson, "Control strategies for battery energy storage for wind farm dispatching," *IEEE Trans. Energy Convers.*, vol. 24, no. 3, pp. 725–732, Sep. 2009.

[109] G. Delille, B. Francois, and G. Malarange, "Dynamic frequency control support by energy storage to reduce the impact of wind and solar generation on isolated power system's inertia," *IEEE Trans. Sustain. Energy*, vol. 3, no. 4, pp. 931–939, Oct. 2012.

[110] D. Gautam, L. Goel, R. Ayyanar, V. Vittal, and T. Harbour, "Control strategy to mitigate the impact of reduced inertia due to doubly fed induction generators on large power systems," *IEEE Trans. Power Syst.*, vol. 26, no. 1, pp. 214–224, Feb. 2011.

[111] L. Xu, "Enhanced control and operation of DFIG-based wind farms during network unbalance," *IEEE Trans. Energy Convers.*, vol. 23, no. 4, pp. 1073–1081, Dec. 2008.

[112] L. Xu, "Coordinated control of DFIG's rotor and grid side converters during network unbalance," *IEEE Trans. Power Electronics*, vol. 23, no. 3, pp. 1041–1049, May 2008.

[113] L. Yang, Z. Xu, J. Ostergaard, Z. Y. Dong, and K. P. Wong, "Advanced control strategy of DFIG wind turbines for power system fault ride through," *IEEE Trans. Power Syst.*, vol. 27, no. 2, pp. 713–722, May 2012.

[114] F. Islam, A. Al-Durra, and S. Muyeen, "Smoothing of wind farm output by prediction and supervisory-control-unit-based FESS," *IEEE Trans. Sustain. Energy*, vol. 4, no. 4, pp. 925–933, Oct. 2013.

[115] Y.-K. Wu and J.-S. Hong, "A literature review of wind forecasting technology in the world," in *Power Tech, 2007 IEEE Lausanne*, pp. 504–509, 2007.

[116] L. Liang, J. Zhong, and Z. Jiao, "Frequency regulation for a power system with wind power and battery energy storage," in *Power System Technology (POWERCON), 2012 IEEE International Conference on*, pp. 1–6, 2012.

[117] H. Holttinen and J. Pedersen, "The effect of large-scale wind power on a thermal system operation," in *Proc. 4th Int. Workshop Large-Scale Integration of Wind Power and Transmission Networks for Offshore Wind Farms*, pp. 20–22, 2003.

[118] Q. Jiang, Y. Gong, and H. Wang, "A battery energy storage system dual-layer control strategy for mitigating wind farm fluctuations," *IEEE Trans. Power Syst.*, vol. 28, no. 3, pp. 3263–3273, 2013.

[119] M. A. Abdullah, K. M. Muttaqi, D. Sutanto, and A. P. Agalgaonkar, "An effective power dispatch control strategy to improve generation schedulability and supply reliability of a wind farm using a battery energy storage system," *IEEE Trans. Sustain. Energy*, vol. 6, no. 3, pp. 1093–1102, Jul. 2015.

[120] A. Ghaeedi and E. Noroozi, "Reliability evaluation of renewable energy-based power system containing energy storage,"

[121] Y. Xu and C. Singh, "Adequacy and economy analysis of distribution systems integrated with electric energy storage and renewable energy resources," *IEEE Trans. Power Syst.*, vol. 27, no. 4, pp. 2332–2341, 2012.

[122] A. S. Awad, T. H. El-Fouly, and M. M. Salama, "Optimal ess allocation for load management application," *IEEE Trans. Power Syst.*, vol. 30, no. 1, pp. 327–336, Jan. 2015.

[123] Y. Wen, C. Guo, H. Pandzic, and D. S. Kirschen, "Enhanced security-constrained unit commitment with emerging utility-scale energy storage," *IEEE Trans. Power Syst.*, vol. 31, no. 1, pp. 652–662, Jan. 2016.

[124] J. Cao, W. Du, and H. Wang, "An improved corrective security constrained opf with distributed energy storage," *IEEE Trans. Power Syst.*, vol. 31, no. 2, pp. 1537–1545, 2016.

[125] J. M. Gantz, S. M. Amin, and A. M. Giacomoni, "Optimal mix and placement of energy storage systems in power distribution networks for reduced outage costs," in *Energy Conversion Congress and Exposition (ECCE), 2012 IEEE*, pp. 2447–2453, 2012.

[126] Department of Energy, "Grid 2030: A national vision for electricity's second 100 years," *US DOE Report*, 2003.

[127] L. Xu, X. Ruan, C. Mao, B. Zhang, and Y. Luo, "An improved optimal sizing method for wind-solar-battery hybrid power system," *IEEE Trans. Sustain. Energy*, vol. 4, no. 3, pp. 774–785, Jul. 2013.

[128] A. Narimani, G. Nourbakhsh, G. Ledwich, and G. R. Walker, "Impact of electric energy storage scheduling on reliability of distribution system," in *Power Electronics and Drive Systems (PEDS), 2015 IEEE 11th International Conference on*, pp. 405–408, 2015.

[129] Z. Gao, P. Wang, and J. Wang, "Impacts of energy storage on reliability of power systems with wtgs," in *Probabilistic Methods Applied to Power Systems (PMAPS), 2010 IEEE 11th International Conference on*, pp. 65–70, 2010.

[130] L. Koh, W. Peng, K. Tseng, and G. ZhiYong, "Reliability evaluation of electric power systems with solar photovoltaic & energy storage," in *Probabilistic Methods Applied to Power Systems (PMAPS), 2014 International Conference on*, pp. 1–5, 2014.

[131] R. Zheng and J. Zhong, "Generation adequacy assessment for power systems with wind turbine and energy storage," in *Innovative Smart Grid Technologies (ISGT), 2010*, pp. 1–6, 2010.

[132] W. Li and B. Bagen, "Reliability evaluation of integrated wind/diesel/storage systems for remote locations," in *Probabilistic Methods Applied to Power Systems (PMAPS), 2010 IEEE 11th International Conference on*, pp. 791–795, 2010.

[133] W. Li and R. Billinton, *Reliability assessment of electric power systems using Monte Carlo methods*. Springer Science & Business Media, 2013.

[134] Department of Trade and Industry, "The energy challenge energy review report 2006," tech. rep., UK, 2006.

[135] G. Lalor, A. Mullane, and M. O'Malley, "Frequency control and wind turbine technologies," *IEEE Trans. Power Syst.*, vol. 20, no. 4, pp. 1905–1913, Nov. 2005.

[136] C. Chompoo-Inwai, W.-J. Lee, P. Fuangfoo, M. Williams, and J. R. Liao, "System impact study for the interconnection of wind generation and utility system," *IEEE Trans. Ind. Appl.*, vol. 41, no. 1, pp. 163–168, Feb. 2005.

[137] A. Esmaili and A. Nasiri, "Energy storage for short-term and long-term wind energy support," in *IECON 2010-36th Annual Conference on IEEE Industrial Electronics Society*, pp. 3281–3286, 2010.

[138] D. Gautam, V. Vittal, R. Ayyanar, and T. Harbour, "Supplementary control for damping power oscillations due to increased penetration of doubly fed induction generators in large power systems," in *Power Systems Conference and Exposition (PSCE), 2011 IEEE/PES*, pp. 1–6, 2011.

[139] G. Cai, Q. Sun, C. Liu, P. Li, and D. Yang, "A new control strategy to improve voltage stability of the power system containing large-scale wind power plants," in *Electric Utility Deregulation and Restructuring and Power Technologies (DRPT), 2011 4th International Conference on*, pp. 1276–1281, IEEE, 2011.

[140] P. Du, Y. Makarov, N. Zhou, and P. Etingov, "Application of virtual energy storage to partially mitigate unscheduled interchange caused by wind power," in *Power Systems Conference and Exposition (PSCE), 2011 IEEE/PES*, pp. 1–5, 2011.

[141] D. Ramos, E. Guarnier, and L. Witzler, "Using the seasonal diversity between renewable energy sources to mitigate the effects of wind generation uncertainties," in *Transmission and Distribution: Latin America Conference and Exposition (T&D-LA), 2012 Sixth IEEE/PES*, pp. 1–7, 2012.

[142] "60 Hz stability on power grid going away?," 2011. [Online]. Available: http://www.radiomagonline.com/deep-dig/0005/60hz-stability-on-power-grid-going-away/33527.

[143] S. J. Chapman, *MATLAB programming for engineers*. Nelson Education, 2015.

[144] "Characteristics and target values of the voltage supplied by the Hydro-Québec medium and low voltage systems," *Hydro-Québec, Tech. Rep*, pp. 30012–01.